Impact of healthy aging on visual internal noise sources

Daphné Silvestre

THÈSE DE DOCTORAT

Spécialité: **Psychophysique**

Ecole doctorale Informatique, Télécommunications et Electronique (Paris)

Présentée par

Daphné SILVESTRE

Pour obtenir le grade de

DOCTEUR de Sorbonne UNIVERSITÉ

Impact of healthy aging on visual internal noise sources

Soutenue le 4 Juin 2019 devant le jury composé de:

Rémy ALLARD – Sorbonne Université, Paris, FR	Directeur de thèse
Angelo ARLEO – Sorbonne Université, Paris, FR	Examinateur
Thérèse COLLINS – Université Paris Descartes, Paris, FR	Examinatrice
Michael HERZOG – EPFL, Lausanne, Switzerland	Rapporteur
Peter NERI – ENS, Paris, FR	Rapporteur

Abstract

The unceasing growth of the aging population worldwide is a major societal issue and particularly a public health concern. The well-being of the elderly needs to be improved in order to increase their autonomy and quality of life. One major factor responsible for the loss of the elderly's autonomy is vision loss. This thesis' aimed to identify the functional and neurobiological alterations responsible for the age-related vision loss. This question was addressed through experimental psychophysics by using an external noise paradigm, which enables the factorization of contrast sensitivity (i.e. measure of visual perception) into equivalent input noise and calculation efficiency. A new paradigm was first developed from the collection of young participants data, in order to have a fundamental understanding of the contrast sensitivity variations with respect to spatial frequency and luminance intensity. This paradigm enabled to differentiate the equivalent input noise estimations into three sources of internal noise at different levels of the visual system (photoreceptor level, retinal level and cortical level), each having an impact on contrast sensitivity at different luminance and spatial frequency ranges. Further fundamental experiments were undertaken in the spatio-temporal domain in order to better characterize the properties of these sources of noise. Finally, our internal noise paradigm was used to investigate the impact of aging on the limiting factors of spatial and temporal contrast sensitivities. This study aimed at estimating the proportion in which the three sources of noise defined by our paradigm were responsible for age-related vision losses. It was found that the elderly population absorbed less photons than the young probably due to less efficient cones (source of noise at the photoreceptor level). The elderly had also more spontaneous neural activity (source of noise at the cortical level), but this was only found for the detection of static visual inputs (i.e. measure of spatial contrast sensitivity) and not

for drifting visual inputs (i.e. measure of temporal contrast sensitivity). Therefore, our internal noise paradigm enabled to estimate the sources of noise considerably impaired with aging and gave us a better comprehension of the underlying causes of the age-related contrast sensitivity loss.

Abbreviations

cpd or cyc/deg — cycles per degree of visual angle

CSF — Contrast Sensitivity Function

LAM — Linear Amplifier Model

MTF — Modulation Transfer Function

PTM — Perceptual Template Model

SF — Spatial frequency

TCSF — Temporal Contrast Sensitivity Function

TF — Temporal frequency

tMTF — temporal Modulation Transfer Function

Contents

List of Figures

List of Tables

Part I

Theoretical framework

Chapter 1

Aging and vision

1.1 General introduction

The unceasing growth of the aged population worldwide is becoming a societal issue, because there are more and more retired people to support. In 2017, there was 962 millions of older adults over 60 years of age worldwide representing 13% of the total population and this population will keep growing at a rate of 3% per year (United Nations, 2017). This aging population growth is especially a public health concern in terms of costs (Mendelson and Schwartz, 1993) since aging impacts many functions such as motor functions, sensory processes and cognitive processes that need to be taken care of to improve the quality of life of the elderly. Furthermore, these different declines occurring with aging affect the autonomy of the elderly in their every day tasks. One major factor responsible for this loss of autonomy is vision loss, with nearly 186 millions of visually impaired older adults (>50 years, in 2010, Pascolini and Mariotti 2012) worldwide. Indeed, it has been reported, for instance, that the elderly have more problems driving at night (Gruber et al., 2013) due to a decrease of their visual faculties in low luminance conditions.

The overall objective of a society to tackle this growth of the aging population is to extend the autonomy of the elderly as long as possible, in order that this population can keep contributing to the society. To reach this objective, new tools need to be develop to diagnose at an early stage impairments that derive from age-related pathologies or healthy

aging and treatments need to be found to restore damaged functions. This thesis will focus on age-related vision loss and aims to understand the causes of this loss that greatly impacts elderly's performance of everyday visual tasks and therefore their overall autonomy.

1.2 Factors impacting age-related vision loss

Age-related visual declines can either be due to healthy or pathological aging. The structural changes of the visual system occurring with healthy aging can be differentiated into optical and neural factors.

The optical factors affect the quality of the image forming on the retina by degrading the visual signal (i.e. light) from its entry in the eye to its focus onto the retina (see Figure 1.1). The light first goes through the cornea, which induce a refraction of the light. The cornea is also accountable for approximately two-thirds of the eye's total optical power. Aging affects the cornea by increasing its curvature resulting in a decrease of the cornea's optical power and therefore in a deterioration of the quality of the retinal image (Baldwin and Mills, 1981; Fledelius, 1988). After the cornea the light goes through the pupil, which is the aperture regulating the amount of light entering the eye. The size of the pupil is controlled by the iris muscle. The diameter of the pupil tends to decrease with aging for a given luminance condition, which is referred to as miosis. The pupil size difference between young (20 years old) and older adults (80 years old) is at its maximum in dim light conditions, where the elderly have a pupil diameter of 4 mm and the young adults a pupil of 8 mm in average leading to a factor 2 of difference (Loewenfeld, 1979). Next, the light passes through the crystalline lens, which refracts and focuses the light onto the retina by changing its shape due to contractile forces exerted by the ciliary muscles. This process called accommodation is accountable of one-third of the eye's total optical power. The accommodative power of the lens decreases with aging due to a loss of elasticity of the lens. Furthermore, the lens' optical density increases with aging resulting in a loss of its transparency and in filtering out particularly short wavelengths light (i.e. blue). The aging lens is also responsible for an increase of the light scatter in the eye, which leads to a blurrier retinal image.

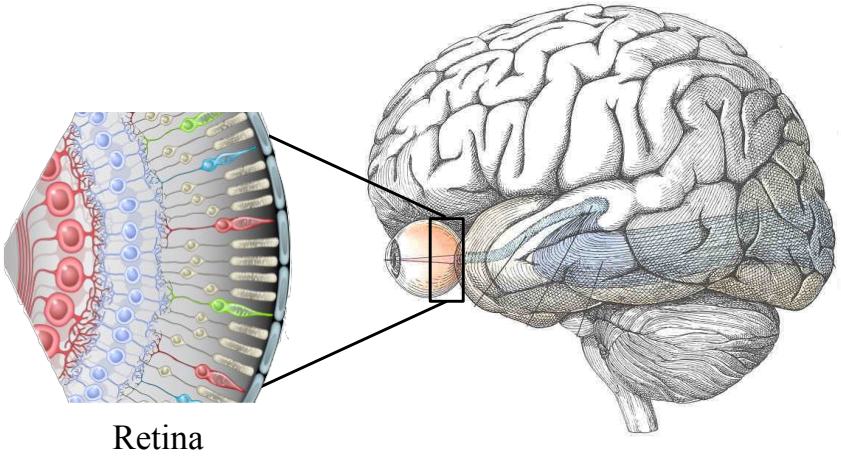

Figure 1.1: The visual system. This schematic representation of the visual system presents on the left, an enlargement of the retina illustrating the different layers of neurons and on the right, the brain with the processing pathway of visual inputs illustrated in blue.

The neural factors affect the quality of the electrical signal, originating from a visual input, that is process by the different neurons of the visual system. The visual input (i.e. light) is first converted into an electrical signal at the photoreceptor level in the retina with what is called the phototransduction, this signal is then processed by the different layers of neurons of the retina (bipolar, amacrine, horizontal and retinal ganglion cells), by the lateral geniculate nucleus, and finally by the visual cortex and other cortical areas. At the photoreceptor level, several studies have shown that aging affects the density of rods (photoreceptors mainly in the periphery) with a 30% loss (Curcio et al., 1990; Panda-Jonas et al., 1995), however the loss of cones (photoreceptors mainly in the center in the macula) with aging is still unclear and debated (Curcio et al., 1993; Gartner and Henkind, 1981). The retinal ganglion cells are also affected with aging with a 16% to a 25% loss in the macula region (Curcio and Drucker, 1993; Gao and Hollyfield, 1992). In the visual cortex and other cortices it was found with aging that the density of the neuron synapses decreases, that the inhibitory neurotransmitter (i.e. GABA) is affected and that there is a degeneration of the myelin around the neuron's axons (Zhang et al., 2008).

Pathological aging was not part of the scope of this thesis, but since visual pathologies are very common in the elderly population, I think it is important to cite the main ones. There are three types of age-related ocular diseases leading to blindness (visual acuity <20/200)

or to low vision (acuity between 20/200 and 20/40), which are glaucoma (damage of the optical nerve), age-related macular degeneration (affecting central vision) and cataract (opacification of the crystalline lens).

As described above, age-related vision loss can be due to many factors that are either optical or neural. However, these factors are rarely easily measurable, especially the neural factors, such as cell density, which are often measured on post-mortem human eye donor or non human primate's eye. Furthermore, it is still unclear in which proportion these different factors affect age-related vision loss. The purpose of this thesis is to quantify the impact of different factors affecting vision loss with healthy aging by using a psychophysical approach.

1.3 Methods to estimate age-related vision loss

Visual perception can be quantified by different methods, the one commonly used in clinic is visual acuity, which is measured by reading black letters on a white chart (e.g. ETDRS chart). In this thesis, a more precise measure was used called contrast sensitivity, which is commonly used in psychophysics to measure visual perception.

1.3.1 Contrast sensitivity

Definition

Contrast sensitivity defines the threshold of an observer between the visible and the invisible (see Figure 1.2). Suppose an observer has to detect a target on a uniform background (e.g. a Gabor represented in Figure 1.2), the contrast of this target may be specified as Weber contrast $\frac{L_{max}-L_{min}}{L_{background}}$, Michelson contrast $\frac{L_{max}-L_{min}}{L_{max}+L_{min}}$ or RMS (Root Mean Square) contrast $\frac{L_\sigma}{L_\mu}$, where $L_{max}, L_{min}, L_{background}, L_\mu$ and L_σ are the luminance maximum, minimum, background, mean and standard deviation, respectively. The contrast threshold of an observer is the contrast required for him to see the target consistently. The inverse of contrast threshold is called contrast sensitivity.

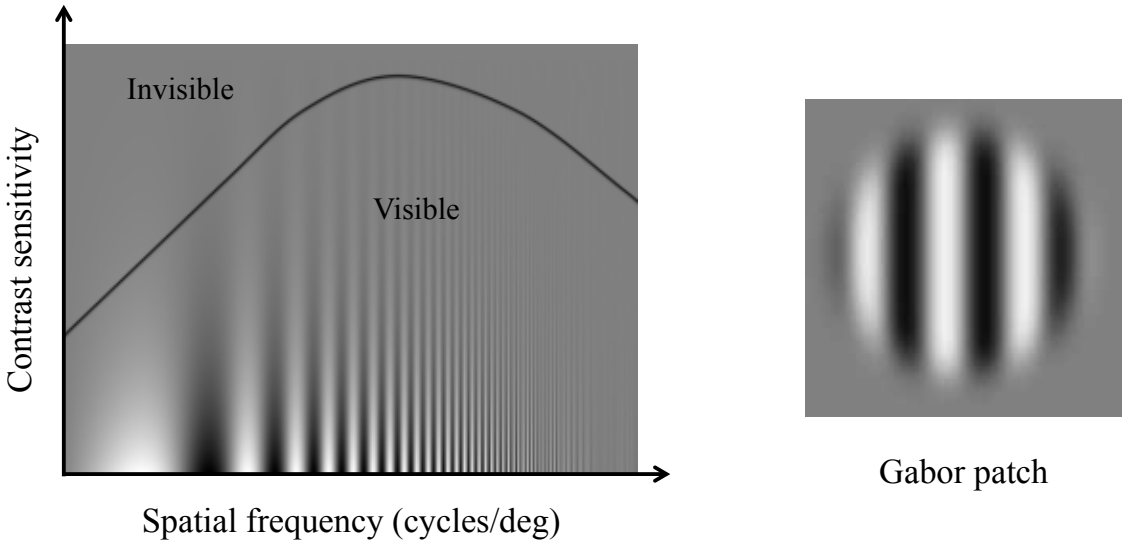

Figure 1.2: Contrast sensitivity function and Gabor patch. Contrast sensitivity as function of spatial frequency is represented on the left. The solid line represents the contrast sensitivity function, which is the threshold between the visible and invisible. A Gabor patch is represented on the right, which is the type of stimulus generally used to measure contrast sensitivity.

Contrast sensitivity varies according to different parameters such as spatial frequency (SF), temporal frequency (TF) and luminance intensity (see Figure 1.3). Contrast sensitivity as a function of SF is called the Contrast Sensitivity Function (i.e. CSF) and is shaped as an inverted « U ». The measure of contrast sensitivity is often carried out by presenting a Gabor, which is a sinusoid convolved with a Gaussian spatial window (Figure 1.2), in order to drive the activity of neurons in the early visual cortex in a controlled manner (e.g. activation of neurons specialized for a specific orientation of the Gabor). The SF of a Gabor is the number of visible cycles per degree of visual angle. The human eye is less sensitive at low and high SFs and reaches a peak of sensitivity around 4 cycles per degree (cpd) for high luminance intensities. Contrast sensitivity as a function of TF is called the Temporal Contrast Sensitivity Function (TCSF) and can be measured by detecting a flickering or a drifting Gabor. The human eye reaches a peak of sensitivity around 8 Hz for high luminance intensities and decreases steeply above this frequency. CSF and TCSF also vary with luminance intensity by decreasing (i.e. observer less sensitive) as luminance intensity decrease. Luminance intensity describes the amount of light that is emitted or

reflected from a surface and falls within a given solid angle (e.g. subtended by the pupil of the eye). Luminance intensity depends on the sensitivity of the human eye and its unit is candela per square meter ($cd.m^{-2}$). Luminance intensity at the retina level is called retinal illuminance and is in Trolands (Td), which corresponds to the luminance intensity ($cd.m^{-2}$) multiplied by the pupil area (mm^2). In this thesis, we wanted the observers to be in the same retinal illuminance conditions, therefore the unit used for luminance intensity was always Trolands.

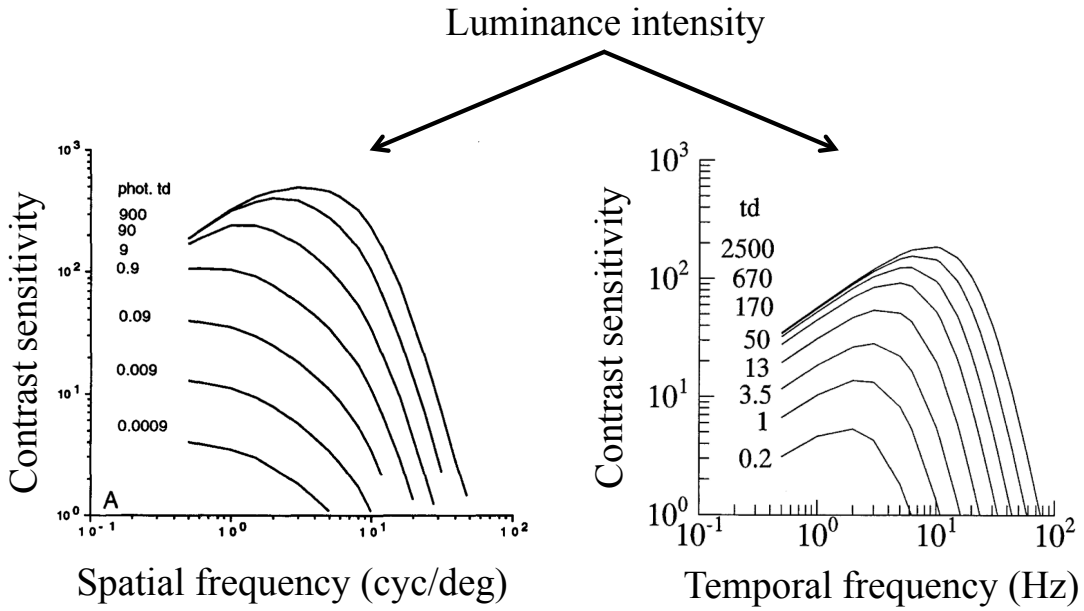

Figure 1.3: Contrast sensitivity functions. On the left, contrast sensitivity as a function of spatial frequency for different luminance intensities (Figure from Rovamo et al. 1994a). On the right, contrast sensitivity as a function of temporal frequency for different luminance intensities (Figure from Rovamo et al. 2000b).

Contrast sensitivity and aging

It has been established since the late 80's that contrast sensitivity declines with healthy aging under photopic conditions at intermediate and high SF, with an increasing effect of this decline at higher SFs (see left graph of Figure 1.4, Derefeldt et al. 1979; Elliott et al. 1990; Owsley et al. 1983; Tulunay-keesey et al. 1988). In the literature (Artal et al., 2002; Elliott et al., 1990; Weale, 1963), this age-related sensitivity loss was mainly explained by a decline of the optical factors with aging, since these factors have a higher impact on high

SFs. It was found that miosis and the yellowing of the lens were the main optical factors accounting for this loss. Indeed, these factors reduce the retinal illuminance of elderly by a factor of 3 (Weale, 1963) and since contrast sensitivity decreases with decreasing luminance intensity this would explain the age-related contrast sensitivity loss.

Aging was also found to affect temporal contrast sensitivity, with a greater loss at high TFs (see right graph in Figure 1.4, Elliott et al. 1990; Kim and Mayer 1994; Mayer et al. 1988). This loss was mainly attributed to a reduction in the neural impulse response speed (Tyler, 1989), meaning that the age-related temporal sensitivity loss was due to neural factors and not to optical factors. Indeed, in this study (Tyler, 1989), the optical factors such as miosis and the yellowing of the lens were controlled for.

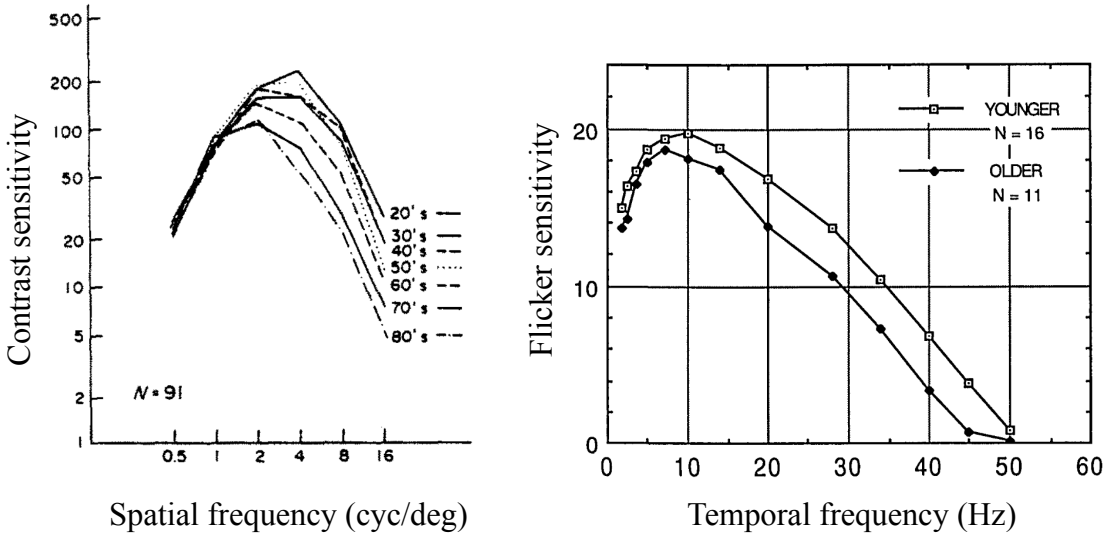

Figure 1.4: Contrast sensitivity functions for different age groups. On the left, contrast sensitivity as a function of spatial frequency for different age groups (Figure from Owsley et al. 1983). On the right, contrast sensitivity as a function of temporal frequency for different age groups (Figure from Mayer et al. 1988).

1.3.2 External noise paradigm

We have seen that contrast sensitivity can quantify the age-related vision loss and give further details about the parameters of the visual information that are lost with aging (e.g. the high SFs). Contrast sensitivity is usually measured by presenting a stimulus on a blank

background (e.g. the Gabor patch in Figure 1.2), but by measuring an additional threshold on a noisy background, contrast sensitivity can be factorized into equivalent input noise and calculation efficiency (Pelli and Farell, 1999). These two factors, being each invariant to a number of properties of the visual input, can procure a better understanding of the processing of visual information. Indeed, equivalent input noise is independent of the nature of the task and relies on the properties of the visual neurons, such as their density, gain and variance. Calculation efficiency is on the other hand independent of many properties of the visual input but dependent on the nature of the task and explains the processing of the the visual information leading to the observer's decision. Therefore, the analysis of these two factors has the advantage of understanding more thoroughly the physiological and functional limitations of contrast sensitivity.

Calculation efficiency is calculated from the signal-to-noise ratio needed to detect the target at threshold. Equivalent input noise is the external noise contrast that has the same impact as the internal noise of the visual system. Figure 1.5 represents contrast threshold (i.e. inverse of contrast sensitivity) as a function of external noise contrast (i.e. the contrast of the noisy background). At low external noise contrast, before the knee of the curve, the external noise has a negligible impact on contrast threshold because internal noise dominates, therefore contrast threshold does not vary with external noise contrast (horizontal dashed line in Figure 1.5). The detection of a signal in this condition will therefore depend on the internal noise of the observer and on his signal-to-(internal)noise ratio at threshold. At high external noise contrast, after the knee of the curve, contrast threshold is limited by external noise (i.e. internal noise is negligible) and therefore increases proportionally with external noise contrast (dashed line with a slope of 1 in log-log units in Figure 1.5). The detection of a signal in this condition will therefore depend only on the signal-to-(external)noise ratio, which can be experimentally measured as the signal and external noise contrast are known and which gives us the calculation efficiency. The junction of the two asymptotes (i.e. the two dashed lines in Figure 1.5) represents the equivalent input noise. At this point, the internal and external noises have the same impact on contrast threshold, which gives a quantification of the impact of the internal noise, that is, the equivalent input noise.

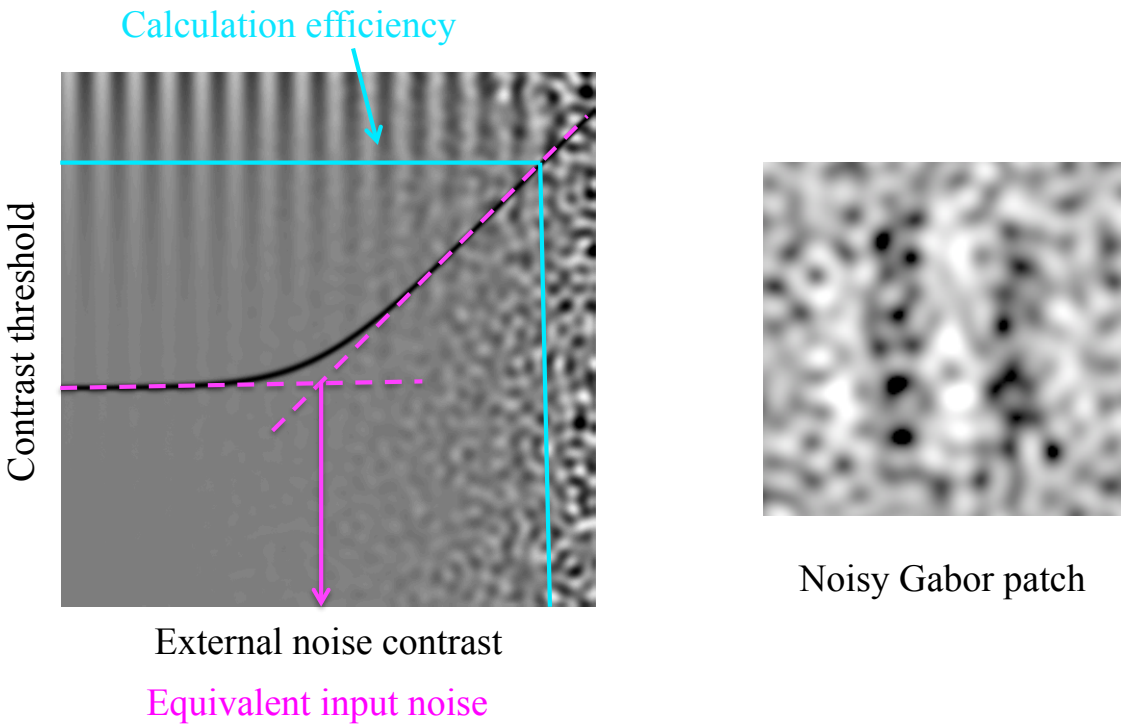

Figure 1.5: External noise paradigm and a noisy Gabor patch. On the left is represented a typical function obtained for a detection task when measuring contrast threshold as a function of external noise contrast (solid black line). The junction of the two asymptotes (dashed lines) represents the equivalent input noise. The signal-to-noise ratio at threshold represents the calculation efficiency. On the right is represented a Gabor patch in a noisy background.

A few studies have used external noise paradigms to further understand the origin of the age-related contrast sensitivity loss (Allard et al., 2013b; Bennett et al., 1999; Pardhan, 2004). The first two studies (Bennett et al., 1999; Pardhan, 2004) found that contrast sensitivity loss was mostly explained by elderly having less calculation efficiency. The equivalent input noise, on the other hand, was only affected by aging at high SF. However, a more recent study (Allard et al., 2013b) found different results, with elderly having more equivalent input noise at low SF and less calculation efficiency at intermediate and high SFs. This study (Allard et al., 2013b) found evidence for this difference with the previous studies and showed that it was due to the type of external noise used. Indeed, Bennett et al. (1999) and Pardhan (2004) used one dimensional and two dimensional local static noise, respectively, whereas Allard et al. (2013b) used a two dimensional extended dynamic

noise. This issue that external noises having different properties (e.g. static or dynamic) may lead to different experimental results will be further investigated in chapter 2. To summarize, age-related contrast sensitivity loss is due to more equivalent input noise at low SF and less calculation efficiency at intermediate and high SF. Therefore, the use of an external noise paradigm enabled to further understand the origin of the age-related loss, with a neural origin at low SF (i.e. more internal noise) and a cortical origin at higher SFs, with an impairment in the processing of the visual information.

1.3.3 Sources of noise

We have seen that equivalent input noise is an estimation of the impact of internal noise of an observer. However, this estimation does not give any information about the origin of the source of noise within the visual system. Lets first clarify the concept of internal noise. Internal noise is defined as any stochastic factor that alters the signal. For instance, before an observer can detect a signal the photons of the signal enter the eye and undergo many processing stages, which will each add noise to the signal. At least two types of noise can be distinguished in the visual system: probability of photon absorption at the photoreceptor level and neural spontaneous activity (see Figure 1.6). The stochastic fluctuations of the number of absorbed photons occurring at the photoreceptor level was found to follow Poisson's distribution. Neural noise occurring at each processing stage of the visual system, from the retina to the different cortical areas involved, is spontaneous activity that is induced by the soma or dendrites of a neuron.

Previous studies (Pelli, 1990; Raghavan, 1995) have defined different sources of internal noise from the estimation of the equivalent input noise. Indeed, the equivalent input noise was defined as the sum of three independent internal noise sources: photon noise, ganglion cell noise and cortical noise. The photon noise was defined as the photon absorption at the photoreceptor level and is inversely proportional to luminance intensity, the ganglion cell noise is inversely proportional to the ganglion cell density and cortical noise is proportional to the signal area. These sources of noise could be estimated because they impact contrast sensitivity in distinct domain (e.g. different eccentricities or luminance intensities) of the stimulus. Although, these sources of noise were estimated over a large

range of the stimulus' parameters, such as the size, the duration, the eccentricity and the luminance intensity, the impact of aging on these or any other sources of noise have not been estimated.

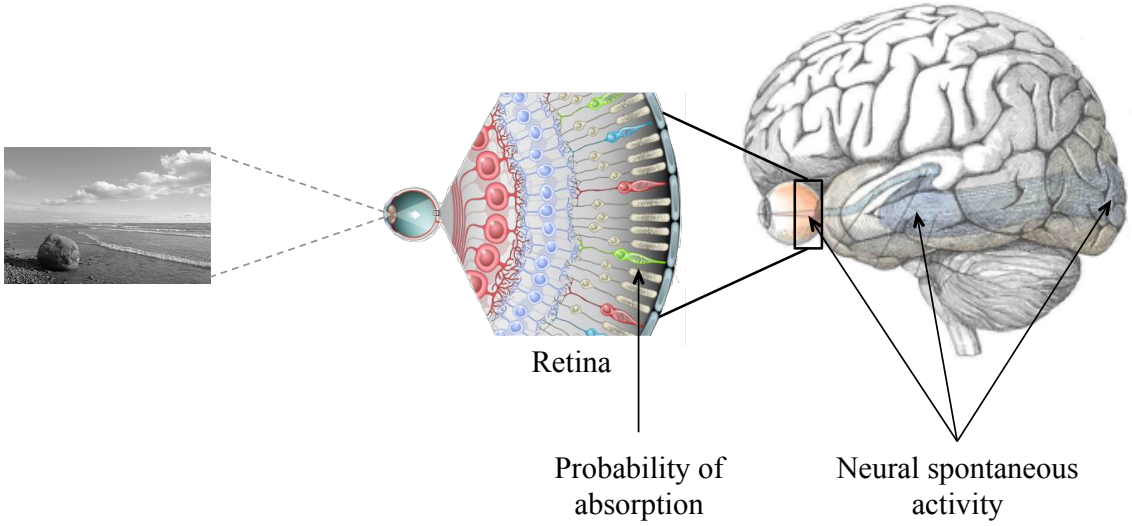

Figure 1.6: The different types of noise in the visual system. In the visual system, at least two types of noise can be distinguished: probability of absorption occurring at the photoreceptor level and neural spontaneous activity occurring at each processing stage of the visual system.

1.4 Objectives of the thesis

The overall aim of this thesis was to further understand the age-related sensitivity loss by estimating the impact of aging on different sources of internal noise of the visual system, which could give more precise information than the equivalent input noise that has been studied so far.

1.4.1 Contributions

The manuscript of my thesis is divided in three parts: the theoretical framework (Part I), the experimental contributions (Part II) and the general discussion (Part III). **Part I** comprises this first chapter that introduces the main question of this thesis by giving

an overview of the literature on this issue. **Part II** is composed of five projects. The first project was on the importance of the noise properties when using an external noise paradigm, related in chapter 2. The second project was on the paradigm we developed to estimate different sources of noise, related in chapter 3. The third project was on the application of this paradigm on aging to estimate the impact of aging on different sources of noise, related in chapter 4. The fourth project was on the extension of our paradigm to the spatio-temporal domain to better characterize the properties and range of impact of the different sources of noise defined by our model, related in chapter 5. Finally the last project was on the impact of aging on the different sources of noise in the temporal domain (i.e. measurement of motion contrast sensitivity), related in chapter 6. This last project was completed as part of Asma Braham Chaouche's master internship under the supervision of Dr. Rémy Allard and myself. All of these projects are presented in the form of published (chapter 2 to 4) or submitted (chapter 5 and 6) articles. Finally, **Part III** comprises the general discussion and conclusions of this thesis, related in chapter 7.

Part II

Experimental contributions

Chapter 2

Adding temporally localized noise can enhance the contribution of target knowledge on contrast detection

Before studying the limitations of contrast sensitivity, we were interested in an unresolved issue in the literature concerning the external noise paradigm and more specifically the choice of the external noise features such as the spatial and temporal characteristics. Therefore, this chapter presents the importance of the choice of the noise features when using an external paradigm.

This work has been previously published under the form of an article:

Daphné Silvestre, Patrick Cavanagh, Angelo Arleo and Rémy Allard (2017) Adding temporally localized noise can enhance the contribution of target knowledge on contrast detection. *Journal of Vision*, 17, 1–10.

Abstract

External noise paradigms are widely used to characterize sensitivity by comparing the effect of a variable on contrast threshold when it is limited by internal versus external noise. A basic assumption of external noise paradigms is that the processing properties are the same in low and high noise. However, recent studies (e.g. Allard and Cavanagh 2011; Allard and Faubert 2014b) suggest that this assumption could be violated when using spatiotemporally localized noise (i.e., appearing simultaneously and at the same location as the target), but not when using spatiotemporally extended noise (i.e., continuously displayed, full-screen, dynamic noise). These previous findings may have been specific to the crowding and 0D noise paradigms that were used so the purpose of the current study is to test if this violation of noise-invariant processing also occurs in a standard contrast detection task in white noise. The rationale of the current study is that local external noise triggers the use of recognition rather than detection and that a recognition process should be more affected by uncertainty about the shape of the target than one involving detection. To investigate the contribution of target knowledge on contrast detection, the effect of orientation uncertainty was evaluated for a contrast detection task in absence of noise and in the presence of spatiotemporally localized or extended noise. A larger orientation uncertainty effect was observed with temporally localized noise than with temporally extended noise or with no external noise indicating a change in the nature of the processing for temporally localized noise. We conclude that the use of temporally localized noise in external noise paradigms risks triggering a shift in process, invalidating the noise-invariant processing required for the paradigm. If instead, temporally extended external noise is used to match the properties of internal noise, no such processing change occurs.

2.1 Introduction

External noise paradigms (Lu and Dosher, 2008; Pelli, 1981; Pelli and Farell, 1999) are widely used to characterize sensitivity by comparing the effect of a variable on contrast thresholds when it is limited by internal versus external noise. An underlying assumption of such external noise paradigm is that the processing properties are the same in presence and absence of external noise. This noise-invariant processing assumption (Allard and Cavanagh, 2011) is generally taken for granted because the visual system has some intrinsic noise, so adding external noise is expected to increase the total amount of noise without triggering a shift in processing properties. However, Allard and colleagues (Allard and Cavanagh, 2011; Allard and Faubert, 2013, 2014a,b; Allard et al., 2013b) recently found evidence that this assumption can be violated for a contrast detection task when the noise is spatiotemporally localized to the target (i.e., appear simultaneously and at the same location as the target), but not when it is spatiotemporally extended (i.e., continuously displayed, full-screen, dynamic noise). Although these studies suggest that localized noise can trigger a change in processing properties, most recent studies using external noise paradigms based on the noise-invariant processing assumption continue to use spatially and/or temporally localized noise (e.g. Baldwin et al. 2016; Bejjanki et al. 2014; Chen et al. 2014; Wyart et al. 2012; Zhao et al. 2015). A potential violation of the noise-invariant processing assumption is probably ignored because the evidence for a shift in processing properties is indirect (e.g. aging, Allard et al. 2013b), is for a specific noise-type (e.g. 0D noise, Allard and Faubert 2013, 2014b), is for a specific task (e.g. motion discrimination, Allard and Faubert 2014a) or relies on a peripheral phenomenon that is not fully understood (e.g. crowding, Allard and Cavanagh 2011). The target of the current study was to directly test if adding noise that is spatiotemporally localized could trigger a shift in processing properties for a standard contrast detection task in central vision.

The most widely used variant of the external noise paradigm is the Linear Amplifier Model (LAM, Pelli 1981, 1990; Pelli and Farell 1999), which is used to factor contrast sensitivity into equivalent input noise and calculation efficiency. Since the impact of

internal noise[1] becomes negligible in high external noise, contrast threshold in high noise depends only on calculation efficiency (calculated from the measured signal-to-(external)noise ratio at threshold, Figure 2.1 bottom). The equivalent input noise can be estimated by assuming that the low-noise calculation efficiency (i.e., the signal-to-(internal)noise ratio at threshold, Figure 2.1 top) is the same as the estimated high-noise calculation efficiency. This noise-invariant calculation efficiency assumption can only be justified if the processing properties are the same in low and high noise. Otherwise, there is no reason to assume that the signal-to-noise ratios at threshold are the same in low and high noise. Thus, the equivalent input noise can be estimated only if the processing properties are the same in low and high noise and a violation of the noise-invariant processing assumption therefore compromises the applicability of the external noise paradigm. Although there are many variants of the observer model (e.g., PTM; Lu and Dosher 2008) they all implicitly assume that the processing properties are the same in low and high noise. Indeed, a key interest of adding external noise is to characterize the processing properties of a stimulus in absence of noise (e.g., estimate equivalent input noise). Consequently, these models implicitly assume that the processing properties are the same in low and high noise (i.e., the noise-invariant processing assumption).

Although it has been suggested that adding localized noise may trigger a shift in processing strategy (Allard and Cavanagh, 2011; Allard and Faubert, 2013, 2014a,b; Allard et al., 2013b), the nature of the strategy operating in localized noise is still elusive. One study suggested that a detection processing strategy may shift to a recognition strategy in localized noise (Allard and Cavanagh, 2011). In this study, crowding was found to affect contrast threshold in localized noise, but not in absence of noise or in extended noise. Given that crowding affects recognition but not detection (Levi, 2008; Pelli et al., 2004), these results suggest that a recognition strategy was used in localized noise and a detection strategy was used in absence of noise and in extended noise. However, crowding is not fully understood and its underlying causes are still widely debated (Dakin et al., 2009; Freeman and Pelli, 2007; Greenwood et al., 2009; Levi, 2008; Pelli et al., 2004). This

[1] In this article the term internal noise refers to additive internal noise. Multiplicative noise was not relevant for the purpose of this article.

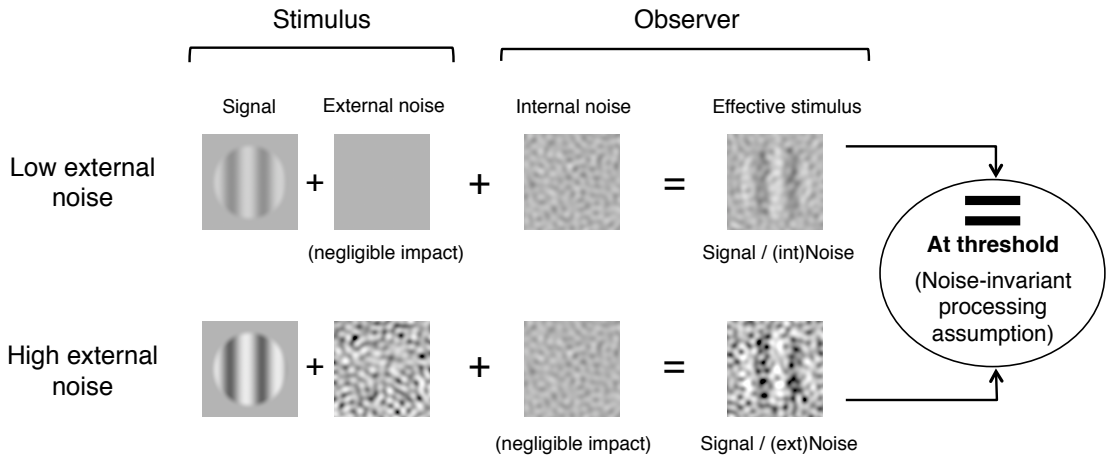

Figure 2.1: Noise-invariant processing assumption. The top row represents a signal presented in low external noise in which case the external noise is dominated by internal noise and therefore has a negligible impact. The detection of this signal would therefore depend on the internal noise of the observer and on his signal-to-(internal) noise ratio at threshold. The bottom row represents a signal in high external noise in which case the internal noise is dominated by external noise and therefore has a negligible impact. The detection of this signal would depend only on the signal-to-(external)noise ratio, which can be experimentally measured as the signal and external noise contrasts are known (Pelli, 1981; Pelli and Farell, 1999). The relative impact of the internal noise (i.e., equivalent input noise) can be estimated by assuming that the signal-to-(internal)noise ratio at threshold is the same as the evaluated signal-to-(external)noise ratio at threshold, which is expected if the same processing strategy operates in low and high external noise (noise-invariant processing assumption).

weakens the interpretation based on a crowding effect. The current study therefore used a paradigm that does not rely on a controversial phenomenon such as crowding. If the processing that operates in localized noise relies on recognizing the shape of the target, then uncertainty about the shape of the target should impair the ability to recognize it. In other words, uncertainty about the shape of the target will degrade its recognition. Thus, if the processing operating in localized noise relies more on target knowledge than does the processing in the absence of noise and in extended noise, then uncertainty about the shape of the target should impair performance more in localized noise than in absence of noise or in extended noise. Note that uncertainty can weakly affect contrast detection in

absence of noise by filtering out noise within irrelevant channels (Davis and Graham, 1981; Davis et al., 1983; Pelli, 1985). Nonetheless, the rationale of the current study was that uncertainty about the shape of the target should have a greater effect on recognition-based processing than on detection-based processing. To measure the effect of shape uncertainty on contrast threshold, the current study investigated contrast detection thresholds when the orientation of the target was known versus unknown to the observer. Orientation uncertainty effects were evaluated in absence of noise and in different noise conditions (spatial and temporal windows each either localized or extended).

2.2 Methods

2.2.1 Observers

Eleven observers, aged from 23 to 39 years old (mean age = 28.73 years, SD = 5.68) with normal or corrected-to-normal vision participated in this study. This study was carried out in accordance with the Code of Ethics of the World Medical Association (Declaration of Helsinki) and informed consent was obtained.

2.2.2 Apparatus

All stimuli were generated by a homemade program and presented on a VIEWPixx/EEG LCD monitor with a refresh rate of 120 Hz and a resolution of 1920×1080 pixels. Stimuli were presented at the center of a grey square of 8.4×8.4 degrees of visual angle (dva) and mean luminance of 50 cd/m^2. The screen being rectangular, the luminance of the unused pixels was minimized. Stimuli were viewed binocularly at a distance of 2 meters. The monitor was the only source of light in the room. The output intensity of each color gun was linearized psychophysically using a homemade program. The Noisy-bit method (Allard and Faubert, 2008), implemented independently to each color gun, made the 8-bit display perceptually equivalent to an analog display having a continuous luminance resolution.

2.2.3 Stimuli/procedure

A two-interval forced-choice procedure was used with an interstimulus interval of 500 ms. The signal was presented in only one of the two 33 ms intervals and each interval was indicated by a synchronized 33 ms sound. The detection task consisted in determining if the stimulus was presented simultaneously with the first or second sound by pressing one of two keys. Auditory feedback was given to the observer. Stimuli were sinusoidal gratings at two cycles per degree having one of eight possible orientations (0, 22.5, 45, 67.5, 90, 112.5, 135 and 157.5 degrees, Figure 2.2). The spatial window of the stimulus had a diameter of 1 dva and its temporal window was 33 ms. A black circle with a 4 dva diameter and centered on the target was continuously presented to maximally reduce spatial uncertainty (Figure 2.3).

Figure 2.2: The 8 possible orientations of the signal. From left to right: 0, 22.5, 45, 67.5, 90, 112.5, 135 and 157.5 degrees. Signals are represented here at 100% contrast.

The noise was sampled from a Gaussian distribution and filtered in the Fourier domain to remove all spatial frequencies above 8 cycles per degree. The rms contrast of the noise was fixed at 20% and the noise was resampled at 30 Hz. The spatial window of the noise was either localized (same spatial window as the target) or extended (covered the entire displayed area) and the temporal window was also either localized (same temporal window as the target, i.e. 33 ms) or extended (continuously displayed during and between trials). The four noises plus no noise conditions are shown in Figure 2.3.

For each noise condition, 8 staircases were performed in which the observer knew the orientation of the target and 8 in which he did not know the orientation of the target. The subject alternated between unknown and known orientation conditions until the 16 staircases for the given noise condition were performed. In the unknown orientation condition, the orientation of the signal was pseudo-randomized at each trial. In the known orientation condition, the orientation was fixed for each staircase (pseudo-randomly selected so that one staircase was performed for each of the 8 orientations), and was known

to the observer. There were a total of 80 conditions: (8 × unknown orientation condition + 8 × known orientation condition) × 5 noise conditions. The subjects carried out 5 testing sessions (i.e. one noise condition per session), which lasted about 30 min each and where spread out over 5 days of testing (not necessarily consecutive).

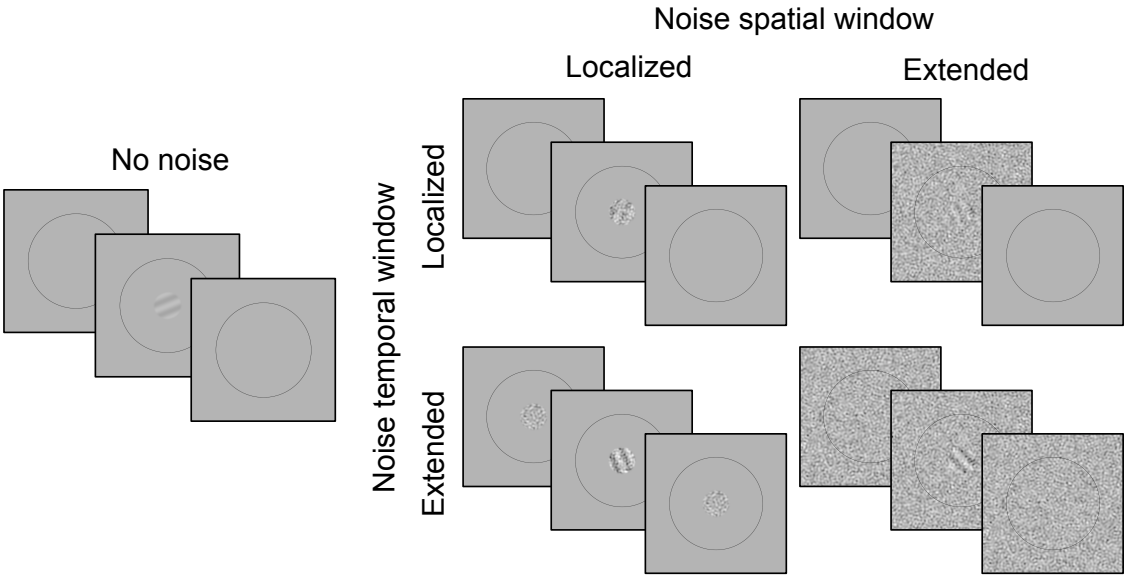

Figure 2.3: The five noise conditions. On the left, the no noise condition. On the right the four different noise conditions. The noise was either spatially localized (noise and signal have the same spatial window, left column) or spatially extended (covered the entire displayed area, right column) and either temporally localized (one 33 ms noise frame, top row) or temporally extended (continuously displayed during and between trials, bottom row).

Contrast detection threshold was measured using a 3down1up staircase procedure (Levitt, 1971) with a step size of 1.25 factor and was interrupted after 12 inversions. Threshold for each staircase was estimated as the geometric mean of the last 10 inversions. For each noise condition, the contrast threshold in the unknown orientation condition was estimated as the geometric mean of the 8 threshold estimations (i.e. 8 staircases with pseudo-randomized orientation) and the contrast threshold in the known orientation condition was the geometric mean of the 8 threshold estimates for the 8 known orientations.

2.3 Results

Contrast thresholds for the known orientation and the unknown orientation conditions are shown in Figure 2.4. Contrast thresholds were substantially higher in noise conditions than in absence of noise (see in Figure 2.4 the different range of the Y-axis). This considerable effect of the noise on the contrast threshold, confirms that the impact of the internal noise was negligible in the four high-noise conditions (Pelli and Farell, 1999).

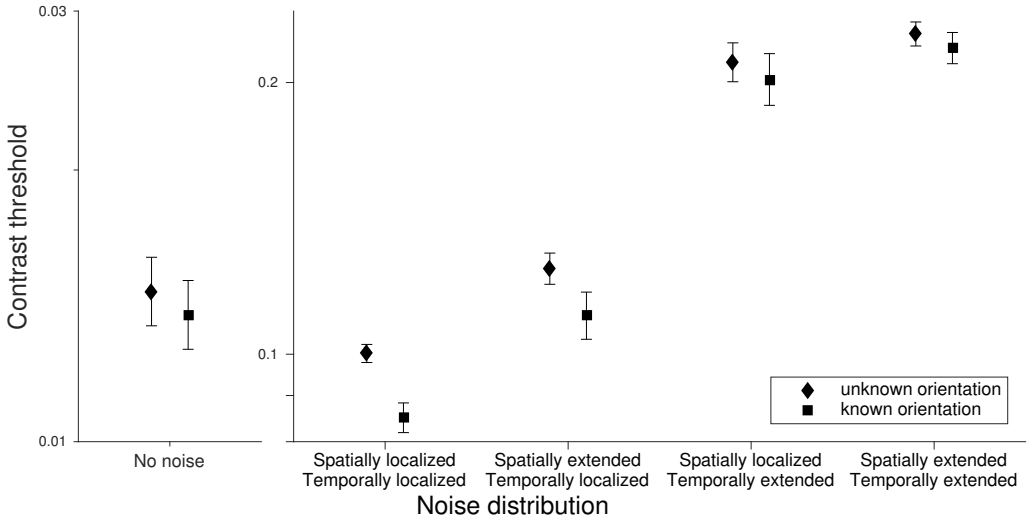

Figure 2.4: Contrast thresholds for the known and unknown orientation conditions. Mean contrast thresholds for the unknown orientation condition (diamonds) and the known orientation condition (squares) for the no noise condition and the four different noise distributions. The error bars represent the standard error of the mean. The two Y-axes cover different ranges, but have the same logarithmic scale.

The orientation uncertainty effect was defined as the contrast threshold ratio between the unknown orientation and known orientation conditions (Figure 2.5). An orientation uncertainty effect greater than 1 represents an advantage of knowing the orientation of the target, whereas an orientation uncertainty effect of 1 (similar contrast thresholds in the two conditions) represents no advantage of knowing the orientation.

One of the aims of the current study was to determine if the processing in spatiotemporally localized and extended noise (second and fifth columns in Figure 2.5, respectively) was the same as the processing in the absence of noise (left column in Figure 2.5). Paired *t* tests showed that the orientation uncertainty effect was significantly greater in spatiotemporally

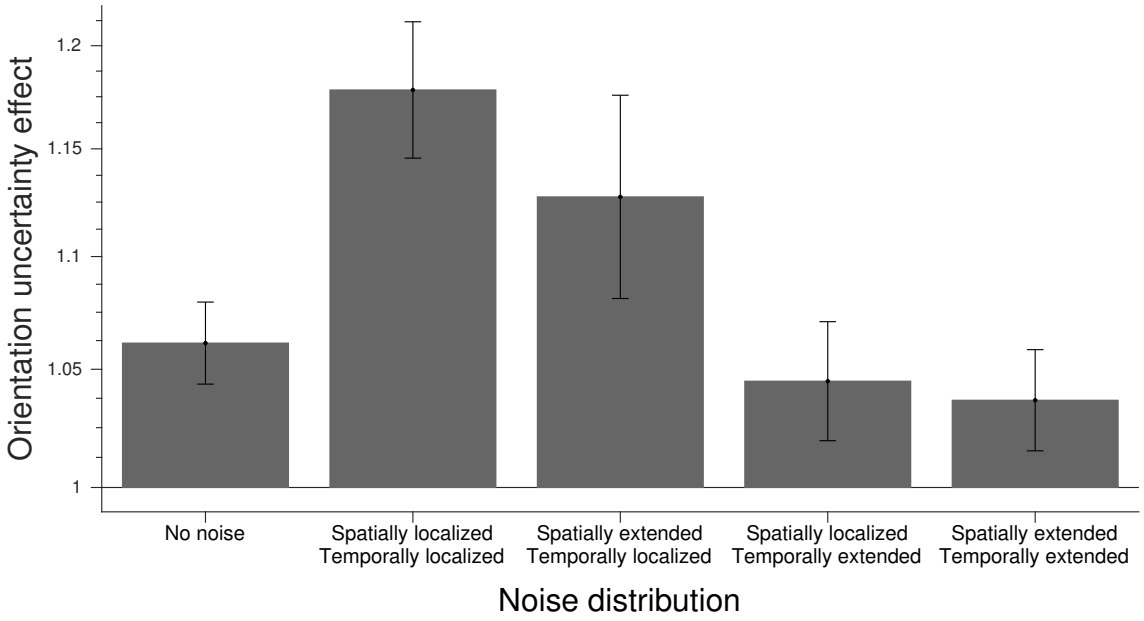

Figure 2.5: Orientation uncertainty effects for the different noise conditions. For each noise condition, an orientation uncertainty effect corresponds to the contrast threshold ratios of the unknown-known orientation conditions (calculated from the data shown in Figure 2.4). A ratio greater than 1 indicates that contrast threshold was greater in the unknown orientation than known orientation conditions. The error bars represent the standard error of the mean.

localized noise than in no noise ($t(10)$=3.0; p<.05) and in spatiotemporally extended noise ($t(10)$=3.7; p<.01). The no noise and the spatiotemporally extended noise conditions did not significantly differed ($t(10)$=1.1; p=.3). Knowing the orientation of the stimulus was therefore more useful in the presence of spatiotemporally localized noise than in the other two conditions, demonstrating additional contribution of target knowledge in spatiotemporally localized noise.

The difference in orientation uncertainty effects between the spatiotemporally localized noise and the spatiotemporally extended noise could be due to the temporal or spatial window of the noise. The orientation uncertainty effect at intermediate noise conditions (i.e. spatially extended and temporally localized noise, and spatially localized and temporally extended noise, third and fourth columns in Figure 2.5, respectively) can be used to test which dimension of the noise was responsible for the greater orientation uncertainty effect in spatiotemporally localized noise. A two-way ANOVA (2 spatial windows × 2

temporal windows) showed a simple main effect of the temporal window ($F(1,10)=19.37$; $p<.01$), but not of the spatial window ($F(1,10)=1.49$; $p=.25$). This suggests that the higher orientation uncertainty effect in the spatiotemporally localized noise was due to the fact that the noise was temporally localized, not that it was spatially localized.

Because the ANOVA showed that the spatial window of the noise had no significant impact on the orientation uncertainty effect, the effect of the temporal window can be examined with additional statistical power by grouping the orientation uncertainty effects that varied only according to the spatial window of the noise (i.e., geometric mean of the orientation uncertainty effects in spatially localized and extended noise for each temporally localized and extended noise) as shown in Figure 2.6. Paired t tests showed that the orientation uncertainty effect in the temporally localized noise was significantly higher than in the no noise condition ($t(10)=2.5$; $p<.05$) and highly significantly higher than in the temporally extended noise condition ($t(10)=4.4$; $p<.01$). Furthermore, the orientation uncertainty effects in the no noise condition and in the temporally extended noise condition did not significantly differed ($t(10)=0.91$; $p=.38$). The greater orientation uncertainty effect in temporally localized noise shows that knowledge about the shape of the target was more relevant to the processing in temporally localized noise than in temporally extended noise or in absence of noise, which reveals additional contribution of target knowledge in temporally localized noise.

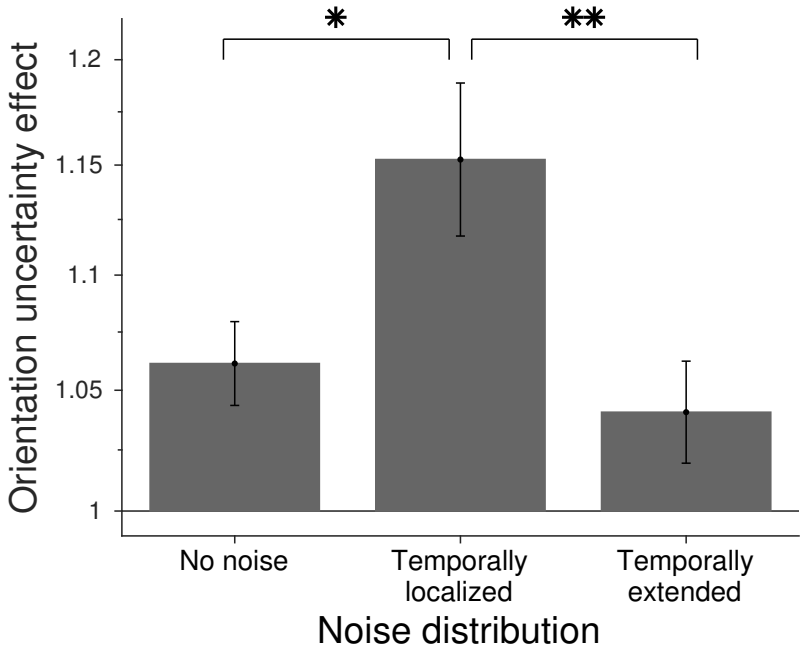

Figure 2.6: Orientation uncertainty effects for the noise conditions regrouped according to their temporal window. Ratio of the unknown-known orientation conditions of the subject's mean for the no noise condition, the temporally localized condition (geometric mean of the spatiotemporally localized noise and the spatially extended and temporally localized noise in Figure 2.5) and the temporally extended condition (geometric mean of the spatiotemporally extended noise and the spatially localized and temporally extended noise in Figure 2.5). The error bars represent the standard error of the mean.

2.4 Discussion

The results of the current study showed that knowing the orientation of the target was more advantageous in temporally localized noise than in the absence of noise or in temporally extended noise. These results revealed additional contribution of target knowledge for detection in temporally localized noise.

External noise paradigms are often used to characterize sensitivity by comparing the effect of a variable on contrast thresholds in low and high noise, that is, threshold limited by internal and external noise, respectively. Given that the contribution of target knowledge depended on the temporal window of the noise, implementing the external noise paradigm

using temporally localized or temporally extended noise would lead to different outcomes and interpretations. For instance, consider the two main variants of the external noise paradigm: the Linear Amplifier Model (LAM, Pelli 1981; Pelli and Farell 1999) and the Perceptual Template Model (PTM, Lu and Dosher 1999, 2008). The LAM has a factor affecting threshold in both low and high noise (namely, calculation efficiency) and another factor affecting threshold only in low noise (namely, equivalent input noise). Based on the greater uncertainty effect in temporally localized noise than in absence of noise, the LAM would suggest that knowing the orientation improved calculation efficiency (equivalent to orientation uncertainty effect in temporally localized noise of Figure 2.6) and surprisingly increased equivalent input noise (lower equivalent input noise when orientation is unknown, first column in Figure 2.7). On the other hand, based on the similar and small uncertainty effects in the absence of noise and in temporally extended noise, the LAM would suggest instead that knowing the orientation did not affect equivalent input noise (right column in Figure 2.7) and slightly improved calculation efficiency (right column in Figure 2.6). Thus, applying the LAM to data collected with different temporal noise windows leads to dramatically different interpretations.

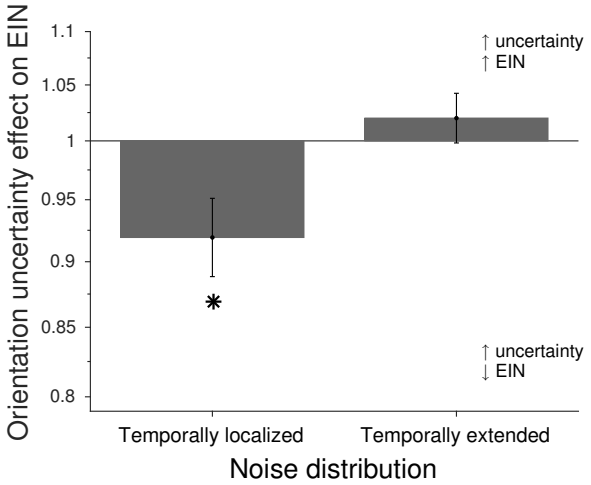

Figure 2.7: Orientation uncertainty effect on Equivalent Input Noise (EIN). EIN ratio of the unknown-known orientation conditions of the subject's mean for the temporally localized condition and the temporally extended condition. A ratio above 1 represents more EIN in the unknown orientation condition, whereas a ratio below 1 represents less EIN in the unknown orientation condition. The error bars represent the standard error of the mean.

Contrary to the LAM, the PTM has a parameter affecting threshold only in high noise: an early perceptual template filtering out irrelevant information operating before the main internal noise (namely, external noise exclusion). Thus, the PTM could explain the greater uncertainty effect in temporally localized noise than in absence of noise due to a better filter tuning along the known orientation, excluding external noise at irrelevant orientations. However, the much smaller uncertainty effect observed in temporally extended noise (Figure 2.6) would rather suggest that knowing the orientation did not considerably filter out external noise at irrelevant orientations. As a result, applying the PTM also leads to drastically different interpretations depending on the temporal window of the noise. More generally, given that the contribution of target knowledge depends on the temporal window of the noise, applying any variant of the external noise paradigm (e.g., LAM, PTM) would result in different interpretations depending on whether the noise is temporally localized or extended.

The rationale of external noise paradigm is to better characterize processing by evaluating performance limited by internal and external noise (i.e., in absence of noise and in high noise, respectively). If different processing properties are observed in temporally localized and extended noises, then the external noise paradigm should be implemented with temporally extended noise to match the properties of internal noise. Indeed, internal noise does not turn on and off with the signal presentation and is therefore temporally extended, so the interpretation from any variant of the external noise paradigm based on temporally localized noise would be invalid. For instance, the LAM assumes that the processing properties that affect contrast threshold in high noise (i.e., calculation efficiency) equally affect contrast threshold in absence of noise. Thus, because internal noise is temporally extended, the greater contribution of target knowledge observed specifically in temporally localized noise could not be interpreted as occurring in absence of noise. In other words, applying the LAM using temporally localized noise would overestimate the contribution of target knowledge on the calculation efficiency effective in absence of noise.

Within the PTM framework, an effect only in high noise suggests a variation in early template tuning occurring *before* the internal noise. Indeed, filtering out noise *after* the limiting internal noise should equally affect contrast threshold in low and high noise,

whereas filtering out noise *before* the limiting internal noise should affect contrast threshold only in high noise. However, given that the greater contribution of target knowledge was specific to temporally localized noise and internal noise is temporally extended, then a process specific to temporally localized noise occurring *after* the internal noise would equally account for the data: affect performance only in temporally localized noise, not in temporally extended noise or in absence of noise. Thus, applying the PTM using temporally localized noise would unjustifiably suggest that target knowledge affects *early* template tuning. In sum, if an effect depends on some property of the noise that differ between internal and external noise, then it compromises the interpretation of any external noise paradigms implicitly assuming that the processing properties are noise-invariant. Therefore, to avoid triggering a potential shift in processing properties and thereby compromise the application of the external noise paradigm, external noise should be temporally extended to match the properties of internal noise.

Why was there a larger contribution of target knowledge in temporally localized noise compared to temporally extended noise and absence of noise? The rationale of the current study was based on a previous study (Allard and Cavanagh, 2011) suggesting that adding localized noise causes a shift from a detection to a recognition strategy. This study found that crowding affected the contrast detection threshold in localized noise, but not in the absence of noise or in extended noise. Given that crowding affects recognition, but not detection (Levi, 2008; Pelli et al., 2004), these results suggest that a recognition strategy operates in localized noise and that a detection strategy operates in the absence of noise and in extended noise. Given that a recognition strategy relies more on target knowledge than does a detection strategy, such a shift in processing strategy can explain the greater contribution of target knowledge in temporally localized noise that is observed in the current study.

This interpretation is consistent with other studies that found a processing strategy shift in localized noise (Allard and Faubert, 2014a,b; Allard et al., 2013b). For instance, Allard and Faubert (2014a) found that the most sensitive detectors for a moving stimulus were direction-selective (e.g. direction-selective complex cells) in the absence of noise and in temporally extended noise, but not in temporally localized noise as the most sensitive

detectors in that case were labeled for orientation, but not direction (e.g. simple cells). The stimulus in the current study was not moving but was briefly presented (33 ms), which makes it probable that the most sensitive detectors were transient-based in the absence of noise and in temporally extended noise. Thus, the involvement of different channels depending on the temporal window of the noise could be part of the reason why the effect of target knowledge depended on the nature of the external noise in the current study.

There is, nevertheless, an alternative explanation that we must consider. A notable property of temporally localized noise is that it reduces temporal uncertainty and the possibility of an interaction between temporal and orientation uncertainty could explain different orientation uncertainty effects in temporally localized and extended noise. In particular, adding uncertainty along one dimension may have a negligible effect when there is a high uncertainty along another dimension. In this case, reducing orientation uncertainty may have no effect when temporal uncertainty is high (absence of noise and in temporally extended noise), but may have an effect when temporal uncertainty is low (temporally localized noise). Consequently, it is theoretically possible that the greater contribution of target knowledge in temporally localized noise could be triggered by a temporal uncertainty reduction.

However, the different processing properties in temporally localized noise compared to temporally extended and absence of noise observed in some previous studies cannot be explained by temporal uncertainty. Indeed, there is no reason for a temporal uncertainty reduction to trigger a crowding effect in a detection task (Allard and Cavanagh, 2011) or cause a shift in processing channel (Allard and Faubert, 2014a). Furthermore, there was little temporal uncertainty to reduce in these studies. Indeed, the temporal window of the signal was longer than in the current study (i.e. $\geq$200 ms compared to 33 ms) and in the crowding study (Allard and Cavanagh, 2011) flankers were presented near the target with the same temporal window as the target. Given that a shift in processing strategy has been observed for a detection task in temporally localized noise and that in the current study temporal uncertainty was minimized with an auditory cue, we consider more likely that the greater contribution of target knowledge in temporally localized noise was due to a shift in processing strategy, rather than an interaction between orientation and temporal

uncertainty.

Most importantly, whether the greater contribution of target knowledge was due to a shift in processing strategy or a reduction in temporal uncertainty does not alter the main implication of the current study. Specifically, the data show that processing properties are noise-dependent and this compromises the interpretation of the external noise paradigms that use temporally localized noise.

Previous studies have suggested that processing strategy shifts in localized noise may be caused by the match between the energy variation of the noise and that of the signal (Allard and Cavanagh, 2011; Allard and Faubert, 2014a,b; Allard et al., 2013b). For the briefly presented signals used in the current study, signal detection in absence of noise and in temporally extended noise is likely to be transient-based. If the same transient-based strategy operated also in temporally localized noise, then similar effects of orientation uncertainty would be expected in all noise conditions. The substantial temporal energy variation caused by temporally localized noise (Figure 2.8, second row) could have impaired the ability to detect the simultaneous signal transients. Noise turning on and off with the target would impair the ability to detect transients caused by the signal, which would increase the relative effectiveness of other strategies (e.g. recognition, or a different processing channel that is not transient-based). On the other hand, the energy fluctuation of temporally extended noise is not synchronous with the signal energy (Figure 2.8, third row) leaving the detection of transients the optimal strategy.

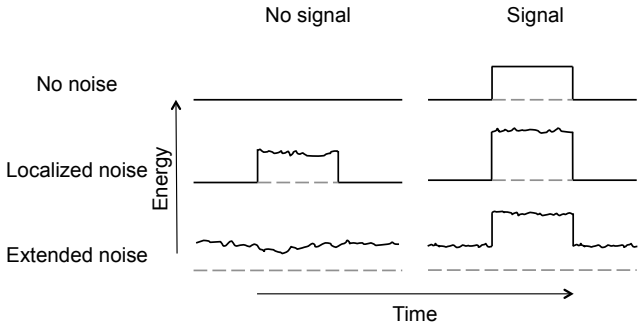

Figure 2.8: Energy levels in the different noise conditions. Energy level when the signal is present (right column) or absent (left column) as a function of a given dimension (e.g. time) for three conditions: no noise (first line), localized noise (second line) and extended noise (third line).

2.5 Conclusion

In conclusion, the contribution of target knowledge was greater in temporally localized noise than in temporally extended noise and in absence of noise. This implies different processing properties between temporally localized external noise and internal noise (which is temporally extended), which violates the noise-invariant processing assumption of external noise paradigms. Therefore, to avoid triggering a potential shift in processing properties and thereby compromise the application of the external noise paradigm, temporally extended noise should be used to match the properties of internal noise.

Chapter 3

Internal noise sources limiting contrast sensitivity

This chapter presents the internal noise paradigm developed during my doctoral studies, which allows us to distinguish different internal noise sources limiting contrast sensitivity to further understand the underlying causes of the limitations of the human visual perception.

This work has been previously published under the form of an article:

Daphné Silvestre, Angelo Arleo and Rémy Allard (2018). Internal noise sources limiting contrast sensitivity. *Scientific Reports*, 8(1):1-11.

Abstract

Contrast sensitivity varies substantially as a function of spatial frequency and luminance intensity. The variation as a function of luminance intensity is well known and characterized by three laws that can be attributed to the impact of three internal noise sources: early spontaneous neural activity limiting contrast sensitivity at low luminance intensities (i.e. early noise responsible for the linear law), probabilistic photon absorption at intermediate luminance intensities (i.e. photon noise responsible for de Vries-Rose law) and late spontaneous neural activity at high luminance intensities (i.e. late noise responsible for Weber's law). The aim of this study was to characterize how the impact of these three internal noise sources vary with spatial frequency and determine which one is limiting contrast sensitivity as a function of luminance intensity and spatial frequency. To estimate the impact of the different internal noise sources, the current study used an external noise paradigm to factorize contrast sensitivity into equivalent input noise and calculation efficiency over a wide range of luminance intensities and spatial frequencies. The impact of early and late noise was found to drop linearly with spatial frequency, whereas the impact of photon noise rose with spatial frequency due to ocular factors.

3.1 Introduction

Contrast sensitivity varies substantially as a function of spatial frequency (SF) and luminance intensity (Barlow, 1956; de Vries, 1943; Fechner, 1860; Rose, 1942; Van Nes and Bouman, 1967) and is limited by many internal factors including optical factors such as diffraction and aberrations of the optical system, stochastic absorption of photons by photoreceptors and neural factors such as stochastic neural activity. The current psychophysical study used an external noise paradigm to quantify the impact of various internal factors on contrast sensitivity as a function of SF and luminance intensity.

At low luminance intensities, increment threshold in absolute units (ΔL) is independent of the background luminance (L) (linear law in Figure 3.1a), which corresponds to contrast sensitivity ($L/\Delta L$) being proportional to the background luminance (Figure 3.1b). This linear law can be explained by spontaneous neural activity occurring early in the visual system (Bulmer et al., 1957; Kelly, 1972) often referred to as the dark light of the eye (Barlow, 1957) (early noise in Figure 3.2). At medium luminance intensities, increment threshold is proportional to the square root of the background luminance (de Vries-Rose law in Figure 3.1a), which corresponds to contrast sensitivity being proportional to the square root of the background luminance (Figure 3.1b). de Vries-Rose law can be explained by the stochastic fluctuations in the number of photon absorbed by the retina due to probabilistic absorption of photons (de Vries, 1943; Rose, 1942) (photon noise in Figure 3.2). Indeed, photon absorption by the retina obeys the Poisson distribution and the number of photon absorbed varies according to Poisson's law with a variance proportional to the luminance intensity and thus a standard deviation proportional to the square root of luminance intensity (Hecht et al., 1942; Mueller, 1951). At high luminance intensities, increment threshold is proportional to the background luminance (Weber's law in Figure 3.1a), which corresponds to contrast sensitivity being independent of background luminance (Figure 3.1b). Weber's law can be explained by neural noise (e.g., spontaneous neural activity) located after contrast normalization (Gregory and Cane, 1955; Pelli, 1990; Rose, 1948; Shapley, 1986) (late noise in Figure 3.2).

Thus, the variation of contrast sensitivity as a function of luminance intensity (three laws in Figure 3.1b) can be explained by the fact that the impact of various internal

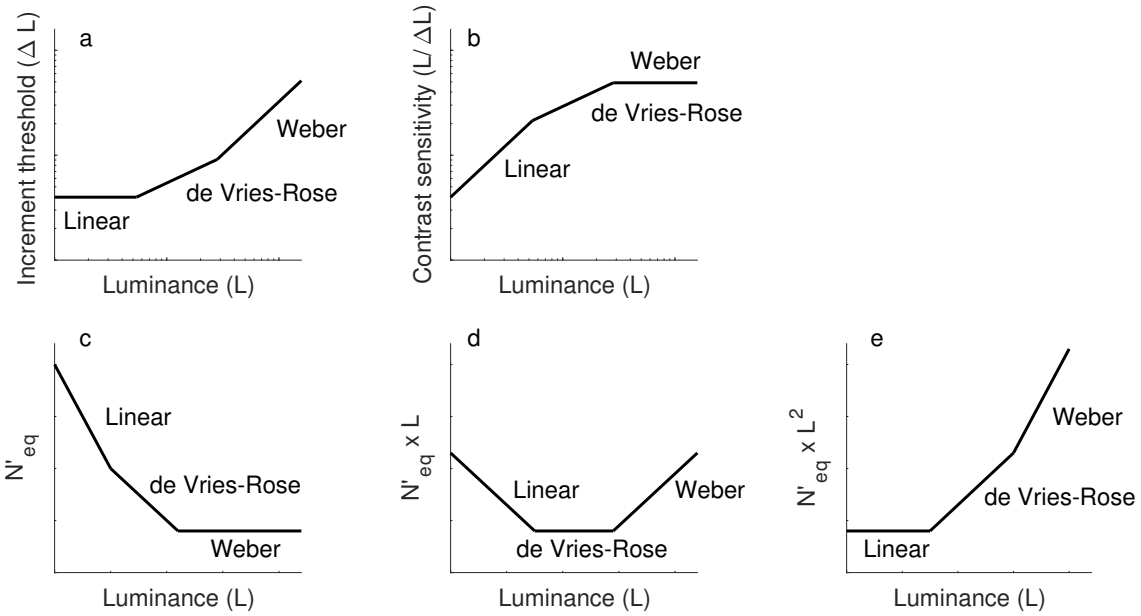

Figure 3.1: The three laws limiting contrast sensitivity and equivalent input noise. (a) The three laws represented with respect to the increment threshold in absolute units (ΔL). (b) The same three laws represented with respect to contrast sensitivity (L/ΔL). The second row represents the three laws limiting equivalent input noise in units where each law is independent of luminance intensity. (c) Weber's law is independent of luminance intensity when equivalent input noise is plotted as a function of luminance intensity. (d) de Vries-Rose law is independent of luminance intensity when equivalent input noise times luminance intensity is plotted as a function of luminance intensity. (e) Linear law is independent of luminance intensity when equivalent input noise times squared luminance intensity is plotted as a function of luminance intensity. These graphs are represented on a log-log scale and (c) to (e) are in energy units.

noise sources varies differently with luminance intensity causing different internal noise sources to dominate at different luminance intensities: early spontaneous neural activity at low luminance intensities (linear law), probabilistic photon absorption at intermediate luminance intensities (de Vries-Rose law) and late spontaneous neural activity at high luminance intensities (Weber's law). However, the impact of these internal noise sources also varies differently as a function of SF causing different internal noise sources to dominate and limit contrast sensitivity at different SFs. For instance, contrast sensitivity saturates (i.e., reach Weber's law) at much lower luminance intensities for low SFs than

for high SFs (Van Nes and Bouman, 1967). The impact of the internal noise can be psychophysically quantified relative to the impact of external noise (i.e., external noise paradigm Pelli and Farell 1999). Varying the contrast of external noise has a negligible impact on contrast threshold if the dominating noise source is internal and considerably affects contrast threshold when it is the dominating noise source. The impact of the internal noise can therefore be quantified relative to the amount of external noise having the same impact as the internal noise, namely, the equivalent input noise. To estimate the impact of the different internal noise sources, the current study used an external noise paradigm to factorize contrast sensitivity into equivalent input noise and calculation efficiency (LAM, Pelli 1981, 1990; Pelli and Farell 1999). Given that calculation efficiency is independent of luminance intensity (Nagaraja, 1964; Pelli, 1981), equivalent input noise (quantified in energy units) is inversely proportional to the squared contrast sensitivity and can therefore be, like contrast sensitivity, related to the three laws (linear, de Vries-Rose and Weber's laws, Figure 3.1c).

The aim of the current study was to characterize how the impact of the three internal noise sources (which varies with luminance intensity according to the three laws) varies with SF, and thereby identify the dominating one as a function of luminance intensity and SF (i.e. spatial-luminance domain). Equivalent input noise was therefore estimated as a function of a wide range of luminance intensities and SFs.

3.2 Model

The observer model used in the current study is illustrated in Figure 3.2 and is divided in three processing stages: optical factors represented by the modulation transfer function (MTF, Charman 1991; Van Nes and Bouman 1967), transduction process of photoreceptors modeled as photon noise added to the retinal image (Pelli, 1990) and the neural processing stage modeled as a combination of early noise occurring before contrast normalization, late noise occurring after the contrast normalization and calculation efficiency, which depends on the signal-to-noise ratio of the effective stimulus after the combination of all the noise sources (Pelli, 1990).

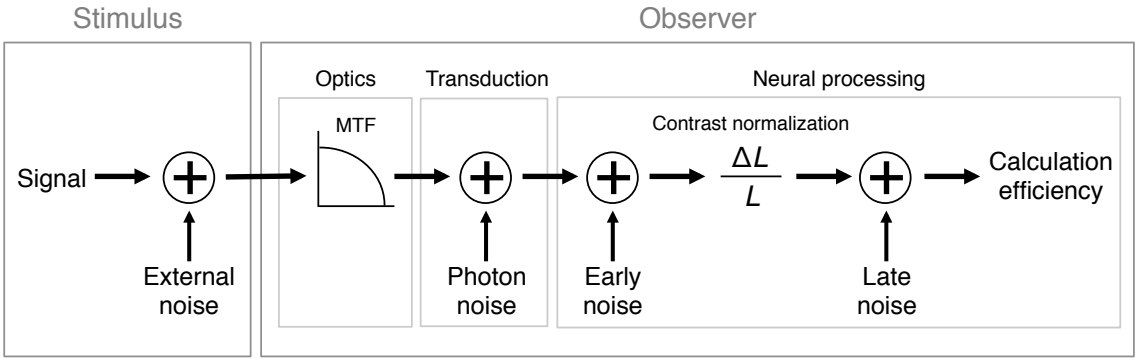

Figure 3.2: Observer model including the MTF, three additive internal noise sources and calculation efficiency. The additive internal noise sources comprise photon noise (i.e. phototransduction), early neural noise arising after optical aberrations modeled by the MTF and late neural noise arising after contrast normalization.

The current study measured the equivalent input noise, which corresponds to the external noise level having the same impact as the total amount of internal noise in the system, that is, the sum of the three internal noise sources in our model. Given that the equivalent input noise is quantified in energy units (i.e., proportional to its variance), the impact of the combination of the three internal noise sources (i.e., equivalent input noise) is equal to the summation of the impact of the different internal sources. Being mainly interested in the neural factors (i.e. the three internal noise sources), let us consider the equivalent input noise at the entry of the retina (N'_{eq}). Equation (3.2.1) represents the equivalent input noise in energy units at the entry of the retina quantifying the impact of the summation of the three sources of noise following the linear law, de Vries-Rose law and Weber's law. L and f represent the luminance intensity and SF, respectively. The impact of photon noise (N_{photon}) on equivalent input noise is inversely proportional to luminance intensity (i.e., de Vries-Rose law in Figure 3.1c). Note that we mathematically defined N_{photon} as independent of luminance intensity and its impact on equivalent input noise (N'_{eq}) is constrained to be inversely proportional to luminance intensity (N_{photon}/L), which is mathematically equivalent to Pelli (1990)'s definition that photon noise is defined as inversely proportional to luminance. This noise being at the photoreceptor level is not spatially correlated and is therefore assumed to be spatially white (Pelli, 1990; Raghavan, 1995), and therefore constrained in our model to be independent of SF. The impact of

early neural spontaneous activity (N_{early}) on equivalent input noise (modeled as early noise in Figure 3.2) is inversely proportional to squared luminance intensity (i.e. linear law, Figure 3.1c). The impact of late neural spontaneous activity (N_{late}) on equivalent input noise (i.e. late noise, Figure 3.2) is independent of luminance intensity (i.e. Weber's law, Figure 3.1c). As a result, the equivalent input noise at the entry of the retina can be defined as a combination of this three internal noise sources:

$$N'_{eq}(L, f) = \frac{N_{photon}}{L} + \frac{N_{early}(f)}{L^2} + N_{late}(f) \tag{3.2.1}$$

However, the current study estimated the equivalent input noise at the entry of the eye (i.e. using a visual stimulus presented on a screen), not at the retina, so it was affected by the optical factors of the eye. The impact of most of the optical factors on contrast sensitivity can be characterized by the Modulation Transfer Function (MTF,Charman 1991; Van Nes and Bouman 1967), which represents the fraction of contrast transferred as a function of SF. Consequently, the contrast at the retina corresponds to the contrast at the input of the eye multiplied by the MTF. Thus, the external noise energy at the entry of the retina is equal to the noise energy at the entry of the eye multiplied by MTF squared. Because the equivalent input noise is quantified relative to the impact of the external noise (in energy units), the equivalent input noise at the entry of the retina (N'_{eq}) is also equal to the equivalent input noise at the entry of the eye (N_{eq}) multiplied by MTF squared:

$$N'_{eq} = MTF^2(f) \times N_{eq}(L, f) \tag{3.2.2}$$

By combining equations (3.2.1) and (3.2.2), the equivalent input noise at the entry of the eye can be defined as a function of the MTF and the three internal noise sources:

$$N_{eq}(L, f) = \frac{1}{MTF^2(f)} \times \left(\frac{N_{photon}}{L} + \frac{N_{early}(f)}{L^2} + N_{late}(f) \right) \tag{3.2.3}$$

As a result, this model of the equivalent input noise as a function of luminance intensity and SF depends on a scalar (N_{photon}) and three functions with respect to SF (MTF(f), N_{early}(f) and N_{late}(f)). Note that no parameter in the model varies with respect to luminance intensity (L). To complete the model these three functions with respect to the SF need to be defined.

3.2.1 MTF

Watson (2013) showed that the MTF can be well modeled with a generalized Lorentzian function:

$$MTF(f) = \left[1 + \left(\frac{f}{u(d)}\right)^2\right]^{-a} \sqrt{D(f, d, 555)} \tag{3.2.4}$$

with *u(d)* representing a second order polynomial depending on d the pupil diameter (here fixed at 3 mm), *D(f,d,555)* representing the diffraction limited MTF depending on SF *(f)*, pupil diameter *(d)* and the wavelength of white light in focus at 555 nm (for details on *u(d)* and *D(f,d,555)* see (Watson, 2013). In his study, Watson (2013) found that an exponent a fixed to 0.62 fitted reasonably well the mean MTF of the 200 eyes tested in his study. In order to model the interindividual differences of the MTF, the current study used this generalized Lorentzian function (equation (3.2.4)) with the exponent a as a free parameter.

3.2.2 Early noise

Early neural noise (N_{early}(f)) represents spontaneous activity occurring before contrast normalization. To characterize how early noise varies with SF, four different functions were tested in the model: no early noise (early noise may not limit contrast sensitivity at any luminance intensities, Rovamo et al. 1994a), a constant (independent of SF), a linear function and a quadratic function, resulting in 0, 1, 2 and 3 degrees of freedom, respectively.

3.2.3 Late noise

Late neural noise (N_{late}(f), i.e. spontaneous activity of neurons processing SF) is known to decrease with SF, which can be explained by the fact that the receptive field size decreases, and the cell density increases, with the cells preferred SF (Raghavan, 1995). Specifically, if the receptive field width of simple cells is inversely proportional to its preferred SF and the cell density is proportional to the preferred SF, the impact of late noise would be expected to drop as a function of SF with a slope of -2 (Raghavan, 1995), which is consistent

with previous observations (Pelli and Farell, 1999; Raghavan, 1995). To characterize how late neural noise varies with SF, three different functions were tested in the model: a linear function with a slope fixed to -2 (i.e. late neural noise inversely proportional to SF squared, Raghavan 1995), a linear function with the slope as a free parameter and a quadratic function, resulting in 1, 2 and 3 degrees of freedom, respectively.

The global model fitting the equivalent input noise in the current study comprised one parameter for the MTF, one for photon noise, and the best functions for the early (0 to 3 parameters) and late neural noise (1 to 3 parameters).

3.3 Methods

3.3.1 Observers

Four observers, aged from 23 to 34 years old (mean age = 27.75 years, SD = 4.57) with normal or corrected-to-normal vision participated in this study. The current study was carried out in accordance with the Code of Ethics of the World Medical Association (Declaration of Helsinki) and informed consent was obtained.

3.3.2 Apparatus

All stimuli were generated by a homemade program and presented on a projector screen. The projector used was a LCD Panasonic PT-EW730Z with a refresh rate of 60 Hz and a resolution of 1280×720 pixels. Stimuli were presented at the center of a grey square of 37×37 cm having a mean luminance of 2300 cd/m^2. Stimuli were viewed monocularly through a 3 mm artificial pupil at a distance of 48.5, 97, 194 and 388 cm from the screen depending on the SF tested. The projector was the only source of light in the room and was set behind the screen for a direct illumination. Luminance intensities of 2300, 230, 23, 2.3, 0.23 and 0.023 cd/m^2 were obtained with neutral density filters with optical density of 0 (no filter), 1, 2, 3, 4 and 5, respectively. The output intensity of each color gun was carefully linearized using a Minolta spectroradiometer CS-1000. The Noisy-bit method

(Allard and Faubert, 2008) implemented independently to each color gun, made the 8-bit display perceptually equivalent to an analog display having a continuous luminance resolution.

3.3.3 Stimuli and procedure

An orientation discrimination task was carried out using a two-alternative forced-choice procedure (vertical or horizontal). Auditory feedback was given to the observer after each response by pressing one of two keys. Stimuli were sinusoidal gratings of one of seven SF (0.25, 0.5, 1, 2, 4, 8 and 16 cpd). The spatial window of the stimulus was a circular aperture with a diameter depending on its SF set to two visible cycles of the grating plus a half-cosine of half cycle. A black annulus centered on the stimulus and three times the size of the aperture (i.e. diameter equal to 6 periods of the grating) was continuously presented to minimize spatial uncertainty. Stimuli were presented for 500 ms.

The noise used was truncated-filtered noise (Jules Étienne et al., 2016). Gaussian noise was spatially low-pass filtered with a cutoff two octaves above the signal frequency; its rms contrast was afterwards scaled to 25% and then truncated at 50%. The noise was resampled at 60 Hz. The resulting noise energies were 1200, 300, 76, 19, 4.7, 1.2 and 0.3 μs.deg^2 for SF of 0.25 to 16 cpd, respectively. To avoid triggering a processing strategy shift, the noise was spatiotemporally extended (i.e. full-screen, continuously displayed, Allard and Cavanagh 2011; Allard and Faubert 2014b; Silvestre et al. 2017).

Contrast detection thresholds were measured using a 3down1up staircase procedure (Levitt, 1971) with a step size of a factor of 1.25 and were interrupted after 12 inversions. Such a staircase converged to a criterion level of 79% correct response corresponding to a d'of 1.16. For each staircase, the threshold was estimated as the geometric mean of the last 10 inversions. Three staircases were performed for each condition. The threshold for each condition was estimated as the geometric mean of the three estimated thresholds.

For each SF and luminance intensity, two contrast thresholds were measured to estimate the equivalent input noise: one in absence of noise *c(0)* and the other in high noise *c(Next)*. To minimize luminance adaptation delays, the testing order was blocked with respect to

the luminance intensity. Within each block of luminance intensity, the order of the SFs was randomized, but to minimized the displacement between testing distance, the three staircases for a given SF were performed one after the other. At low luminance intensities (i.e. 2.3 cd/m^2 to 0.023 cd/m^2), subjects adapted for 20 minutes in the dark (eyes closed) and contrast sensitivity at some high SFs was too low to be measured.

Given that calculation efficiency is independent of luminance intensity (Nagaraja, 1964; Pelli, 1981) (also confirmed by a pilot study) contrast thresholds in noise were measured only at the highest luminance intensity (i.e. 2300 cd/m^2). The energy threshold E (squared of the stimulus'contrast function summed over space and time, Pelli and Farell 1999, i.e. proportional to the squared contrast threshold) is known to be linearly related to the external noise energy N_{ext} (Pelli and Farell, 1999). When the phase of the signal is unknown, this linear function can be represented as (Bennett et al., 1999):

$$E(N_{ext}) = \frac{(d' + \sqrt{0.5})^2}{k}(N_{ext} + N_{eq}) \tag{3.3.5}$$

where k is the calculation efficiency. As a result, the energy threshold in absence of noise (N_{ext}=0) is:

$$E(0) = \frac{(d' + \sqrt{0.5})^2}{k}N_{eq} \tag{3.3.6}$$

Calculation efficiency (k) in energy units was calculated by combining equation (3.3.5) and (3.3.6):

$$k = \frac{(d' + \sqrt{0.5})^2 N_{ext}}{E(N_{ext}) - E(0)} \tag{3.3.7}$$

Given that calculation efficiency is independent of luminance intensity, the threshold in high noise (E(Next)) and the calculation efficiency was estimated only at the highest luminance intensity (2300 cd/m^2) for each SF. Based on equation (3.3.6), equivalent input noise was estimated for each condition based on the energy threshold in absence of noise (*E(0)*) and the calculation efficiency (k) estimated at 2300 cd/m^2 for the given SF:

$$N_{eq} = \frac{k}{(d' + \sqrt{0.5})^2}E(0) \tag{3.3.8}$$

3.3.4 Analysis

In the present study, the model characterizing the equivalent input noise at the entry of the eye had four components: the MTF, the photon noise, the early noise and the late neural

noise (see Model section for details). The different parameters relating to each of these components were independently defined for each subject. The MTF and photon noise were each estimated with only one parameter. For early and late neural noise, different functions were tested. The statistical analysis to determined the best fitting model for early and late neural noise was performed at the group level in order to define the general trend of the shape of these functions. In other words, the best fitting model was constrained to be the same for all subjects (i.e. same number of free parameters), but the value of each free parameter was independent across subjects.

The estimation of early and late noise being relatively independent one of the other (i.e. each dominating in a different luminance range), finding the best fitting function for each noise can be analyzed separately. The best fitting function was first analyzed for the early noise. For this analysis, the late noise was fitted with seven independent variables (one parameter for each SF). Given that the early noise was modeled with zero to three free parameters per subject (i.e. no early noise, a constant, a linear function and a quadratic function respectively), the different tested models comprised nine to twelve free parameters per subject (i.e. one for the MTF, one for the photon noise, seven for the late noise and zero to three for early noise). Model comparisons using F-tests enabled to determine the number of free parameters that were statistically justified for the early noise.

Afterwards, to analyze the best fitting model for the late noise, the early noise was modeled with the best fitting model found previously (linear function, i.e. 2 free parameters, see result section). Given that the late noise was modeled with one to three free parameters per subject (i.e. a linear function with a slope fixed to -2, as suggested by Raghavan (1995), a linear function and a quadratic function, respectively, see Model section), the different tested models comprised five to seven free parameters per subject (i.e. one for the MTF, one for the photon noise, two for the early noise and one to three for late noise). Model comparison with F-tests enabled to determine the number of free parameters that were statistically justified for the late noise.

To determine the number of free parameters statistically justified to fit the calculation efficiency as a function of the SF, F-tests were also performed. The different models tested were a constant (independent of SF), a linear function, a quadratic function and a

cubic function.

All analyses were performed in log units. This fitted calculation efficiency using the best fitting model was used for the estimation of the equivalent input noise (equation (3.3.8)).

3.4 Results

Contrast sensitivity

Contrast sensitivity functions at different luminance intensities are shown in the first row of Figure 3.3. As typically observed (Rovamo et al., 1994a; van Meeteren and Vos, 1972; Van Nes and Bouman, 1967), contrast sensitivity functions were band-pass at high luminance intensities and low-pass at low intensities. Contrast sensitivity gradually improved with luminance intensity until it reached saturation (Weber's law). To illustrate the effect of luminance intensity on contrast sensitivity, the data are re-plotted as a function of luminance intensity in Figure 3.4 separately for each SF. At low SFs (i.e. from 0.25 to 4 cpd), contrast sensitivity generally followed the linear law at low luminance intensities and Weber's law at high luminance intensities. At high SFs (i.e. from 8 to 16 cpd), contrast sensitivity generally followed de Vries-Rose law at low luminance intensities and Weber's law at high luminance intensities.

Calculation efficiency

Calculation efficiencies estimated at the highest luminance intensity based on energy thresholds in presence and absence of noise (equation (3.3.7)) are represented in the second row of Figure 3.3. Model comparisons were performed to investigate the shape of the calculation efficiency function (Table 3.1). Analyses favored a linear function over a constant function ($F_{(4,20)}$=4.95; p<0.01) and a quadratic function over a linear function ($F_{(4,16)}$=3.44; p<0.05). This shows that the calculation efficiency was not independent of the SF.

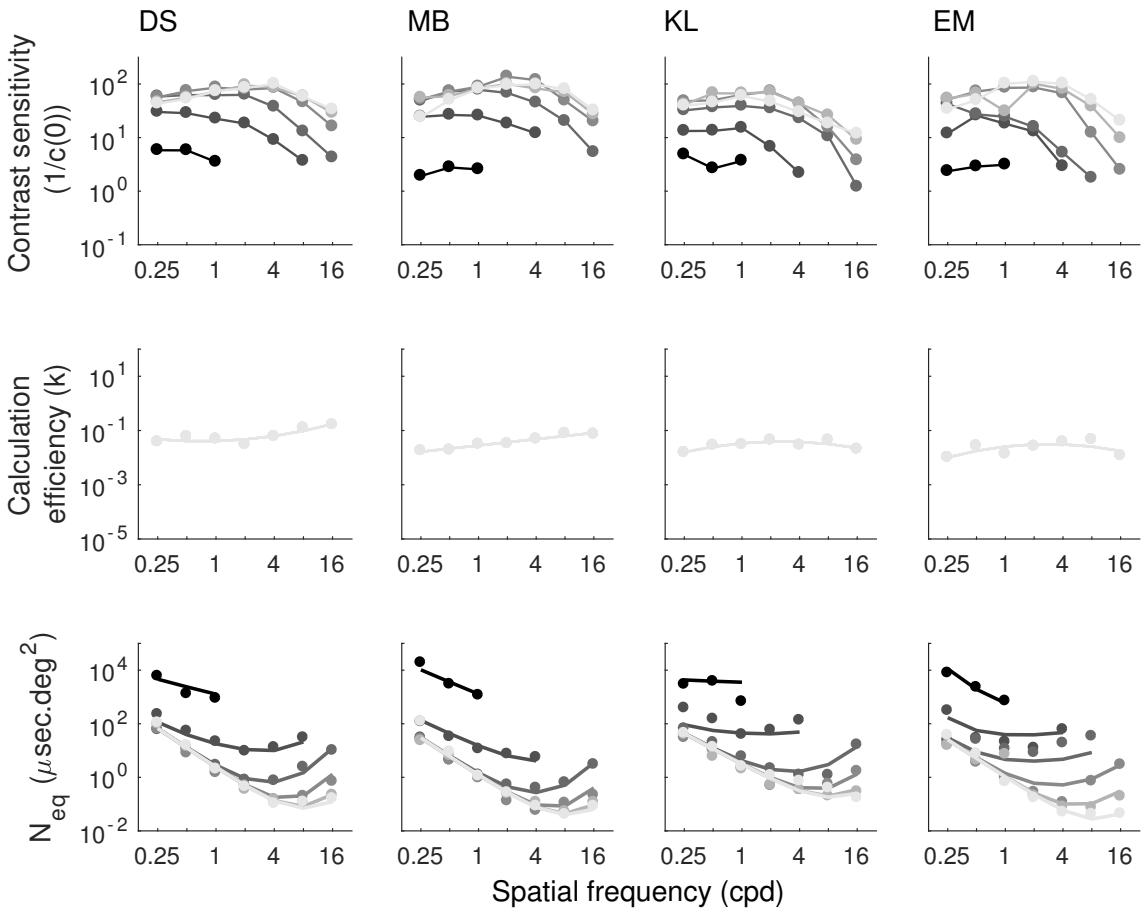

Figure 3.3: Contrast sensitivity function, calculation efficiency (k) and equivalent input noise (N_{eq}). The first row represents contrast sensitivity of the four subjects (DS, MB, KL and EM) as a function of SF for different luminance intensities. The data points were connected with lines for clarity. The second row represents calculation efficiency estimated at 16261 Td for each subject (dots) and fitted with quadratic functions (lines). The third row represents equivalent input noise estimated for the whole range of luminance intensities (i.e. from 0.16 to 16261 Td) represented by dots and fitted with the best model (see Model section) represented by lines. Data are represented on a log-log scale and calculation efficiency and equivalent input noise are in energy units. Luminance intensities range in log steps from 0.16 to 16261 Td. The color gradation from the darkest to the lightest color represents the lowest to the highest luminance intensity, respectively.

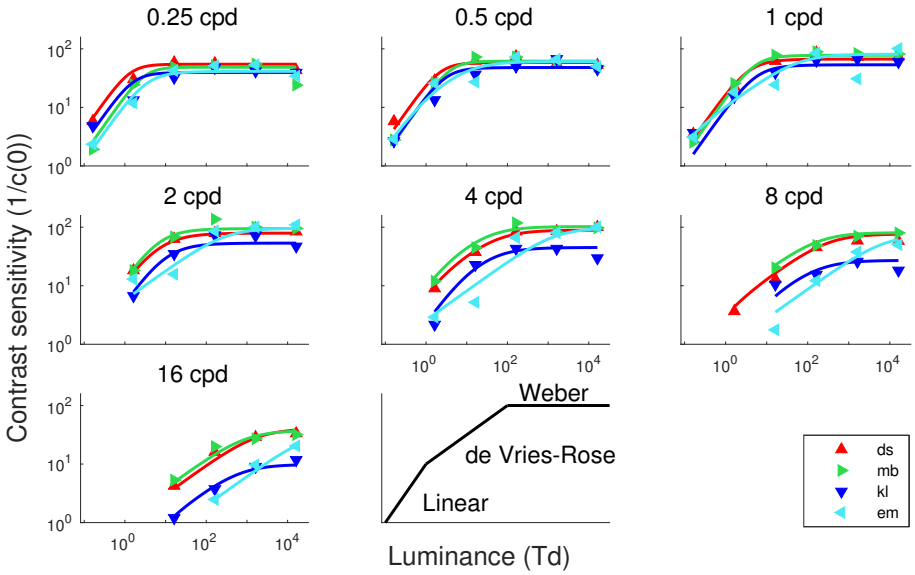

Figure 3.4: Contrast sensitivity as a function of luminance. Each graph represents the contrast sensitivity as a function of luminance of the four subjects for one SF on a log-log scale. Triangles (red, green, blue and cyan) represent the data for each subject and the lines represent the fit of the data with the best model (see Model section). The last graph (bottom right) represents reference lines for the linear law (slope of 1), deVries-Rose's law (slope of 0.5) and Weber's law (null slope). This representation of the three laws allows us to make an analogy with the data above.

Calculation efficiency (k)					
Functions				Model comparison	
Function	**df**	**SSr**	**r²**	***F* value**	***p* value**
Constant	4	1.38	-0.87		
Linear	8	0.69	0.06	$F_{(4,20)}= 4.95$	$p < 0.01$
Quadratic	12	0.37	0.49	$F_{(4,16)}= 3.44$	$p < 0.05$
Cubic	16	0.30	0.6	$F_{(4,12)}= 0.75$	$p = 0.58$

Table 3.1: *F*-tests for the different calculation efficiency functions. Functions depending on SF tested to fit calculation efficiency are a constant, a linear function, a quadratic function and a cubic function. df is the degree of freedom of the function times the number of subjects (statistics at the group level). SSr is the sum of squared residuals and r^2 is the coefficient of determination.

Equivalent input noise

Given the fitted calculation efficiency, equivalent input noise was estimated at various SFs and luminance intensities (bottom row of Figure 3.3) using equation (3.3.8), that is, based on the measured energy thresholds in absence of noise and the fitted calculation efficiency, which was assumed to be independent of the luminance intensity. Statistical analyses regarding the shape of the early noise function rejected the absence of early noise and the constant early noise in favor of an early noise varying linearly with SF (Table 3.2). This shows that there were conditions under which early noise was the dominant noise source and this noise varied with SF. Statistical analyses regarding the shape of the late noise function rejected the linear model with a slope fixed to -2 in favor of a linear model with the slope as a free parameter (Table 3.3).

Early noise (N_{early})					
Functions				Model comparison	
Function	**df**	**SSr**	**r²**	***F* value**	***p* value**
No N_{early}	36	21.94	0.90	$F_{(4,104)}$= 32.37	$p < 0.001$
Constant	40	9.77	0.96	$F_{(4,100)}$= 13.61	$p < 0.001$
Linear	44	6.33	0.97	$F_{(4,96)}$= 1.32	$p = 0.27$
Quadratic	48	6.00	0.97		

Table 3.2: *F*-tests for the different early noise functions. Functions depending on SF tested to fit early noise are no early noise in the model, a constant, a linear function and a quadratic function. df is the degree of freedom of the fixed parameters in the model (i.e. 4 subjects × 9 parameters) plus the different functions defining the early noise (i.e. (0 to 3) × 4 subjects). SSr is the sum of squared residuals and r^2 is the coefficient of determination.

In sum, the best model fitting the equivalent input noise as a function of luminance intensity and SF had 6 degrees of freedom: 1 parameter for the MTF, 1 parameter for the photon noise and linear functions for the early and late noise (2 parameters each). The fitting curves of the equivalent input noise in Figure 3.3, Figure 3.5 and Figure 3.6 correspond to the fit of this model.

Late noise (N_{late})					
Functions				Model comparison	
Function	**df**	**SSr**	**r²**	***F* value**	***p* value**
Slope -2	20	8.66	0.96	$F_{(4,120)}$= 5.41	$p < 0.001$
Linear	24	7.33	0.97	$F_{(4,116)}$= 2.31	$p = 0.06$
Quadratic	28	6.79	0.97		

Table 3.3: *F*-tests for the different late noise functions. Functions depending on SF tested to fit late noise are a linear function with a slope of -2, a linear function and a quadratic function. df is the degree of freedom of the fixed parameters in the model (i.e. 4 subjects × 4 parameters) plus the different functions defining the late noise (i.e. (1 to 3) × 4 subjects). SSr is the sum of squared residuals and r^2 is the coefficient of determination.

To visualize the estimated MTF resulting from this global fit, Figure 3.5 plots the equivalent input noise multiplied by the luminance intensity ($N_{eq} \times L$). Based on equation (3.2.3), we get:

$$N_{eq}(L, f) \times L = \frac{1}{MTF^2(f)} \times \left(N_{photon} + \frac{N_{early}(f)}{L} + L \times N_{late}(f) \right) \tag{3.4.9}$$

which shows that the impact of photon noise is independent of luminance intensity in these units (i.e. $N_{eq} \times L$; dash lines in top row of Figure 3.5) and therefore sets a lower bound for the equivalent input noise: the impact of the sum of the noises at any luminance intensity cannot be less than the luminance-independent impact of only photon noise (see Figure 3.1d). For low SFs at which photon noise was not the dominating noise source at any luminance intensities (only linear law and Weber's law in Figure 3.4), this lower bound was not reached at any luminance intensities. At high SFs, the fit rather suggests that photon noise was the dominating noise source over a wide range of luminance intensities (de Vries-Rose law in Figure 3.4). Assuming that photon noise is spatially white (Pelli, 1990; Raghavan, 1995), the rise in equivalent input noise with SF would be due to the MTF of the eye. Indeed, the MTF affects the contrast of the signal differently according to its spatial frequency by adding some blur to the signal but not to the photon noise. The bottom row of Figure 3.5 is the classical representation of the MTF (i.e. contrast gain as a function of SF, equation (3.2.4)). The exponent of the general Lorentzian fitting the

MTF slightly differed between the subjects and was similar to what would be expected from the literature (based on a large sample, a mean exponent of 0.62 was found, Watson 2013).

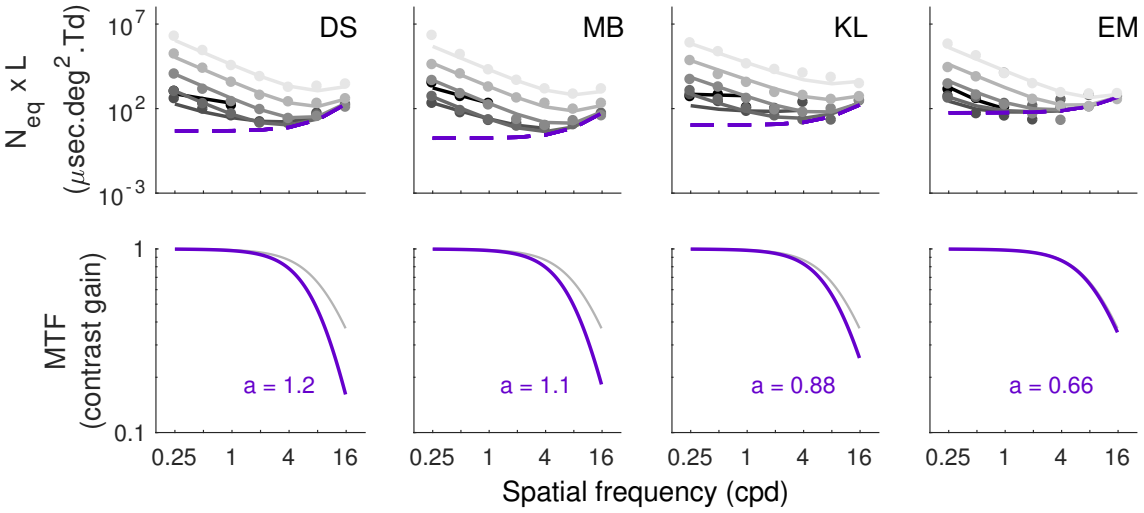

Figure 3.5: MTF estimation. The estimation of the equivalent input noise at the entry of the eye times luminance intensity ($N_{eq} \times L$) is represented in the first row of the graph. The impact of photon noise modulated by the MTF of the eye, which is independent of luminance intensity in these units, is represented by the lower limit (purple dashed line). This line depends on the photon noise and MTF. The second row of the graph represents the MTF of each subject estimated by our model (purple line) and the MTF estimated by Watson's model(Watson 2013) (grey line). The indicated values represent the value of the exponent of the general Lorentzian (equation (4)) found for each subject.

Given the MTF, equivalent input noise at the entry of the retina (N'_{eq}, equation (3.2.2)) can be represented by factorizing out the impact of the MTF from the equivalent input noise at the entry of the eye (N_{eq}). In other words, the impact of the three internal noise sources can be estimated after compensating for the effect of the MTF. To illustrate the impact of each noise source as a function of SF, equivalent input noises were plotted in units so that the impact of photon, early or late noise were independent of luminance intensity ($N'_{eq} \times L$, $N'_{eq} \times L^2$ or N'_{eq}, respectively, Figure 3.1). Thus, in each of their respective units, the impact of a noise source was independent of luminance intensity and corresponded to a lower bound reached when it was the dominating noise source. Figure 3.6 represents the three noise sources to be independent of luminance intensity to highlight their relation

with SF. As in the first row of Figure 3.5, the first row of Figure 3.6 represents photon noise as the limiting input noise, but now corrected for the optical aberrations (MTF). Therefore, photon noise was assumed to be spatially white (blue dashed line) as the rise in its impact was attributed to the MTF (Figure 3.5). We can see that the data matching this lower bound (blue dashed line) are found at medium luminance intensities and high SF, thus for these conditions photon noise was the dominating internal noise source as expected from Figure 3.4.

Early noise being inversely proportional to luminance intensity squared, its relation with SF is represented by the lower limit of the graphs on the second row of Figure 3.6 (red dashed line). We can see that the data matching this lower bound was found at low luminance intensities and low SF as expected from Figure 3.4. Thus, contrast sensitivity was limited by early noise in these conditions. Note that a substantial inter-subject variability was observed regarding the log-log slopes of the linear functions (i.e. -1.0, -1.5, -0.2 and -3.0 for subjects DS, MB, KL and EM, respectively), but the precision of these slopes are likely to be low due to the small number of conditions under which early noise was the dominating noise source (low SFs and low luminance intensities).

Late noise being independent of luminance intensity, its relation with SF is represented by the lower limit of the graphs in the last row of Figure 3.6 (green dashed line). The inter-subject variability regarding the log-log slopes of the linear function modeling the late noise was relatively low (i.e. -2.4, -2.3, -1.9 and -2.3 for subjects DS, MB, KL and EM, respectively, mean of -2.2). We can see that the data matching this lower bound (green dashed line) was found at high luminance intensities and across the whole range of SFs, thus late noise was the dominating noise source in these conditions.

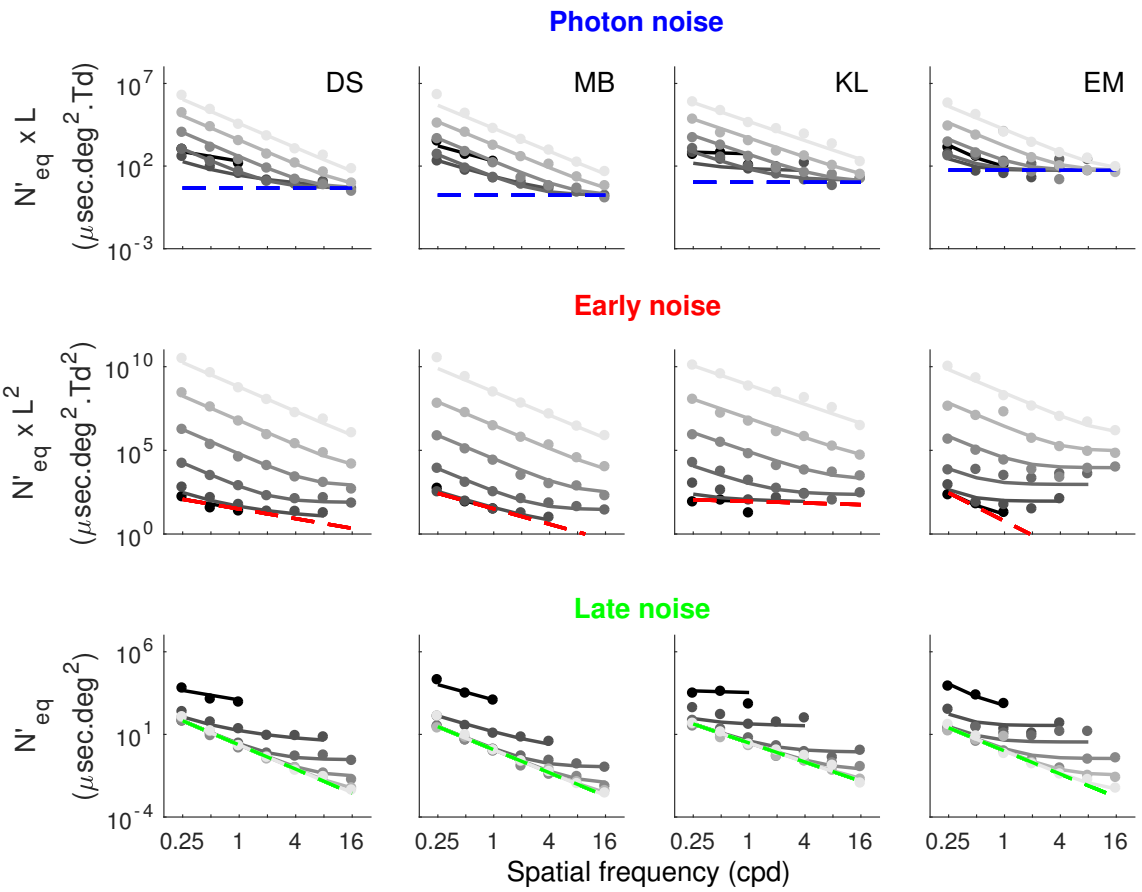

Figure 3.6: Equivalent input noise corrected for the MTF (N'_{eq}). The equivalent input noise at the entry of the retina (N'_{eq}) of each subject as a function of SF is represented in three different ways in order to represent the three sources of noise to be independent of luminance intensity. The first row represents N'_{eq} times luminance intensity and the lower bound (blue dashed line) is the photon noise estimated by our model. The second row represents N'_{eq} times luminance intensity squared and the lower bound (red dashed line) is the early noise estimated by our model. The third row represents N'_{eq} and the lower bound (green dashed line) is the late noise estimated by our model. The data for each luminance (in Td) is fitted with our model (grey gradation lines). The data is represented on a log-log scale and is in energy units.

3.5 Discussion

Contrast sensitivity variations as a function of luminance intensity and SF were mainly due to variations in equivalent input noise as calculation efficiency is independent of luminance intensity and varied little with SF. Moreover, because calculation efficiency is independent of luminance intensity, the three laws characterizing contrast sensitivity as a function of luminance intensity (i.e. the linear law, de Vries-Rose law and Weber's law) can be equally reformulated to characterize equivalent input noise as a function of luminance intensity (Figure 3.1c; equation (3.2.1)) and therefore suggests the existence of three noise sources: photon noise, neural noise occurring before contrast normalization and neural noise occurring after contrast normalization. The advantage of relating these three laws directly to the equivalent input noise rather than contrast sensitivity was to determine how each of these noise sources varies as a function of the SF. Indeed, the contrast sensitivity variation with SF is caused by a variation in both calculation efficiency and equivalent input noise (Figure 3.3). By factorizing out the calculation efficiency from the contrast sensitivity, the equivalent input noise can be independently investigated.

The model used in the current study to fit the data comprised early and late noise decreasing linearly with SF and photon noise being spatially white. Photon noise was the dominating noise at medium luminance intensities (1.6 to 162 Td) and high SFs ($\geq$2 cpd), early noise was the dominating noise at low luminance intensities (0.16 to 1.6 Td) and low SFs (<2 cpd) and late noise was the dominating noise at high luminance intensities (>1626 Td) and across the whole range of SFs tested.

By measuring equivalent input noise across a wide range of SFs and luminance intensities, the current study could estimate the MTF, photon noise, early noise and late noise. While photon noise and late noise have been estimated in other studies (Pelli, 1990; Raghavan, 1995), early noise, to our knowledge, has never been estimated with an external noise paradigm. Nevertheless, contrast sensitivity has been studied as a function of luminance intensity and related to the three laws (de Vries-Rose, linear and Weber's law). In most of these studies (Losada et al., 1993; Mustonen et al., 1993; Van Nes and Bouman, 1967) only de Vries-Rose law and Weber's law were considered. Kelly (1972), on the other hand, considered all three laws, but observed the linear law only at high temporal frequencies,

which were not evaluated in the current study. For static stimuli, Kelly found that contrast sensitivity followed Weber's law at low SF and de Vries-Rose law at high SF at a luminance intensity of 50 Td, which is consistent with our results. In the current study, the spatial-luminance domain where early noise was the dominating internal noise source was low SFs ($\leq$2 cpd) and low luminance intensities ($\leq$1.6 Td).

The model that we develop in the current study is similar to the one developed by Rovamo et al. (1994a) which also takes into account the MTF of the eye, quantal noise (i.e. photon noise related to deVries-Rose's law) and neural noise (related to Weber's law), but not early noise. An important difference between these models is that their model was applied to contrast sensitivity, whereas ours was applied to the equivalent input noise. As a result, they could not directly quantify how the impact of the internal noise sources varies with SF because the contrast sensitivity depends on equivalent input noise and calculation efficiency. Conversely, we were able to quantify how the impact of the internal noise sources varies with SF.

The current approach enabled us to estimate the MTF of the eye psychophysically. A similar approach has been used by Rovamo et al. (1994b) who also estimated the MTF by estimating equivalent input noise. However, the method they used relied on the assumption that photon noise was limiting contrast sensitivity at low luminance intensities, across all SFs. If photon noise was indeed limiting contrast sensitivity across the entire range of SFs tested, then the rise in equivalent input noise with SF would be due to the MTF (given that photon noise is spatially white, Pelli 1990; Raghavan 1995). However, the current study found that at low SFs and at low luminance intensities contrast sensitivity was limited by early noise, not photon noise, which implies that the impact of photon noise was less than the estimated equivalent input noise. Overestimating the impact of photon noise at low SFs reduces its estimated rise with SF, resulting in an underestimation of the drop of the MTF. This could explain their finding of a higher contrast gain for the MTF compared to other studies that estimated the MTF using other techniques.

At high luminance intensities (i.e. $\geq$1626 Td), equivalent input noise was independent of luminance intensities across the whole range of SF tested (i.e. up to 16 cpd), which is consistent with Weber's law and with noise arising after contrast normalization. To

our knowledge, the current study estimated this late noise at high SF for the first time. A previous study (Raghavan, 1995), for the same luminance range (i.e 1600 Td), did not reach Weber's law at high SF and therefore could not estimate late noise for these SFs. This study rather found photon noise (i.e. noise at the photoreceptor level) at high SF suggesting that higher luminance intensities would have been required to reach saturation and thereby estimate late noise. We do not know what could explain these diverging results. Perhaps their subjects had greater photon noise relative to late noise (e.g. subject EM in the current study had relatively more photon noise than the others) or there is some difference in the experimental protocols. At this stage, any interpretation is speculative. What is clear in the current study is that contrast sensitivity reached saturation at the highest luminance intensities even at high SFs (except for subject EM, who did not reach saturation at high SFs), thereby enabling to estimate late noise across a wide range of SFs.

The late noise estimated in our study was found to drop with SF following a linear function with a slope of -2.2 (mean of the subjects), which is similar, but significantly different, from a slope of -2 found by Pelli (Pelli and Farell, 1999; Raghavan, 1995). Pelli suggested that a slope of -2 would be expected if neural density were inversely proportional to receptive field size and receptive field size were inversely proportional to squared SF. Our results are consistent with this explanation although one of these relations should be nuanced or other physiological mechanisms should be taken into account in order to reflect the slightly steeper slope found for the late noise.

In conclusion, the current study shows that the main variation in contrast sensitivity as a function of SF and luminance intensity can be explained by the fact that the impact of various internal noise sources varies with these parameters causing different internal noise sources to dominate in different conditions. More specifically, the equivalent input noise can be well modeled with a model having 6 degrees of freedom: 1 for the MTF of the eye, 1 for the photon noise and 2 for each of the two neural noise sources (early and late noise). Depending on the luminance intensity and the SF, contrast sensitivity variations could either be due to photon noise, early noise or late noise.

Chapter 4

Healthy aging impairs photon absorption efficiency of cones

This chapter presents the application of the internal noise paradigm (described in chapter 3) on aging. This work has been previously published under the form of an article:

> Daphné Silvestre, Angelo Arleo and Rémy Allard (2019). Healthy Aging Impairs Photon Absorption Efficiency of Cones. *Invest. Ophthalmol. Vis. Sci.*, 60(2):544-551.

This work has also led to the filing of a patent with Essilor International:

> Rémy Allard and Daphné Silvestre (2018). Method and system for characterizing the visual system of a subject, EP18305379.2. 2018/03/30. France.

Abstract

Purpose. Vision decline with healthy aging is a major public health concern with the unceasing growth of the aged population. In order to prevent or remedy the age-related visual loss, a better understanding of the underlying causes is needed. The current psychophysical study used a novel noise paradigm to investigate the causes of age-related contrast sensitivity loss by estimating the impact of optical factors, absorption rate of photon by photoreceptors, neural noise, and calculation efficiency on contrast sensitivity.

Methods. The impact of these factors on contrast sensitivity was assessed by measuring contrast thresholds with and without external noise over a wide range of spatial frequencies (0.5–16 cycles per degree [cyc/deg]) and different luminance intensities for 20 young (mean = 26.5 years, SD = 3.79) and 20 older (mean = 75.9 years, SD = 4.30) adults, all having a good visual acuity ($\geq$ 6/7.5).

Results. The age-related contrast sensitivity losses were explained by older observers absorbing considerably fewer photons ($\times$4), having more neural noise ($\times$1.9), and a lower processing efficiency ($\times$1.4). The aging effect on optical factors was not significant.

Conclusions. The age-related contrast sensitivity loss was mostly due to less efficient cones absorbing four times fewer photons than young adults. Thus, besides the ocular factors known to be considerably affected with aging, the decline of absorption efficiency of cones is also responsible for a considerable age-related visual decline, especially under dim light.

4.1 Introduction

Vision decline with healthy aging is a major public health concern with the unceasing growth of the aged population (Mendelson and Schwartz, 1993). To prevent or remedy this age-related vision loss, a better knowledge about the underlying causes is needed. A classical approach to quantify visual perception is to measure contrast sensitivity, which declines with healthy aging (Owsley, 2011) due to optical factors such as pupillary miosis and yellowing of the lens, as well as neural factors such as an increase of neural spontaneous activity and lower neural efficiency (Birren and Schaie, 2006; Zhang et al., 2008). Nevertheless, another factor that is neither optical nor neural is often overlooked: the absorption rate of photoreceptors. The current study aimed at quantifying the impact of healthy aging on absorption rate of photoreceptors and various neural factors.

Noise paradigms have been used to investigate the causes of age-related sensitivity losses by factorizing contrast sensitivity into equivalent input noise, which quantifies the sum impact of all internal noise sources, and calculation efficiency (also termed central efficiency, Barlow 1977), which is equivalent to the signal-to-noise contrast ratio required to detect the signal (Allard et al., 2013b; Bennett et al., 1999; Pardhan, 2004). The current study used an elaborated noise paradigm (Silvestre et al., 2018) to further decompose the equivalent input noise into the Modulation Transfer Function of the eye (MTF, which is accountable for the impact of most optical aberrations, Fry 1969; Lombardo and Lombardo 2010), stochastic absorption rate of photons, and neural noise (see Figure 4.1). The impacts of these components on contrast sensitivity can be disentangled because they vary differently as a function of the spatial frequency (SF) and because different sources of internal noise limit contrast sensitivity at different luminance intensities (Kelly, 1972; Raghavan, 1995; Rovamo et al., 1994a; Silvestre et al., 2018). The current study therefore evaluated the impact of healthy aging on various factors (photon noise, neural noise, MTF, and calculation efficiency) by measuring contrast sensitivity at different luminance intensities, SFs, and with and without external noise for healthy young and older observers.

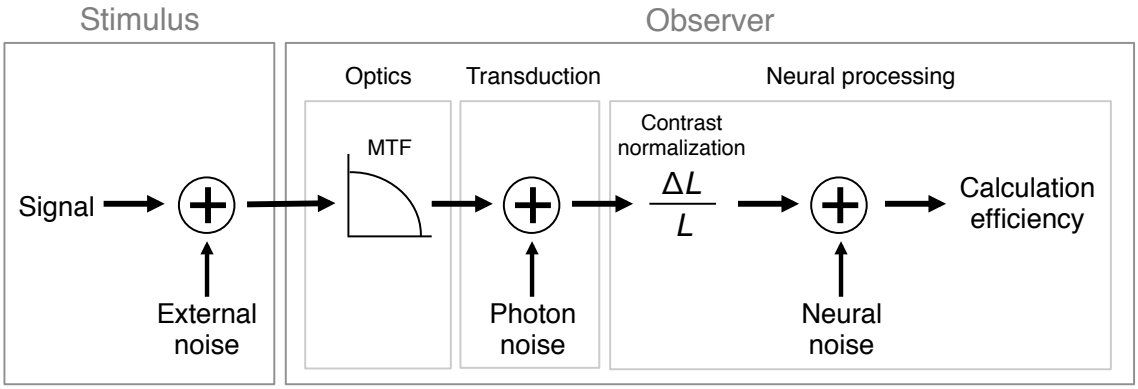

Figure 4.1: Observer model comprising the MTF, photon noise, neural noise, and calculation efficiency. The MTF models most of the optical factors; the photon noise represents the fluctuations of phototransduction, and the neural noise could represent, for instance, the spontaneous activity of neurons located after the contrast normalization.

4.2 Methods

4.2.1 Observers

Twenty young adults (mean age = 26.5 years, SD = 3.79; 12 females) and 20 older adults (mean age = 75.9 years, SD = 4.30; 11 females) from the Silversight cohort (Vision Institute, Paris, France) participated in the current study after giving their informed consent. All participants were screened and included only if they had no known visual, audiovestibular, sensorimotor, neuropsychological, or cognitive pathologies, and a good visual acuity (≥6/7.5) with their dominant eye (estimated by using the hole-in-card test). The screening of the participants was undertaken by an otorhinolaryngologist (audiometric and vestibular tests), a neuropsychologist (Mini Mental State Examination [MMSE], General Health Questionnaire [GHQ], medical history questionnaire), and an ophthalmologist (optical coherence tomography, fundus photography, visual acuity with an ETDRS chart viewed at 2 m, contrast sensitivity with a Pelli-Robson chart). No participants were under any medication known to alter visual perception, such as benzodiazepine (Giersch et al., 2006). Participants were wearing trial frames with trial lenses adjusted to their optimal correction according to each testing distance, which varied across conditions. The visual correction of each subject was estimated before the experiment by an orthoptist.

Ethical approval was obtained from the Comité de Protection des Personnes Ile de France V in agreement with the Declaration of Helsinki, and the clinical screening was carried out under medical supervision at the Clinical Investigation Center of the Quinze-Vingts Hospital, Paris.

4.2.2 Apparatus

All stimuli were generated by a homemade program and presented on a projector screen. The projector used was a LCD Panasonic PT-EW730Z (Kadoma, Osaka, Japan) with a refresh rate of 60 Hz and a resolution of 1280 × 800 pixels; it could project a luminance intensity up to 3700 cd/m^2. This projector was chosen for its brightness, which was essential to measure the impact of neural noise across a wide range of SFs (contrast sensitivity saturates at higher luminance intensities for higher SFs, Silvestre et al. 2018). The projector was the only source of light in the room and was set behind the screen for a direct retroillumination. The output intensity of each color gun was carefully linearized using a Minolta spectroradiometer CS-1000 (Ramsey, NJ, USA). The Noisy-bit method (Allard and Faubert, 2008) implemented independently to each color gun made the 8-bit display perceptually equivalent to an analog display having a continuous luminance resolution.

4.2.3 Stimuli and procedure

An orientation discrimination task was carried out using a two- alternative forced-choice procedure (vertical or horizontal). To help the observer to stay focused and motivated, auditory feedback was given after each response made by pressing one of two keys. Note that such an orientation discrimination task using an external noise paradigm induces no considerable perceptual learning after two experimental sessions (as in the current study) even with feedback (Lu and Dosher, 2004).

The signal was a sinusoidal grating with a SF of 0.5, 1, 2, 4, 8, or 16 cycles per degree (cyc/deg), depending on the testing condition. The spatial window of the signal was a circular aperture with a diameter that depended on the SF of the signal and was set to

eight visible cycles of the signal grating plus a half-cosine of half a cycle. To minimize spatial uncertainty, a black annulus centered on the stimulus and 2.5 times the size of the aperture was continuously displayed. Stimuli were presented for 500 ms plus an on and off half-cosine ramp of 250 ms each, resulting in a total presentation duration of 1 second. Stimuli were presented at the center of a gray square of 41 × 41 cm and were viewed monocularly through a 2.5-mm artificial pupil at a distance of 97, 194, and 388 cm from the screen depending on the SF of the stimulus (see Figure 4.2 for a representation of the stimuli). For better comfort, participants monocularly viewed the stimuli with their dominant eye.

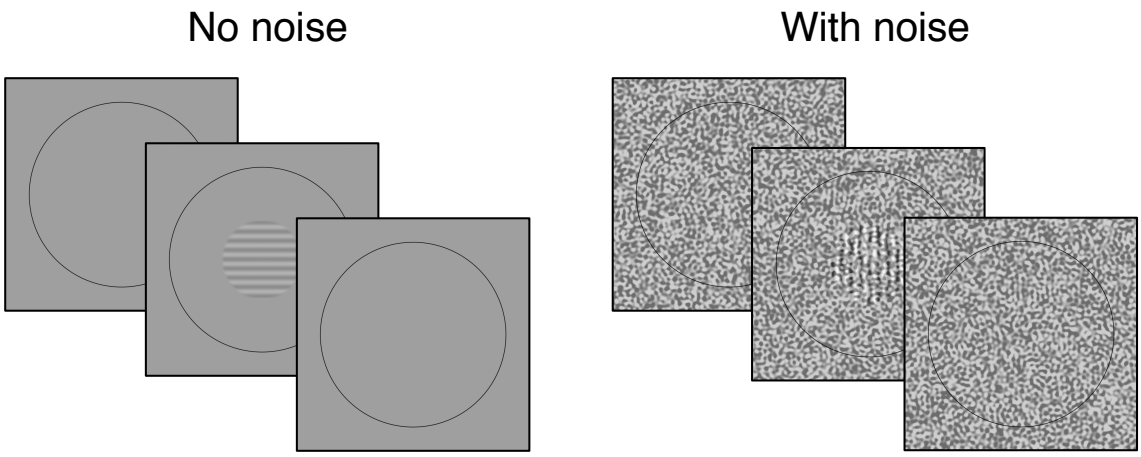

Figure 4.2: Stimuli samples without (*left*) and with (*right*) external noise. The stimulus was either vertical or horizontal and changed randomly at each trial.

Given that calculation efficiency (i.e., contrast threshold in high noise) is independent of luminance intensity (Nagaraja, 1964; Pelli, 1981; Silvestre et al., 2018), contrast thresholds in noise were measured only at the highest luminance intensity (i.e., 9145 trolands [Td]). The noise used was truncated-filtered noise (Jules Étienne et al., 2016) with a SF cutoff two octaves above the SF of the signal, temporally white (refreshed at 30 Hz), and its contrast was truncated at 1 standard deviation, which corresponded to 50%. The noise was spatiotemporally extended (i.e., full-screen and continuously displayed) to avoid triggering a shift in processing strategy (Allard and Cavanagh, 2011; Allard and Faubert, 2014b; Silvestre et al., 2017). For the highest SF of 16 cyc/deg, a pilot study revealed that this noise had little impact on contrast sensitivity of older adults, which compromised the estimation of the calculation efficiency at this SF. Therefore, to estimate the calculation

efficiency at 16 cyc/deg, the calculation efficiencies measured for the other SFs (0.5–8 cyc/deg) were fitted with a quadratic function (Silvestre et al., 2018), which was then used to extrapolate and estimate the calculation efficiency at 16 cyc/deg. The resulting noise energies were 1300, 324, 81, 20, and 5.1 μs.deg^2 for SF of 0.5 to 8 cyc/deg, respectively.

Contrast thresholds in absence of external noise were measured at different luminance intensities. For the highest luminance intensity, at which neural noise was expected to limit contrast sensitivity, the retinal illuminance was 9145 Td and the whole range of SFs (0.5–16 cyc/deg) was tested. For the low luminance conditions, only the high SFs were tested (4–16 cyc/deg), at which photon noise was expected to limit contrast sensitivity. For 4 and 8 cyc/deg, the retinal illuminance was set to 9.1 Td, which was obtained by placing a neutral density filter with an optical density of 3 (which reduces luminance intensity by a factor of 1000) on the trial frames of the observer. For 16 cyc/deg, the retinal illuminance was set to 91 Td (trial frames with an optical density of 2), because contrast sensitivity was too low to be measured at 9.1 Td for the older adults.

Control conditions were designed to evaluate the age- related impact of the yellowing of the lens on contrast sensitivity by presenting stimuli on a red background. Long wavelengths (e.g., red) are little affected by the yellowing of the lens, which mainly blocks shorter wavelengths (Mellerio, 1987). This control condition was done at high luminance intensity (1446 Td) with a SF of 0.5 cyc/deg, at which observers were expected to be limited by neural noise (Silvestre et al., 2018), and at low luminance intensity (91 Td) with a SF of 16 cyc/deg, at which observers were expected to be limited by photon noise (Silvestre et al., 2018) obtained with a neutral density filter with an optical density of 1 and the red background (i.e., red color gun projecting wavelength longer than 580 nm) luminance fixed at 185 cd/m^2.

To evaluate the impact of age-related optical factors on contrast sensitivity, a control condition was conducted in which the impact of optical factors was neutralized using a 1-mm artificial pupil, which makes the impact of a small defocus negligible (Thibos et al., 2002). This control condition was conducted for the SF at which the optical factors had the greatest impact, that is, 16 cyc/deg. For comparative reasons, this control was conducted

for a gray and a red background of 91 Td (by setting the luminance of the screen at 1170 and 370 cd/m^2, respectively, and adding a neutral density filter with an optical density of 1 and 0.5, respectively). Note that for all the experimental parameters (i.e., the different luminance intensities, SFs, and color of the background) the cones were mainly activated, because either the luminance intensity was too high for rods to be effective (they were saturated, Kandel et al. 2000) or the degree of visual angle of the observer was too small to activate photoreceptors outside of the fovea (i.e., mostly cones, Kandel et al. 2000).

Contrast detection thresholds were measured using a 3down1up staircase procedure (the contrast of the stimulus decreases by one step after three consecutive correct answers and increases by one step after every wrong answer, Levitt 1971) with a step size of a factor of 1.25 and terminated after 14 reversals. Such a staircase converged to a criterion level of 79.4% correct response (Levitt, 1971) corresponding to a *d'* of 1.16. For each staircase, the threshold was estimated as the geometric mean of the last 10 reversals. Two staircases were performed for each condition. The threshold for each condition was estimated as the geometric mean of the two estimated thresholds.

Participants completed the experiment in two sessions lasting approximately 2 hours each, and many breaks were provided in each session in order to keep the participants motivated and alert. The first session covered the highest luminance intensity conditions, whereas the second session covered the lowest luminance intensities and controlled conditions, for which participants were light-adapted for 30 minutes by wearing on the trial frames neutral optical density filters of 3. For each session the order of the SFs was randomized, but to minimize the displacement between testing distances, the two staircases for each SF were blocked. For the first session at the highest luminance intensity, two contrast thresholds were measured for each SF to estimate the equivalent input noise and the calculation efficiency: one in absence of noise *c(0)* and the other in high noise $c(N_{ext})$ (except at 16 cyc/deg, at which $c(N_{ext})$ could not be measured). The control condition with a red background corresponding to a retinal illuminance of 1446 Td was also tested at the end of this session. For the second session, the participants were adapted to the lowest luminance intensity (9.1 Td), were tested at that luminance intensity, and then were tested at 91 Td, at which the remaining control conditions were also tested.

The energy threshold E (square of the stimulus' contrast function summed over space and time, Pelli and Farell 1999) is known to be linearly related to the external noise energy N_{ext} (Pelli and Farell, 1999). When the phase of the signal is unknown, this linear function can be represented as (Bennett et al., 1999):

$$E(N_{ext}) = \frac{(d' + \sqrt{0.5})^2}{k}(N_{ext} + N_{eq}) \tag{4.2.1}$$

where k represents the calculation efficiency. Thus, for each SF at which threshold in high noise was measured (0.5–8 cyc/ deg), the calculation efficiency (k) in energy units was calculated based on the energy thresholds in absence of noise (*E(0)*) and in high noise (*E(Next)*) at the highest luminance intensity of 9145 Td:

$$k = \frac{(d' + \sqrt{0.5})^2 N_{ext}}{E(N_{ext}) - E(0)} \tag{4.2.2}$$

The estimated calculation efficiencies as a function of the SF of each observer were fitted with quadratic functions (Silvestre et al., 2018) and these fits (i.e., k_{fit}) were then used to estimate the calculation efficiency at each relevant SF (0.5–16 cyc/deg) and estimate the equivalent input noise at the various luminance intensities. Based on Equation 4.2.1, equivalent input noise for each condition was estimated based on the energy threshold in absence of noise (*E(0)*) and the fit of the calculation efficiency (k_{fit}) estimated for the given SF:

$$N_{eq} = \frac{k_{fit}}{(d' + \sqrt{0.5})^2} E(0). \tag{4.2.3}$$

4.2.4 Model

A model recently developed (Silvestre et al., 2018) was used to decompose the equivalent input noise into the MTF of the eye, photon noise, and neural noise. This model was applied on the estimated equivalent input noise of each subject and had four degrees of freedom; one for the optical aberrations (i.e., MTF modeled with a generalized Lorentzian function with a free exponent, Watson 2013), one for the photon noise (constant with respect to SF), and two for the neural noise (affine function in log-log units with respect to SF). In the current study, the model had only four degrees of freedom compared to six degrees of freedom in the original model (Silvestre et al., 2018) because the very low

luminance intensities at which early noise (i.e., retinal neural noise occurring prior to the contrast normalization) dominates were not investigated. The spatial and luminance conditions were chosen with respect to a previous study (Silvestre et al., 2018), in order to estimate the MTF, photon noise, and neural noise.

4.2.5 Data Statistics

The contrast thresholds, calculation efficiency, and equivalent input noise data were analyzed by means of 2-way repeated measures analysis of variance (ANOVA; age × SF), to take into account that a same participant was tested for the different SFs. The analysis was done for high and low luminance intensities conditions separately. The effect of SF on contrast thresholds and equivalent input noise, for the low luminance intensities conditions, was not reported because there were two different luminance intensities, making the data incomparable. The parameters of the model (MTF, photon noise, and neural noise) were analyzed with a 2-sample *t*-test.

The effect size for the 2-way ANOVAs was estimated with ω^2. A ω^2 near 0.01 is a small effect, near 0.06 is a medium effect, and near 0.14 is a large effect (ω^2 is between -1 and 1). The effect size for the *t*-tests were estimated with Hedges' *g* coefficient (Cohen, 1988; Hedges, 1981). A *g* near 0.2 is a small effect, near 0.5 is a medium effect, and near 0.8 is a large effect.

Pearson partial correlations were used to test if aging effects were due to potential confounding factors affecting contrast sensitivity. Partial correlations were evaluated between the dependent variables (MTF, photon noise, neural noise, and calculation efficiency) and age after controlling for the effects of sex (male or female), smoking (yes or no), education (score from 0 to 5), cognitive impairments (score of MMSE), and depression (score of GHQ).

4.3 Results

Contrast sensitivity

Contrast sensitivity functions for young and older adults at high and low luminance intensities are represented in Figure 4.3. Older adults were less sensitive than young adults across the whole SF range for the high and low luminance conditions. Moreover, the contrast sensitivity functions were less band-pass (i.e., slope less steep at low SF) than what is typically observed in the literature (Owsley et al., 1983), which was expected (Mustonen et al., 1993; Virsu and Rovamo, 1979) given that the stimulus had a fixed number of visible cycles causing the stimulus size to be greater at lower SFs.

A 2-way ANOVA (age × SF) of the contrast sensitivity at high luminance intensity showed a significant large effect of age ($F(1,38) = 33$, $P < 0.001$, $\omega^2 = 0.4$), a significant large effect of SF ($F(5,190) = 151$, $P < 0.001$, $\omega^2 = 0.8$), and a significant interaction between these factors ($F(5,190) = 8.3$, $P < 0.001$, $\omega^2 = 0.2$), which can be explained by the greater age-related sensitivity loss at high SFs.

A 2-way ANOVA (age × SF) of the contrast sensitivity at low luminance intensities also showed a significant large effect of age ($F(1,38) = 34$, $P < 0.001$, $\omega^2 = 0.5$) and a significant interaction between age and SF ($F(2,76) = 7.8$, $P < 0.001$, $\omega^2 = 0.2$), which can also be explained by the greater age-related sensitivity loss at higher SFs.

To visualize the difference between contrast sensitivity at low and high luminance intensities, Figure 4.4 represents the data using Bland-Altman plots. A contrast sensitivity ratio higher than one indicates that the observer was more sensitive at high luminance intensity than at low luminance intensity. The fact that contrast sensitivity was always higher at high luminance intensity for all observers and all SFs is consistent with the expectation that at low luminance intensity the observers were limited by photon noise.

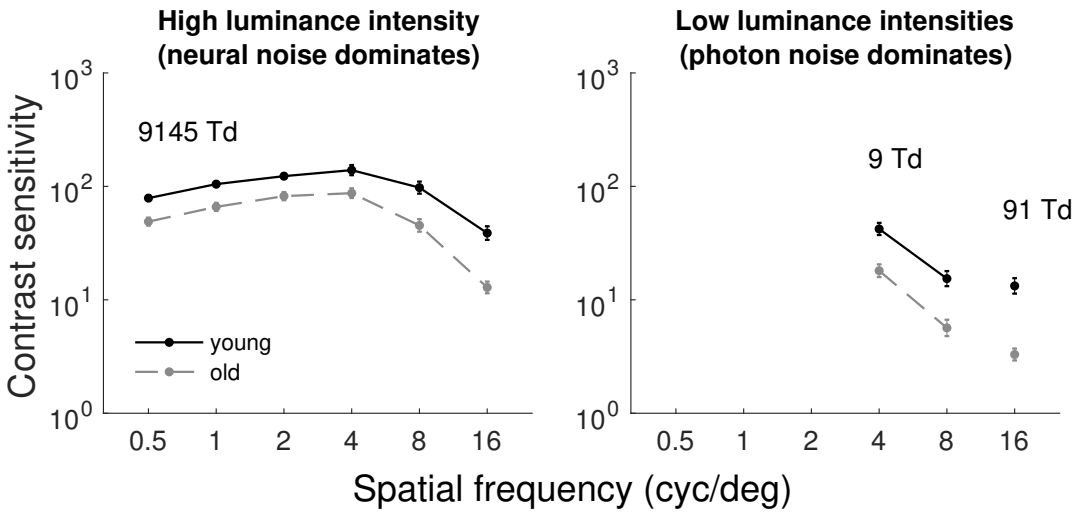

Figure 4.3: Contrast sensitivity of young and older adults. On the *left*, contrast sensitivity as a function of SF at 9145 Td is represented for the older adults (*gray dots* connected with *dashed lines*) and the young adults (*black dots* connected with *solid lines*). On the *right*, contrast sensitivity is represented for the older adults at 9 Td (*gray dots* connected with a *dashed line*) and at 91 Td (*gray dot*) and for the young adults at 9 Td (*black dots* connected with a *solid line*) and at 90 Td (*black dot*). The error bars represent the standard error of the mean (some of them are not visible, being smaller than the size of the marker).

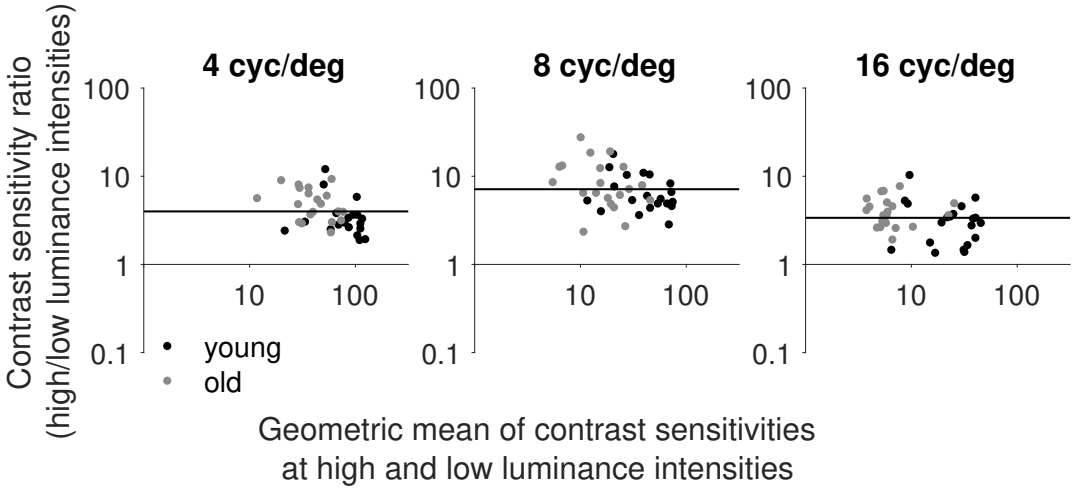

Figure 4.4: Bland-Altman plots. Comparison of contrast sensitivities at high and low luminance intensities for 4 cyc/deg (*left graph*), 8 cyc/deg (*middle graph*), and 16 cyc/deg (*right graph*). The older adults' data are represented by *gray dots* and the young adults' data by *black dots*. The *black lines* represent the geometric mean of the data.

Calculation efficiency

Calculation efficiencies measured at high luminance intensity for young and older adults varied little with SF (Figure 4.5), which is expected when the number of visible cycles is constant (Virsu and Rovamo, 1979). A 2-way ANOVA (age × SF) showed a significant large effect of age ($F(1,38) = 14$, $P < 0.001$, $\omega^2 = 0.3$; older adults were less efficient than young adults by a factor of approximately 1.4 in energy units), a significant large effect of SF ($F(4,152) = 15$, $P < 0.001$, $\omega^2 = 0.3$), which is consistent with previous findings (Silvestre et al., 2018), and no interaction ($F(4,152) = 1.1$, $P = 0.36$).

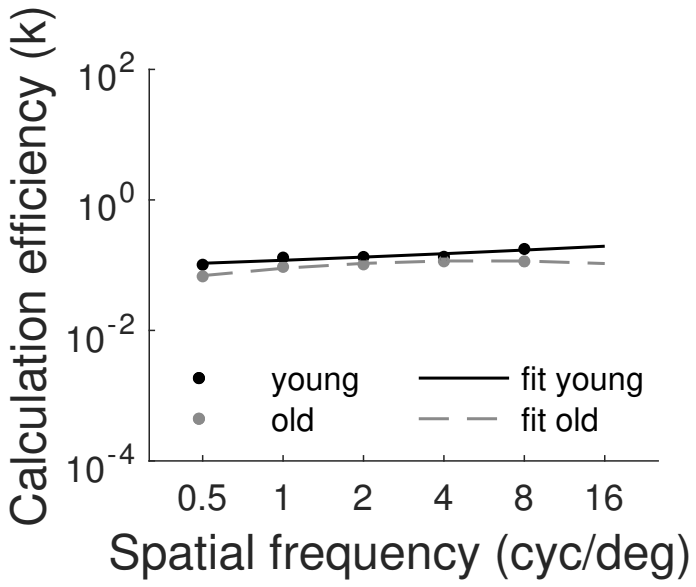

Figure 4.5: Calculation efficiency of young and older adults. Calculation efficiency (k, in energy units) as a function of SF at 9145 Td is represented for older adults (*gray dots*) fitted with our model with *dashed lines* (k_{fit}) and for young adults (*black dots*) fitted with our model with *solid lines*. The error bars represent the standard error of the mean (they are not visible, being smaller than the size of the marker). Note that at 16 cyc/deg the calculation efficiency could not be measured so only the fits are represented.

Equivalent input noise

Equivalent input noises (Figure 4.6) were estimated using Equation 4.2.3 based on the contrast sensitivities at various luminance intensities and SFs and on the calculation efficiency fits at various SFs (Figure 4.5). The mean equivalent input noise of older observers was greater than the mean of young adults at all SFs and luminance intensities.

For the high luminance conditions, a 2-way ANOVA (age × SF) showed a significant large effect of age ($F(1,38) = 20$, $P < 0.001$, $\omega^2 = 0.3$) and SF ($F(5,190) = 401$, $P < 0.001$, $\omega^2 = 0.9$), as well as an interaction between these factors ($F(5,190) = 4.4$, $P < 0.001$, $\omega^2 = 0.1$), which can be explained by the greater aging effect at high SFs.

For the low luminance conditions, a 2-way ANOVA (age × SF) showed a significant large effect of age ($F(1,38) = 24$, $P < 0.001$, $\omega^2 = 0.4$; older adults had more equivalent input noise than young adults) and no interaction between SF and age ($F(2,76) = 2.2$, $P = 0.11$).

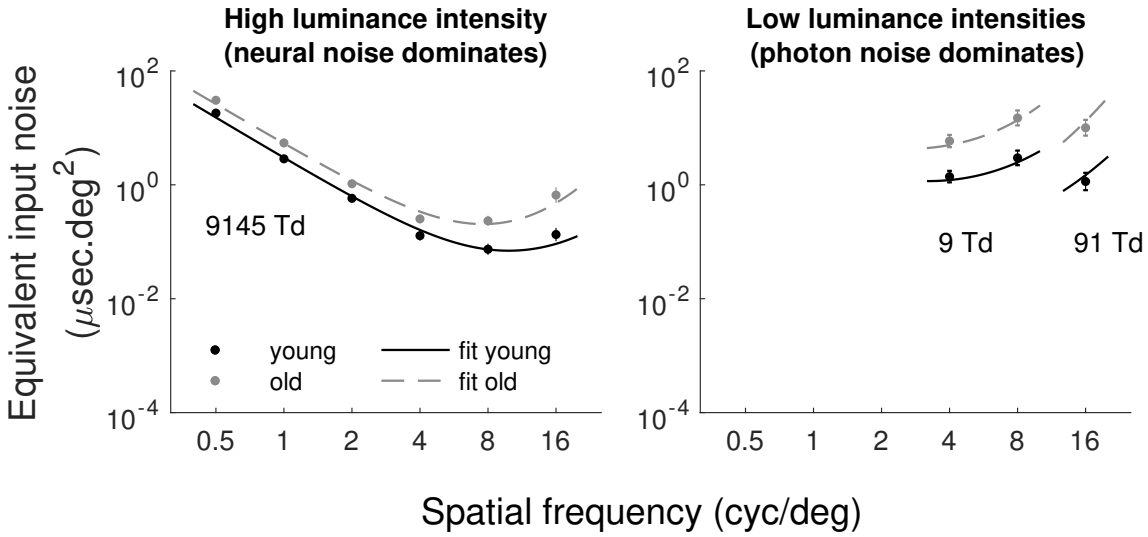

Figure 4.6: Equivalent input noise of young and older adults. On the *left*, equivalent input noise as a function of SF at 9145 Td is represented for the older adults (*gray dots* fitted with our model with *dashed lines*) and for the young adults (*black dots* fitted with our model with *solid lines*). On the *right*, equivalent input noise as a function of SF at 9 Td and 91 Td is represented for the older adults (*gray dots* fitted with our model with *dashed lines*) and for the young adults (*black dots* fitted with our model with *solid lines*). The error bars represent the standard error of the mean (most of them are not visible, being smaller than the size of the marker).

Internal noise sources and MTF

Using an elaborated noise model (Silvestre et al., 2018), equivalent input noises were decomposed for each participant into the optical aberrations modeled by the MTF of the eye, photon noise caused by stochastic absorption of photons, and neural noise (Figure 4.7). Optical factors (MTF) affected slightly more the older observers (up to a factor of 2.3 in energy units at 16 cyc/deg), but this effect was not statistically significant ($t(38) = 1.7$, $P = 0.10$). A significant aging effect on photon noise was found ($t(38) = 3.4$, $P < 0.01$, $g = 1$), suggesting that older adults had more photon noise than young adults by a factor of 4.0 in energy units. This greater amount of photon noise suggests that photoreceptors of the older adults absorbed approximately 4.0 times fewer photons than the young adults. No significant aging effect was found on the slope of the affine function fitting neural noise ($t(38) = 0.4$, $P = 0.71$), but a significant aging effect was found on the neural noise's mean across the SFs ($t(38) = 2.5$, $P < 0.05$, $g = 0.8$), which suggests that the older adults had 1.9 times more neural noise than the young adults.

The age-related effects described above on the photon noise, neural noise, and calculation efficiency show significant differences between young and older groups. These effects could be due to age or some other confounding factor differing between the two groups such as education, sex, smoking, cognitive impairments, and depression, which can affect contrast sensitivity (Fernandes et al., 2017; Swenor et al., 2018; Wesner and Tan, 2006). Partial correlations between each dependent variable and age were evaluated while controlling for the effects of sex (male or female), smoking (yes or no), education (score from 0 to 5), cognitive impairments (score of MMSE), and depression (score of GHQ). The aging effects on photon noise, neural noise, and calculation efficiency all remained significant after controlling for these factors ($r = 0.38$, $P < 0.05$; $r = 0.36$, $P < 0.05$; $r = 0.62$, $P < 0.001$, respectively), which shows that the observed aging effects cannot be explained by these factors (sex, smoking, education, cognitive impairments, and depression).

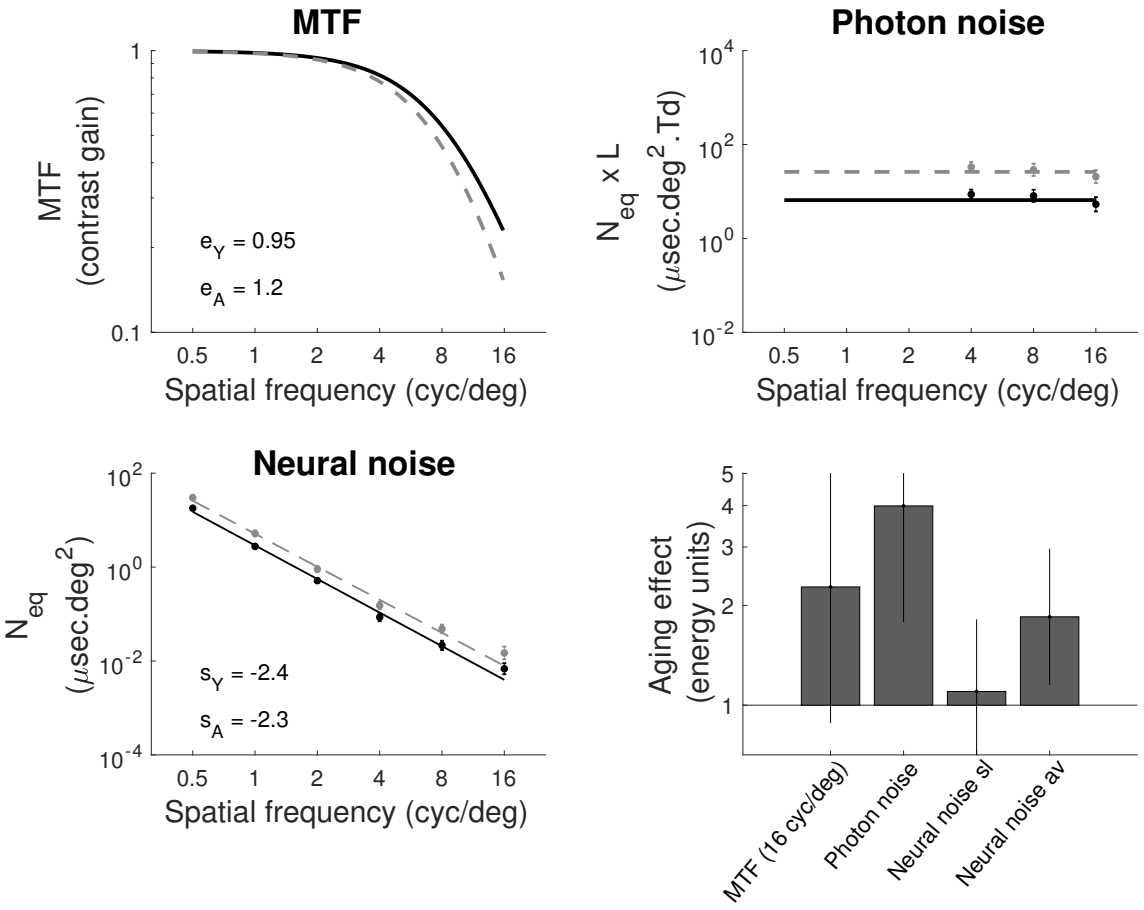

Figure 4.7: Internal noise sources. The *top left* graph represents the MTF of the eye as a function of SF for the older (*dashed line*) and the young adults (*solid line*). The exponent of the generalized Lorentzian function is represented by e_A for the older adults and by e_Y for the young adults. The *top right* graph represents equivalent input noise of the low luminance conditions multiplied by luminance intensity ($N_{eq} \times L$) as a function of SF, at which photon noise was the dominating noise source. The *bottom left* graph represents equivalent input noise (N_{eq}) at the high luminance condition as a function of SF at which neural noise was the dominating noise source. The slopes of the fits are represented by s_A for the older adults and by s_Y for the young adults. The data are represented by *gray dots* fitted by our model with *dashed lines* for the older adults and by *black dots* fitted with our model with *solid lines* for the young adults. Data are all in energy. The error bars represent the standard error of the mean (most of them are not visible, being smaller than the size of the marker). The *bottom right* graph summarizes the aging effect in energy units on each parameter of the model, which are the Modulation Transfer Function (MTF) at 16 cyc/deg, the photon noise, the neural noise slope (sl) and the neural noise average (av) across SF. The error bars represent the 95% confidence interval.

Yellowing of the lens and MTF controls

All the controlled conditions for the yellowing of the lens showed a similar age-related sensitivity loss (i.e., aging effect) using a gray or red background (Figure 4.8), which suggests that the older adults did not have a yellowing of their lens considerably affecting contrast sensitivity. Moreover, the similar age-related sensitivity losses observed with a 2.5- and a 1-mm artificial pupil (right graph in Figure 4.8) suggest that there was no considerable aging effect on optical aberrations, which is consistent with the nonsignificant aging effect found on the MTF of our model (see top left graph of Figure 4.7).

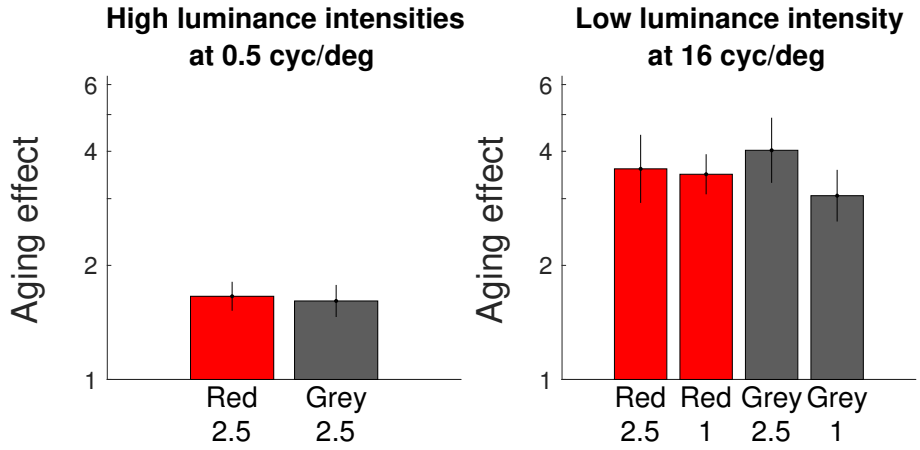

Figure 4.8: Experimental controls. The first graph on the *left* represents the aging effect of the experiment controlling for the effect of the yellowing of the lens at high luminance intensities and at 0.5 cyc/deg, at which neural noise is the dominating source of noise (gray background at 9145 Td versus red background at 1446 Td). The second graph on the *right* represents the aging effect of the experiment controlling for the effect of the yellowing of the lens at low luminance intensity (91 Td) and at 16 cyc/deg, at which the photon noise is the dominating noise source (gray background versus red background for a 2.5- and a 1- mm pupil). The error bars represent the 68% confidence interval.

4.4 Discussion

Healthy aging was found to affect contrast sensitivity across a wide range of SFs at high and at low luminance intensities. By measuring contrast thresholds in high noise and using an elaborated noise model, contrast sensitivity was decomposed into various

factors: the MTF of the eye, photon noise (caused by probabilistic absorption), neural noise, and calculation efficiency. The age-related impacts of these internal factors on sensitivity (in energy units) are summarized in Figure 4.9. Calculation efficiency (CE) dropped by a factor of approximately 1.4 (averaged across SFs). Though the impact of optical aberrations on sensitivity (i.e., MTF) at high SFs was greater for older adults (2.3× at 16 cyc/deg), this effect was not statistically significant. Neural noise, which affected sensitivity at the high luminance intensity (left graph), was affected by a factor of approximately 1.9 (averaged across SFs), whereas photon noise, which affected sensitivity at the low luminance intensities (right graph), was affected by a factor of 4.0.

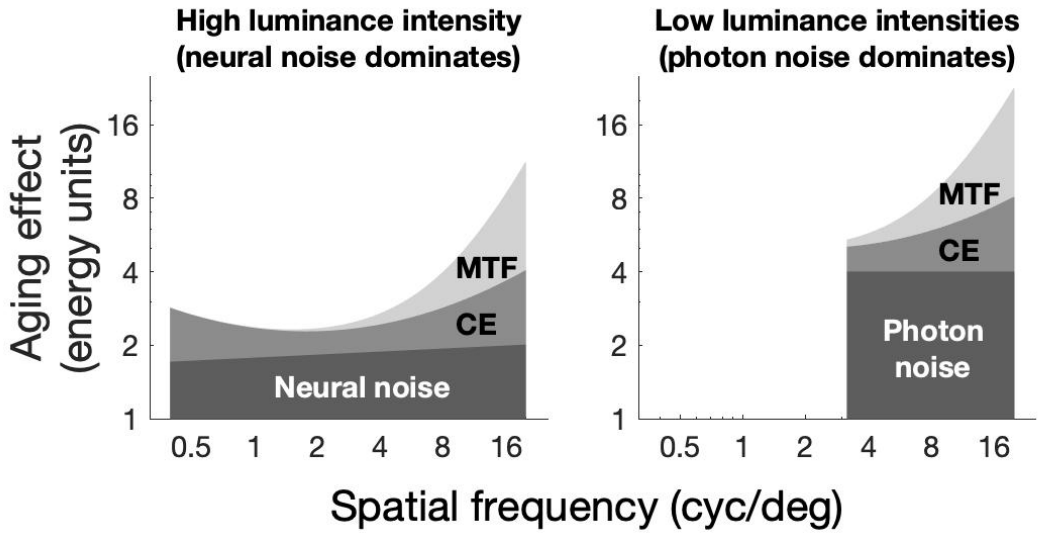

Figure 4.9: Impact of the different internal factors on the age-related sensitivity loss. The age-related sensitivity loss is represented for the different SFs at high luminance intensity on the *left* graph and at low luminance intensities on the *right* graph. Each factor responsible for the aging effect is represented with a different graduation of gray.

The 4-fold age-related increase in photon noise found in the current study suggests that the cones of older adults absorbed four times fewer photons than the ones of the young adults. This lower absorption rate cannot be due to age-related miosis (i.e., smaller pupil) because observers were wearing an artificial pupil equating the amount of photons entering the eye. Furthermore, the lower absorption rate cannot be due to an age-related yellowing of the lens reducing the amount of short-wavelength photons reaching the retina, because a similar age-related effect was observed even when using only high wavelengths (i.e.,

red, Figure 4.8) that are little affected by the yellowing of the lens. The absence of a considerable age-related yellowing of the lens effect in the current study can be explained by the strict inclusion criteria, which asserted that participants were healthy and had a good visual acuity (≥6/7.5). We conclude that the main known age-related factors reducing retinal illumination, namely, miosis and the yellowing of the lens, had little impact on the age-related contrast sensitivity losses observed in the current study.

If the lower number of photons absorbed by the elderly was not due to a reduction in the number of photons reaching the retina, then it must be due to a loss of cones or a lower absorption efficiency of cones. The exact loss of cones with aging remains debated (Curcio et al., 1993; Gartner and Henkind, 1981) but no study found evidence of a large loss of cones with aging that could explain the 4-fold decrease of photon absorption rate observed in the current study. This suggests that the age-related decrease in photon absorption rate was mainly due to lower absorption efficiency of the cones, not to a loss of cones. The results of the current study therefore suggest that a lower absorption efficiency of the cones considerably affects vision of older observers in low-brightness environments (e.g., driving at night, Gruber et al. 2013). This conclusion differs from the one reached by previous studies (Owsley et al., 1983; Weale, 1963) which mainly attributed age-related contrast sensitivity losses to an increase of the lens opacity and miosis reducing the amount of light reaching the retina, whereas the current study mainly attributes them to less efficient cones. Note that both conclusions suggest that persons who are elderly absorb fewer photons, but only our conclusion is consistent with our data as the pupil diameter was controlled for using an artificial pupil and similar age-related sensitivity losses were observed when using only high wavelengths (i.e., red), which are little affected by the yellowing of the lens.

A possible explanation of the lower absorption rate of cones is a change of morphology related to the decreased density of rods (i.e., approximately a 30% loss, Curcio et al. 1993; Gao and Hollyfield 1992; Panda-Jonas et al. 1995) occurring with aging. Indeed, the loss of rods disorganizes the alignment of the cones by giving less support to the cones and therefore induces a change in the orientation of the cones, reducing their absorption rate (Cunea and Jeffery, 2007).

Optical aberrations (i.e., MTF) were found in the literature to greatly degrade contrast sensitivity with aging (Artal et al., 2002, 2003). A reason that the aging effect on the MTF was not significant in the current study could be that the older participants had to have a good acuity (≥6/7.5) and healthy eyes to be included in the study, and a relatively small artificial pupil (2.5 mm) was used, which reduces the impact of optical aberrations. Consequently, the absence of a considerable age-related increase in optical aberrations observed in the current study is likely not representative of the elderly population.

The 2-fold increase in neural noise with aging found in the current study could be due to various age-related neurobiological alterations such as more spontaneous activity, less inhibition, a decrease of the myelin density, or fewer synapses (Xie et al., 2014; Zhang et al., 2008). In any case, this aging effect on neural noise was not specific to some SFs, which suggests that there was not a greater loss in density of neurons sensitive to low SFs than neurons sensitive to high SFs.

A modest age-related decline in calculation efficiency was observed and this effect was similar across SFs (i.e., no interaction between SF and age; Figure 4.5). Taken alone, this result could be due to numerous factors affecting the ability of elderly persons to perform the task such as cognitive impairment, attention, lack of motivation, or fatigue. Indeed, an age-related factor affecting performance in both absence and presence of noise would affect calculation efficiency, not equivalent input noise (and thus, not the MTF, photon noise, or neural noise). The fact that the effect of aging on calculation efficiency was modest suggests that age-related effects not related to perception per se, were, at most, modest. Nonetheless, combining the current results with the ones of a previous study (Allard et al., 2013b) suggests that this modest age-related decline in calculation efficiency was due to a less efficient spatial integration, not to a nonperceptual factor like cognitive impairment, attention, or fatigue. This previous study (Allard et al., 2013b) found no aging effect on the calculation efficiency at 1 cyc/deg, a modest decline at 3 cyc/deg, and a greater decline at 9 cyc/deg. The absence of an aging effect on calculation efficiency at 1 cyc/deg was due to the fact that young and older adults had similar contrast thresholds in high noise, which rules out any effect due to cognitive impairment, attention, lack of motivation, or fatigue, and implies that the effect observed in the other conditions was specific to perception per

se. Because this previous study (Allard et al., 2013b) used a spatial window with a size fixed to 4° of visual angle, the number of visible cycles of the signal increased with the SF (4, 12, and 36 visible cycles, respectively). Given that the number of cortical neurons stimulated is proportional to the number of visible cycles (Virsu and Rovamo, 1979), the ability to integrate across many cortical neurons would be more useful when more cortical neurons are stimulated (i.e., more visible cycles). Consequently, if older observers were less efficient at integrating across many visible cycles, then age-related calculation efficiency declines would be greater when more cycles are visible. In the current study, the same number of visible cycles were presented for all SFs (eight visible cycles for which it has been shown that contrast sensitivity reaches a plateau, Robson and Graham 1981) and the modest aging effect was similar across SFs. Taken together, the results of the current and the previous study (Allard et al., 2013b) suggest that healthy aging impairs spatial integration as the decline in calculation efficiency depends on the number of visible cycles of the signal.

A limitation of the current study was that older adults were not representative of the aging population, having, for instance, higher visual acuity. However, we would expect a similar or lower absorption rate by photoreceptors in a more representative aging population, which would only reinforce the main finding of the current study. Another limitation was that a cross-sectional paradigm was used, so it is possible that the age-related effects may not be due to aging per se but to other confounding factors. To minimize the impact of this limitation, partial correlations were used to control for the more likely confounding factors. Another limitation is that the interpretation of the underlying causes of age-related contrast sensitivity loss (e.g., absorption rate of photoreceptors) relies on the application of a psychophysical noise paradigm (Silvestre et al., 2018). The current conclusion that aging affects the absorption rate of photoreceptors is currently being tested by combining physiological and psychophysical approaches.

4.5 Conclusion

To summarize and in conclusion, the current study suggests that an age-related increase in neural noise (e.g., spontaneous neural activity) considerably impairs contrast sensitivity at high luminance intensities, whereas a considerable decline in the ability of cones to absorb photons greatly impairs contrast sensitivity at low luminance intensities. Furthermore, an age-related decline in calculation efficiency likely due to a decline in spatial integration would also impair contrast sensitivity to large targets at all luminance intensities.

Thus, besides the optical factors and the neural factors, the absorption rate of cones is an important factor impaired with aging that has been overlooked and considerably affects vision under dim light. In order to prevent this age-related decline, additional studies should investigate the causes of less efficient cones (e.g., morphologic changes).

Chapter 5

Spatio-temporal properties of three internal noise sources limiting contrast sensitivity

This chapter presents the extension of the internal noise paradigm to the spatio-temporal domain. This study aimed at characterizing the spatial and temporal properties of the internal noise factors limiting the spatio-temporal contrast sensitivity function.

Abstract

Spatial and temporal contrast sensitivities are limited by many internal factors and the comprehension of these factors could enable us to better understand the limitations of the visual system. However, the properties of these factors are still unclear and need to be further investigated. The current study used a recently developed paradigm (internal noise paradigm) to distinguish three different sources of noise located at the photoreceptor (photon noise), retina (early noise) and cortical level (late noise). To estimate these noise sources, contrast thresholds were measured for two young adults over a large range of spatial frequencies (0.5 to 16 cpd), temporal frequencies (0 to 15 Hz) and luminance intensities (0.35 to 353 Td), in presence and absence of external noise. In the temporal domain, the observer's model constrained the photon noise and early noise to be temporally white and model comparisons analyses suggested that late noise followed a second-degree polynomial function. In the spatial domain, model comparisons analyses suggested that photon noise, early noise and late noise followed linear functions. Moreover, it was found that the spatio-temporal contrast sensitivity function was limited by photon noise over a wide range of the spatio-temporal domain at photopic light levels, by early noise at high temporal frequencies over a wide range of luminance intensities and by late noise at low temporal frequencies and high luminance intensities.

5.1 Introduction

Contrast sensitivity and flicker sensitivity functions quantify the limits of the visual system in the spatial and temporal domain, respectively. These limits are due to a combination of many internal factors. A better comprehension of these limiting factors may allow us, for instance, to better characterize visual loss due to aging or pathologies. These factors impact the visual signal at various levels of the visual system, such as the optical aberrations of the eye (e.g. diffraction), the retinal temporal diffusion and internal noise at different stages of the visual system. Optical aberrations and retinal temporal diffusion have been well characterized and estimated in the literature, either psychophysically (Kelly and Wilson, 1978; Watson, 2013) or with other techniques (e.g. double-pass ophthalmoscopic methods, Charman 1991). However, the properties of the internal noise are still unclear and need to be further investigated. A recently developed paradigm (Silvestre et al., 2018), named internal noise paradigm, allows us to estimate the impact of three different sources of noise occurring at different levels of the visual system (see Figure 5.1): the stochastic absorption rate of photons (i.e. photon noise), neural noise at the retina level (i.e. early noise) and neural noise at the cortical level (i.e. late noise). Using an observer's model, we were able to estimate the spatial properties of these sources of noise and also to identify the main internal noise source limiting contrast sensitivity as a function of the spatial frequency and luminance intensity (Silvestre et al., 2018). However, in the temporal domain (e.g. using flickering stimuli) and moreover in the spatio-temporal domain, the properties of these sources of noise have not yet been defined. Few studies have measured the spatio-temporal contrast sensitivity function (Kelly, 1972; Rovamo et al., 2000a), therefore little is known by its limiting factors.

The current study will characterize the spatio-temporal properties of three sources of noise (photon noise, early noise and late noise), by using flickering stimuli at different spatial frequencies (SFs), temporal frequencies (TFs) and luminance intensities, which will enable to derive which internal noise source is limiting sensitivity as a function of SF, TF and luminance intensity.

5.2 Model

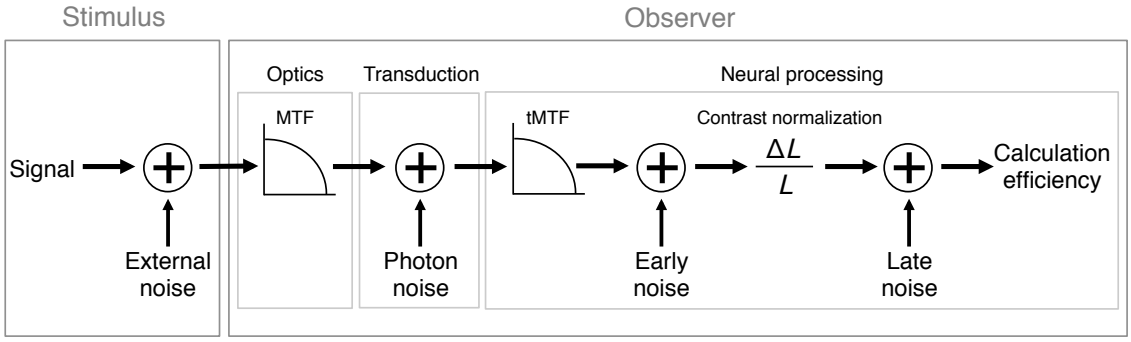

Figure 5.1: Observer's model. The model comprises the spatial and temporal MTFs, three additive internal noise sources and calculation efficiency. The first additive internal noise source is the photon noise (i.e. phototransduction) arising after the spatial MTF (i.e. optical aberrations). The second internal noise source is the early noise (i.e. neural noise at the retina level) and it arises after an additional factor being the temporal tMTF. The third internal noise source is the late noise, which is neural noise occurring after the contrast normalization.

The observer's model, illustrated in Figure 5.1, is based on a recently developed model (Silvestre et al., 2018) that decompose equivalent input noise into three sources of noise, which are photon noise, early and late noise that are related to de Vries-Rose law, the linear law and Weber's law, respectively. In the current study, this model was adapted to also take into account the temporal domain and is represented by equation (5.2.1):

$$N_{eq}(L,s,t) = \frac{1}{MTF^2(s)}\left(\frac{N_{photon}(s)}{L} + tMTF^2(t)\left(\frac{N_{early}(s)}{L^2} + N_{late}(s,t)\right)\right) \qquad (5.2.1)$$

This model of the equivalent input noise as a function of luminance intensity (L), SF (s) and TF (t) depends on five factors that vary with SF, TF or both ($MTF(s)$, $N_{photon}(s)$, $tMTF(t)$, $N_{early}(s)$ and $N_{late}(s,t)$). These five factors are defined as follows:

MTF. The Modulation Transfer Function ($MTF(s)$) representing the optical aberrations and depending only on SF is modeled with a generalized Lorentzian function with a free exponent (Watson, 2013), resulting in a function with one degree of freedom.

Photon noise. Photon noise ($N_{photon}(s)$) represents the stochastic absorption rate of photons at the photoreceptor level and should be spatially and temporally white (Pelli,

1990; Raghavan, 1995). However, after viewing preliminary results of the current study, it was decided to test different functions depending on SF to fit the photon noise estimations. Three different functions were tested: a constant (independent of SF), a linear function and a quadratic function, resulting in 1, 2 and 3 degrees of freedom, respectively.

tMTF. The temporal Modulation Transfer Function (*tMTF(t)*) representing the retinal temporal diffusion resulting into a low-pass filter with respect to the TF is modeled by the diffusion model of Kelly and Wilson (1978), resulting in a function with one degree of freedom (i.e. argument of the exponential function).

Early noise. Early noise ($N_{early}(s)$) represents spontaneous neural activity at the retinal level, more specifically before contrast normalization presumably occurring at the retinal ganglion cells level. Given that spontaneous neural activity is not temporally correlated (Raghavan, 1995), it was therefore constrained in our model to be temporally white. Three different functions depending on SF were tested to fit the early noise estimations: a constant (independent of SF), a linear function and a quadratic function, resulting in 1, 2 and 3 degrees of freedom, respectively.

Late noise. Late noise ($N_{late}(s,t)$) represents for instance spontaneous neural activity occurring after the contrast normalization. Six different second-degree polynomial functions depending on SF and TF and with or without a spatio-temporal interaction (see Table 5.4) were tested to fit the late noise estimations, resulting in 3 to 6 degrees of freedom.

The global model fitting the equivalent input noise in the current study comprised one parameter for the MTF and one for the tMTF and the best fitting functions for the photon noise (1 to 3 parameters), early noise (1 to 3 parameters) and late noise (3 to 6 parameters).

5.3 Methods

5.3.1 Observers

Two observers of 26 and 28 years old with normal or corrected-to-normal vision participated to the current study and one of the observer is an author of this study. The

participants were taken from the Silversight cohort and informed consent were obtained. The participants had a good visual acuity (>6/6 or >10/10 in decimals) with their dominant eye and they wore trial frames with trial lenses adjusted to their optimal correction according to the testing distance. The visual correction of the participants was estimated before the experiment by an orthoptist. Ethical approval was obtained from the 'Comité de Protection des Personnes Ile de France V', which is in agreement with the Declaration of Helsinki.

5.3.2 Apparatus

All stimuli were generated by a homemade program and presented on a VIEWPixx/EEG LCD monitor with a refresh rate of 120 Hz, a resolution of 1920 × 1080 pixels and had a maximum luminance intensity of 100 cd/m^2. The monitor was the only source of light in the room. The output intensity of each color gun was carefully linearized using a Minolta spectroradiometer CS-1000. The Noisy-bit method (Allard and Faubert, 2008), implemented independently to each color gun, made the 8-bit display perceptually equivalent to an analog display having a continuous luminance resolution.

5.3.3 Stimuli and procedure

An orientation discrimination task was carried out using a four-alternative forced-choice procedure (vertical, horizontal, 45° and -45°). Auditory feedback was given to the observer after each response by pressing one of four keys.

The signal was a flickering sinusoidal grating with a SF of 0.5, 1, 2, 4, 8 or 16 cpd and a TF of 0, 0.94, 1.88, 3.75, 7.5 or 15 Hz depending on the testing condition. The spatial window of the signal was a circular aperture with a diameter that depended on the SF of the signal and was set to four visible cycles of the signal plus a half-cosine of half a cycle. To minimize spatial uncertainty a black annulus was centered on the stimulus, which was 5.5 times the size of the aperture and was continuously displayed. Stimuli were presented for 250 ms with an on and off half-cosine ramp of 250 ms each, resulting in a total duration presentation of 750 ms. Stimuli were presented at the center of a grey square of 8.3 × 8.3

degrees of visual angle (dva), which had a mean luminance intensity of 50 cd/m^2. The screen being rectangular, the luminance intensity of the unused pixels was minimized. Stimuli were viewed monocularly at a 2 meters distance through a 3 mm artificial pupil, with the observer's dominant eye.

Contrast thresholds were measured using a 1down1up staircase procedure (Levitt, 1971) with a step size of a factor 1.25 and were interrupted after 12 inversions. Such a staircase converged to a criterion level of 50% correct response. The threshold of each staircase was estimated as the geometric mean of the last 10 inversions.

Given that calculation efficiency (i.e. contrast threshold in high noise) is independent of luminance intensity (Silvestre et al., 2018), contrast thresholds in noise were measured only at the highest luminance intensity (353 Td). The external noise used was a truncated-filtered noise (Jules Étienne et al., 2016) with a SF cutoff two octaves above the SF of the signal, temporally white (refreshed at 60 Hz) and its contrast was truncated at 1 standard deviation, which corresponded to 50%. The noise was spatiotemporally extended (i.e. full-screen and continuously displayed) to avoid triggering a shift in processing strategy (Allard and Cavanagh, 2011). The noise energies were 649, 162, 41, 10, 2.5 and 0.6 μs.deg^2 for 0.5, 1, 2, 4, 8 and 16 cpd, respectively.

Contrast thresholds in absence of external noise were measured at different luminance intensities ranging in half log steps from 0.35 to 353 Td and were obtain by adding a neutral density filter ranging from 3 to 0, respectively. From 35 Td to the lowest luminance intensity, the observers were light-adapted for 20 minutes by wearing on the trial frames of the corresponding neutral optical density filter. A pilot experiment presenting the stimulus on a red background (i.e. rods are little sensitive to this light wavelength), showed similar contrast threshold when the screen's luminance intensity was equated in photopic trolands, which confirms that even in the lowest luminance conditions, vision was mediated by cones.

The experiment was divided in 8 blocks of about 30 min, each block comprised all the SF and TF conditions for a given luminance intensity (except for the conditions at which threshold could not be measured because sensitivity was too low) and no external noise, and one block comprised the conditions with external noise for all the SF and TF conditions

at 353 Td. In each block the order of the spatiotemporal conditions was randomized. Participants completed the experiment in different sessions over a week. Each session lasted maximum 2 hours.

The energy thresholds E is known to be linearly related to the external noise energy N_{ext} (Pelli and Farell, 1999) and can be represented as:

$$E(N_{ext}) = \frac{(N_{ext} + N_{eq})}{k} \tag{5.3.2}$$

where k represents the calculation efficiency and N_{eq} the equivalent input noise. Thus the calculation efficiency (k) in energy units was calculated based on the energy thresholds in absence of noise ($E(0)$) and in high noise ($E(N_{ext})$) at the highest luminance intensity of 353 Td:

$$k = \frac{N_{ext}}{E(N_{ext}) - E(0)} \tag{5.3.3}$$

The estimated calculation efficiencies as a function of SF and TF of each observer were fitted with a second-degree polynomial function in log-log units (i.e. a linear combination of a linear function with respect to SF and a second-degree polynomial function with respect to TF, thus four degrees of freedom, see Analysis section). These fits (i.e. k_{fit}) were then used to estimate the equivalent input noise at the various luminance intensities. Based on equation (5.3.2), the equivalent input noise for each condition was estimated based on the energy threshold in absence of noise ($E(0)$) and the fit of the calculation efficiency (k_{fit}):

$$N_{eq} = k_{fit}E(0) \tag{5.3.4}$$

5.3.4 Analysis

In the current study, the observer's model characterizing the equivalent input noise had five factors and the free parameters of each factor were independently fitted for each participant. The low-pass functions fitting the MTF and tMTF were defined based on previous studies (Kelly and Wilson, 1978; Watson, 2013) and had each one degree of freedom. On the other hand, for the photon noise, early noise and late noise different functions were tested. The statistical analysis to determined the best fitting functions for photon noise, early noise and late noise was performed at the group level in order to define the general trend of the

shape of these functions. In other words, the best fitting model was constrained to be the same for both participants (i.e. same number of free parameters), but the value of each free parameter was independently fitted for each participant.

The estimation of photon noise, early noise and late noise being relatively independent of one another (i.e. each dominating in a different luminance range), finding the best fitting function for each noise can be analyzed separately. The best fitting function was first analyzed for the photon noise. For this analysis, early noise and late noise were fitted with second-degree polynomials (i.e. 3 and 6 degrees of freedom, respectively) to not constrained these sources of noise to unsuitable functions (i.e. with a number of degree of freedom too small). Given that photon noise was modeled with one to three free parameters per participant (i.e. a constant, a linear function and a quadratic function with respect to SF, respectively), the different tested models comprised twelve to fourteen free parameters per participant (i.e. one for the MTF, one to three for the photon noise, one for the tMTF, three for the early noise and six for the late noise). Model comparisons using F-tests enabled to determine the number of free parameters that were statistically justified for the photon noise (Silvestre et al., 2018).

Next, to analyze the best fitting model for the early noise, the photon noise was modeled with the best fitting function found previously (linear function with respect to SF, i.e. 2 free parameters, see Results section). Given that the early noise was modeled with one to three free parameters per participant (i.e. a constant, a linear function and a quadratic function with respect to SF, respectively), the different tested models comprised eleven to thirteen free parameters per participant (i.e. one for the MTF, two for the photon noise, one for the tMTF, one to three for the early noise and six for the late noise). Model comparisons using F-tests enabled to determine the number of free parameters that were statistically justified for the early noise.

Finally, to analyze the best fitting model for the late noise, the early noise was modeled with the best fitting model found previously (linear function with respect to SF, i.e. 2 free parameters, see Results section). Given that the late noise was modeled with three to six free parameters per participant (i.e. different second-degree polynomial functions with respect to SF and TF), the different tested models comprised nine to twelve free parameters

per participant (i.e. one for the MTF, two for the photon noise, one for the tMTF, two for the early noise and three to six for the late noise). Model comparison with F-tests enabled to determine the number of free parameters that were statistically justified for the late noise.

Likewise, F-tests were also performed to determine the number of free parameters statistically justified to fit the calculation efficiency as a function of SF and TF. The functions tested were different second-degree polynomial functions with respect to SF and TF ranging from four to six degree of freedom. All the analysis describe above were performed in log units.

5.4 Results

Spatial and temporal contrast sensitivity functions

Contrast sensitivity functions (CSF) and temporal contrast sensitivity functions (TCSF) of both observers are represented in Figure 5.2. As typically observed (Rovamo et al., 1994a; van Meeteren and Vos, 1972; Van Nes and Bouman, 1967), the contrast sensitivity functions were band-pass at high luminance intensities and low-pass at low luminance intensities. Note that these functions were less band-pass at high luminance intensities (i.e. slope less steep at low SF) than what is generally observed in the literature (Owsley, 2003), which is expected (Rovamo et al., 1993) for stimulus having a fixed number of visible cycles and thus bigger stimulus at lower SFs. The temporal sensitivity functions declined (i.e. downward shift) and were more low-pass as the luminance intensity decreased, which is in agreement with the literature (Rovamo et al., 2000b; Watson, 1986).

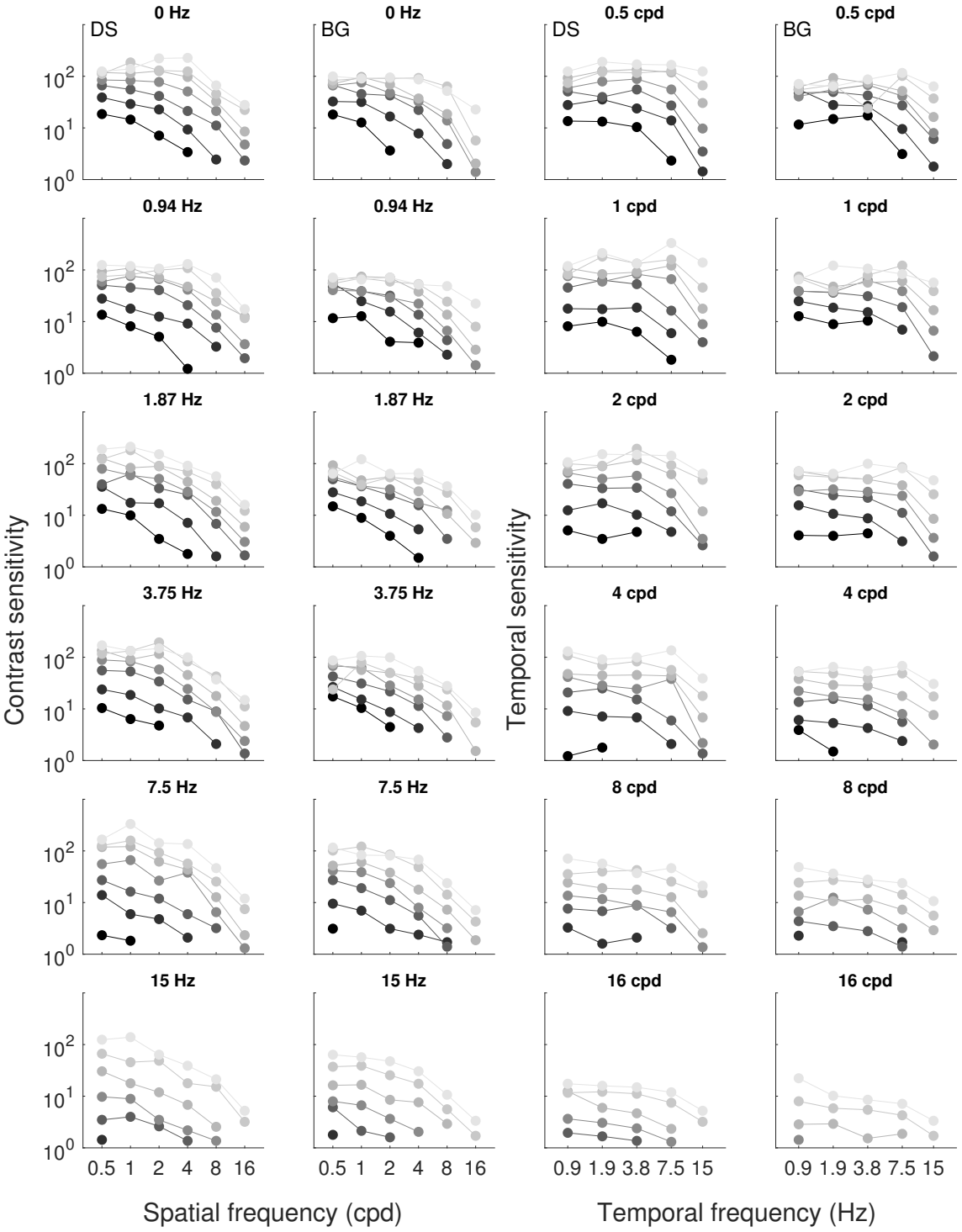

Figure 5.2: CSF and TCSF. The two columns on the left represent the contrast sensitivity functions at different TFs for observers DS (first column) and BG (second column). The two columns on the right represent the temporal contrast sensitivity functions at different SFs for observers DS (third column) and BG (fourth column). The gradation from the darkest to the lightest gray represents the lowest to the highest luminance intensity, respectively. Luminance intensities range in half log steps from 0.35 to 353 Td.

Calculation efficiency

Calculation efficiencies as a function of SF and TF measured at the highest luminance intensity of both observers are represented in Figure 5.3. Model comparisons were performed to investigate the shape of the calculation efficiency function (Table 5.1). Analyses favored a linear combination of a linear function with respect to SF and a second-degree polynomial function with respect to TF (last row in Table 5.1) over second-degree polynomials with an interaction between SF and TF (first row in Table 5.1) or with a second order SF component (second row in Table 5.1). This shows that calculation efficiency depends on SF and TF, but there was no interaction between these two factors. Calculation efficiency varied little as a function of SF with a slope of 0.17 and 0.25 log for DS and BG, respectively and decreased with TF with a slope of 0.76 and 0.66 log (i.e. slopes measured based on the maximum and minimum values) for DS and BG, respectively.

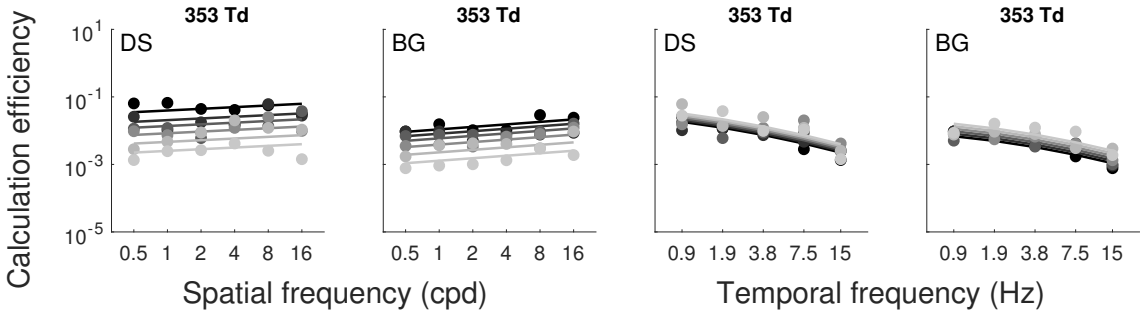

Figure 5.3: Calculation efficiency. The two first graphs represent calculation efficiencies as a function of SF for observer DS (first graph) and BG (second graph). The two last graphs represent calculation efficiency as a function of TF for observer DS (third graph) and BG (fourth graph). The gradation from the darkest to the lightest gray represent the lowest to the highest TF, for the two graphs on the left and SF, for the two graphs on the right. Data were measured at the highest luminance intensity of 353 Td. The data are fitted with a linear combination of a linear function with respect to SF and a second-degree polynomial function with respect to TF.

Calculation efficiency (k)				
Functions			Model comparison	
Function	**df**	**SSr**	***F* value**	***p* value**
$b_1x^2+b_2y^2+b_3x+b_4y+b_5xy+b_6$	12	0.70	$F_{(2,60)}= 1.79$	$p = 0.18$
$b_1x^2+b_2y^2+b_3x+b_4y+b_5$	10	0.76	$F_{(2,62)}= 12.56$	$p < 0.01$
$b_1x^2+b_2x+b_3y+b_4$	8	1.26	$F_{(2,62)}= 0.91$	$p = 0.41$
$b_1y^2+b_2x+b_3y+b_4$	8	0.77		

Table 5.1: *F*-tests for the different calculation efficiency functions. To fit calculation efficiency different second-degree polynomial functions depending on SF (x) and TF (y) were tested. df is the degree of freedom of the function times the number of participants (statistics at the group level). SSr is the sum of squared residuals.

Equivalent input noise

The equivalent input noise as a function of SF and TF (Figure 5.4) were estimated using equation (5.3.4) based on the energy thresholds in absence of noise and the fit of the calculation efficiency. Equivalent input noise increased as the luminance intensity decreased, which is in agreement with previous studies (Allard and Arleo, 2017; Silvestre et al., 2018).

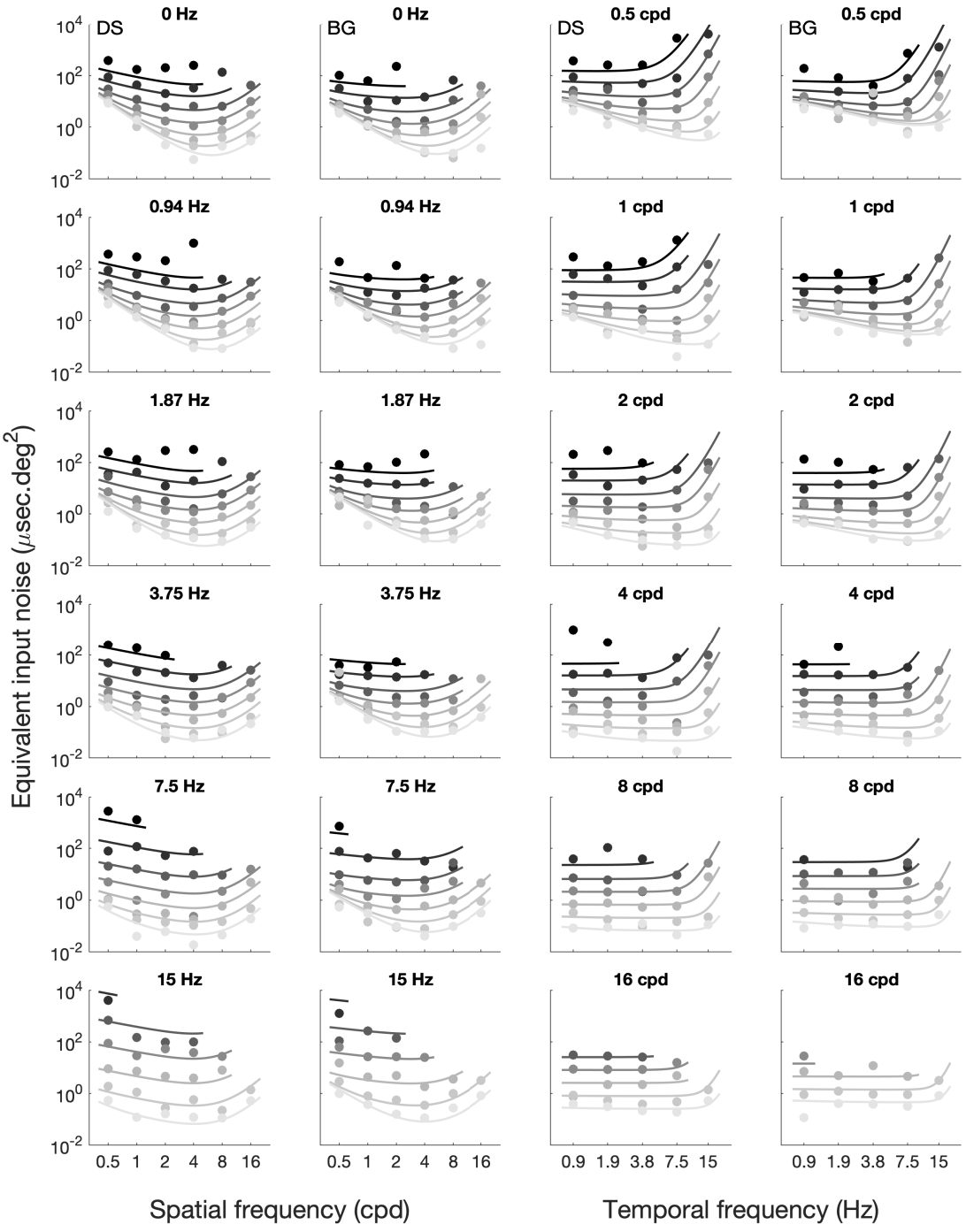

Figure 5.4: Equivalent input noise. The two columns on the left represent equivalent input noises as a function of SF at different TFs for observer DS (first column) and BG (second column). The two columns on the right represent equivalent input noises as a function of TF at different SFs for observer DS (third column) and BG (fourth column). The gradation from the darkest to the lightest gray represents the lowest to the highest luminance intensity, respectively. Luminance intensities ranges in half log steps from 0.35 to 353 Td. The data points were fitted with our model.

Spatio-temporal maps

The spatio-temporal maps of each noise (photon, early and late noise) for both observers are represented in Figure 5.5. The model fitting the equivalent input noise constrained the photon and early noise to be temporally white, but model comparisons were performed to investigate the shape of photon noise and early noise with respect to SF. Table 5.2 shows that, for the photon noise, analyses favored a linear function over a constant ($F_{(2,410)}$= 26.87; $p < 0.01$), but a quadratic function was not statistically justified ($F_{(2,408)}$= 1.99; p = 0.14). This suggests that photon noise varied with SF and it was found to decrease with SF with a slope of 0.75 and 0.29, for observers DS and BG, respectively. Analyses of the model comparisons for early noise are represented in Table 5.3 and a linear function was favored over a constant ($F_{(2,412)}$= 16.84; $p < 0.01$), but a quadratic function was not statistically justified ($F_{(2,410)}$= 0.19; p = 0.83). This suggests that early noise varied with SF and it was found to decrease with SF with a slope of 0.72 and 0.41, for observers DS and BG, respectively.

Analyses of the model comparisons for late noise in the temporal and spatial domain are represented in Table 5.4 and a linear combination of a linear function with respect to SF and a second-degree polynomial with respect to TF, in log-log units was favored (fourth row in Table 5.4). This suggests that late noise depends on SF and TF but there is no interaction between these two factors. Late noise decreased with SF with a slope of 2.6 and 2.3 and decreased with TF with a slope of 4.9 and 4.6 (i.e. slopes measured based on the maximum and minimum values), for observers DS and BG, respectively.

Photon noise (N_{photon})				
Functions			Model comparison	
Function	**df**	**SSr**	***F* value**	***p* value**
Constant	24	11.1	$F_{(2,410)}$= 26.87	$p < 0.01$
Linear	26	9.67	$F_{(2,408)}$= 1.99	$p = 0.14$
Quadratic	28	9.55		

Table 5.2: *F*-tests for the different photon noise functions. Functions depending on SF tested to fit photon noise are a constant, a linear function and a quadratic function. df is the degree of freedom of the fixed parameters in the model (i.e. 2 participants × 11 parameters) plus the different functions tested for the photon noise (i.e. (1 to 3) × 2 participants). SSr is the sum of squared residuals.

Early noise (N_{early})				
Functions			Model comparison	
Function	**df**	**SSr**	***F* value**	***p* value**
Constant	22	11.1	$F_{(2,412)}$= 16.84	$p < 0.01$
Linear	24	9.68	$F_{(2,410)}$= 0.19	$p = 0.83$
Quadratic	26	9.67		

Table 5.3: *F*-tests for the different early noise functions. Functions depending on SF tested to fit early noise are a constant, a linear function and a quadratic function. df is the degree of freedom of the fixed parameters in the model (i.e. 2 participants × 10 parameters) plus the different functions tested for the early noise (i.e. (1 to 3) × 2 participants). SSr is the sum of squared residuals.

Late noise (N_{late})				
Functions			Model comparison	
Function	**df**	**SSr**	***F* value**	***p* value**
$b_1x^2+b_2y^2+b_3x+b_4y+b_5xy+b_6$	24	9.68	$F_{(2,412)}= 0.19$	$p = 0.82$
$b_1x^2+b_2y^2+b_3x+b_4y+b_5$	22	9.69	$F_{(2,414)}= 159.6$	$p < 0.01$
$b_1x^2+b_2x+b_3y+b_4$	20	20.6	$F_{(2,414)}= 0.91$	$p = 0.40$
$b_1y^2+b_2x+b_3y+b_4$	20	9.69	$F_{(2,416)}= 273.9$	$p < 0.01$
$b_1x^2+b_2x+b_3$	18	26.8	$F_{(2,414)}= 0.30$	$p = 0.74$
$b_1y^2+b_2x+b_3y+b_4xy+b_5$	22	9.68		

Table 5.4: *F*-tests for the different late noise functions. Functions depending on SF (x) and TF (y) tested to fit late noise are different second-degree polynomials with or without an interaction between SF and TF. df is the degree of freedom of the fixed parameters in the model (i.e. 2 participants × 6 parameters) plus the different functions tested for the late noise (i.e. (3 to 6) × 2 participants). SSr is the sum of squared residuals.

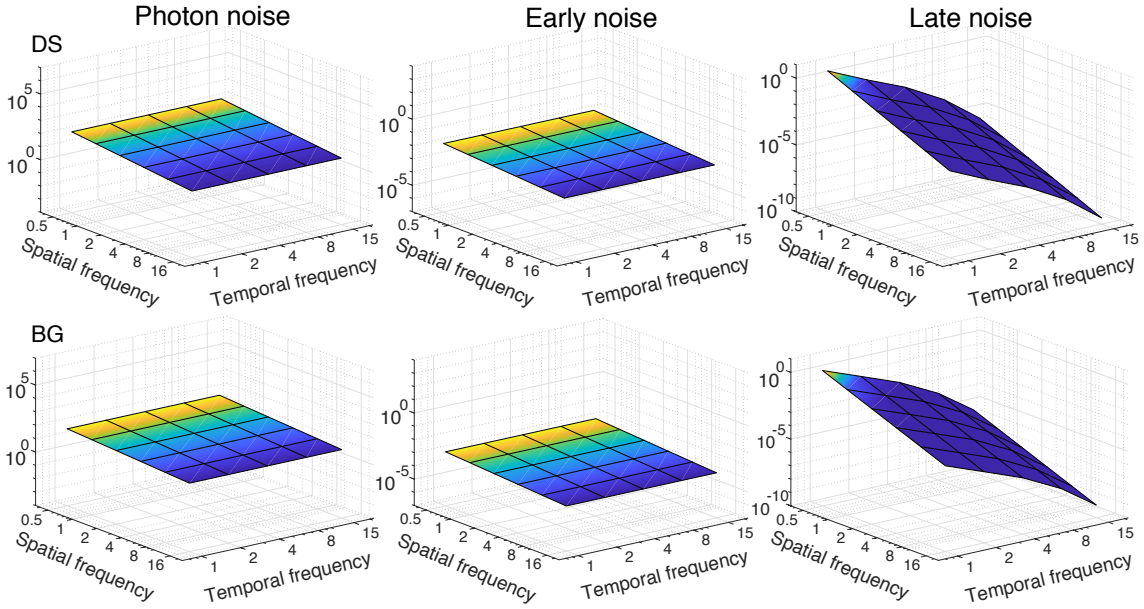

Figure 5.5: Spatio-temporal maps of the 3 internal noise sources. The spatio-temporal properties of the photon noise are represented on the left, of the early noise in the middle and of the late noise on the right for observers DS (top row) and BG (bottom row). Data are represented on a log-log scale.

Spatio-temporal and luminance domain of the noises

The spatio-temporal and luminance domain where each noise limits spatial and temporal contrast sensitivity for both observers are represented in Figure 5.6. Notice that photon noise limits contrast sensitivity over a broad range of spatio-temporal frequencies and luminance intensities. The spatio-temporal and luminance domains of the three internal noise sources are also presented with 3D graphics in Figure 5.7 for a better view of the range of each noise's domain.

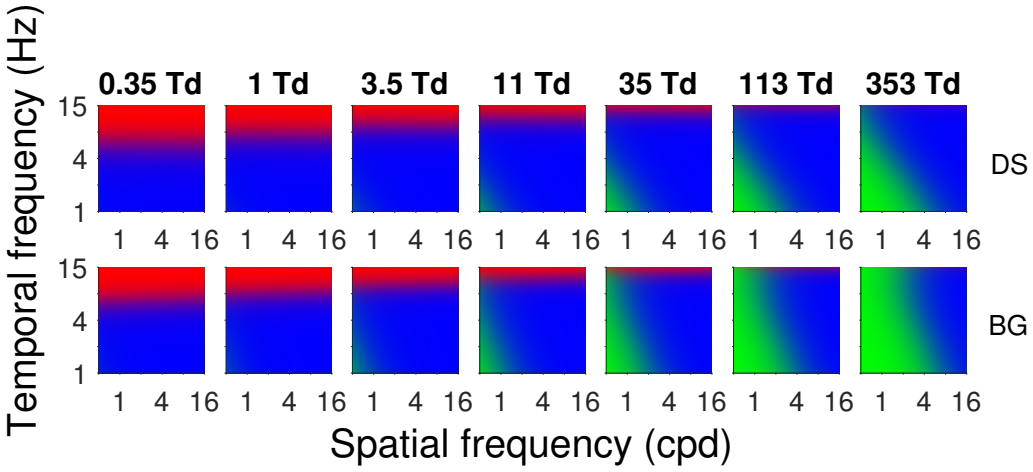

Figure 5.6: Spatio-temporal and luminance domain of the 3 internal noise sources. The spatio-temporal domain where each source of noise is the dominating noise source limiting contrast sensitivity at each luminance intensity is represented on the first row for observer DS and on the second row for observer BG. Photon noise is represented by the color blue, early noise by the color red and late noise by the color green.

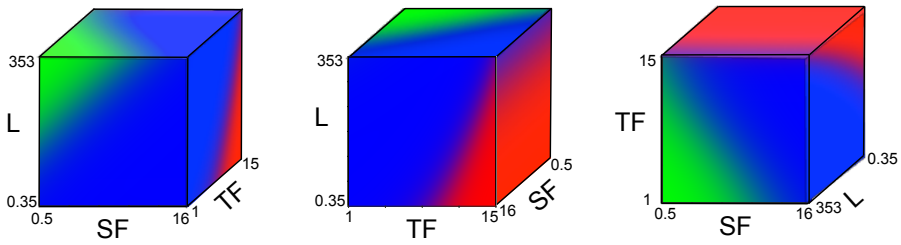

Figure 5.7: Spatio-temporal and luminance 3D domain. The results of observer DS are represented with three different orientations of the same cube, in order to see the extend of the domain of each noise. Data are represented on a log-log scale.

5.5 Discussion

The variations of the spatio-temporal contrast sensitivity function were mainly attributed to equivalent input noise variations, since calculation efficiency varied little with SF and TF. The internal noise paradigm applied to the equivalent input noise, allowed us to distinguish three sources of noise, which are photon noise, early noise and late noise. In the temporal domain, photon noise and early noise were constrained to be temporally white and late noise was found to decreased greatly with TF (log-log slope of -5, approximately). In the spatial domain, photon noise and early noise varied little, but significantly, with SF (log-log slopes <-1) and late noise decreased greatly with SF (log-log slope of -2.4, approximately). No interactions between SF and TF were found for these factors. These sources of noise have an impact on the spatio-temporal contrast sensitivity function at different range of the spatio-temporal and luminance domain and it was found that sensitivity is limited by photon noise over a wide range of the spatio-temporal domain at photopic light levels, by early noise at high TFs over a wide range of luminance intensities and by late noise at low TFs and high luminance intensities (photopic vision).

Photon noise was found in the current study to decrease with SF with a slope of -0.52 log (mean of the observers), however in the literature photon noise has been assumed to be spatially white (Pelli, 1990; Raghavan, 1995; Silvestre et al., 2018), since this noise is at the photoreceptor level, the processing of the signal is not spatially correlated. One hypothesis is that in the current study the stimuli did not stimulate the same amount of cones due to the varying size of the stimulus depending on its SF, which leads to a different amount of noise at each SF. For instance, high SF stimuli were small and stimulated only the fovea of the retina and low SF stimuli were larger and stimulated a more peripheral region of the retina than just the fovea. The cone density decreases with eccentricity, thus, the transduction efficiency (i.e. the number of isomerizations per photon) also decreases with eccentricity, which leads to an increase of photon noise with eccentricity. Thus, low SF stimulus covering a larger retina area should induce a higher amount of noise than a high SF stimulus covering only the fovea. This could explain why we found more photon noise at low SF than at high SF.

Little is known about the properties and location of early noise, since it has been estimated

only recently in one of our previous study assessing spatial contrast sensitivity (Silvestre et al., 2018). In the current study, we found that early noise decreased with SF with a slope of -0.57 log (mean of the observers), whereas in our previous study (Silvestre et al., 2018) a slope of -1.4 log was found. One plausible explanation for this difference is the large variance found for the estimation of the slope of the early noise in our previous study due to the small number of conditions in which contrast sensitivity was limited by early noise. In the current study, more conditions were limited by early noise, i.e., a greater range of SFs and luminance conditions followed the linear law, so we may assume that the slope found may be more precise. The precise location of the early noise in the visual system is still speculative, but our model allowed us to constrain it to a limited region. Indeed, in our observer's model early noise is located before contrast normalization occurring in the retinal ganglion cells (Shapley and Enroth-Cugell, 1984) and after the transduction process. Thus, early noise could be spontaneous activity arising from different retinal neurons such as photoreceptors, horizontal cells, bipolar cells and amacrine cells or from the dendrites connecting these different cells.

Late noise was found in the current study to decrease with SF with a slope of -2.4 log (mean of the observers) and decrease with TF with a slope of -4.7 log (mean of the observers). Its decrease with SF is in agreement with our previous study (Silvestre et al., 2018), which found a slope of -2.2 log. Other studies (Pelli and Farell, 1999; Raghavan, 1995) found a slope of -2 log and explained this result with the fact that neural density is inversely proportional to receptive field size and receptive field size is inversely proportional to squared SF. However, our previous study found that the slope of late noise was statistically different than -2 and thus one of the relations explained above should be a bit nuanced. The current study supports our previous argument that the slope of late noise with respect to SF is higher than -2, leading to a more complex explanation than the simple neural density proportional to the preferred SF of V1 receptors given by Pelli and colleagues.

Our internal noise paradigm allowed us to determine the spatio-temporal and luminance domain (see Figures 5.6 and 5.7) where each noise was the limiting noise source of the spatio-temporal contrast sensitivity function. These spatio-temporal maps at different luminance intensities are consistent with a previous study (Kelly, 1972) that estimated

contrast sensitivity at different spatio-temporal and luminance conditions in order to build a spatio-temporal map at a given luminance intensity delimiting the three adaptation laws (de Vries-Rose, Weber and linear). This previous study only showed spatio-temporal maps for two luminance intensities (i.e. 50 and 200 Td), but by comparing with our spatio-temporal maps taken at similar luminance intensity (i.e. 35 and 113 Td), we find that the spatio-temporal domain of the three noise sources (photon noise, early noise and late noise) correspond to the same spatio-temporal domain of the three laws (with de Vries-Rose law related to the photon noise, linear law to the early noise and Weber law to late noise). The novelty of the spatio-temporal maps estimated in the current study compared with this previous study is that we presented the maps for each luminance intensity tested and we looked at lower luminance intensities, which unravelled a larger region of the early noise domain. Furthermore, these maps could be of interest if one wants the observer to be limited by a specific location of the visual system (i.e. either the photoreceptor, retina or cortical level) in order to study for instance a pathology affecting specifically one of these locations. For instance to detect age-related macular degeneration at an early stage (before the symptoms appear), one could test the observer in a photon noise limiting condition in order to record any abnormal change in the photon noise level.

5.6 Conclusion

The variations of the spatio-temporal contrast sensitivity function is mainly due to the variations of the different internal noise sources. The internal noise paradigm of the current study allowed us to characterize the spatio-temporal properties of three different sources of noise of the visual system (i.e. photon noise, early noise and late noise). Furthermore, the spatio-temporal and luminance domain where each noise source limits the spatio-temporal contrast sensitivity function is define over a wide range of spatio-temporal frequencies and luminance intensities, which could be used for clinical applications to detect eye pathologies at an early stage.

Chapter 6

Underlying causes of age-related motion sensitivity loss

This chapter presents the application of the internal noise paradigm adapted to the temporal domain (i.e. measure of the temporal contrast sensitivity function) on aging. This project was done during Asma Braham Chaouche's master internship under the supervision of Dr. Rémy Allard and myself. Therefore, this chapter was mainly written by Dr. Rémy Allard and Asma Braham Chaouche. My contribution to this research project was the elaboration of the experimental protocol, the analysis of the data, the elaboration of the figures and a general supervision of the project.

Abstract

The purpose of the current study was to investigate the underlying causes of age-related motion sensitivity losses. Using the external noise paradigm, motion sensitivity was factorized into equivalent input noise, which quantifies the impact of internal noise, and calculation efficiency, which is related to the signal-to-noise ratio required to detect the signal. Furthermore, the internal noise paradigm was used to decompose the equivalent input noise into temporal modulation transfer function (tMTF, which correspond to temporal blur) and 3 different sources of internal noise: the stochastic absorption of photons by photoreceptors (i.e. photon noise), neural noise occurring at the retina level (i.e. early noise) and neural noise occurring at the cortical level (i.e. late noise). The impact of healthy aging on these various factors was evaluated by measuring motion sensitivity of young and older healthy observers at different luminance intensities, temporal frequencies and with/without external noise. Elderly were found to have more photon noise attributed to a lower photon absorption rate of cones. When roughly equating the amount of photons being absorbed by the photoreceptors, elderly had lower calculation efficiencies, but no significant aging effect was found on tMTF, early noise and late noise. These results suggest that age-related motion sensitivity losses are mainly due to a lower absorption rate by photoreceptors and a lower processing efficiency, not to an increase in neural noise, nor to additional temporal blur due to longer integration time from early retinal processes.

6.1 Introduction

Motion perception is essential for many daily activities such as walking in a crowded environment, practicing a sport, crossing a street and driving. However, motion perception is affected with healthy aging (Allard et al., 2013a; Habak and Faubert, 2000), which can reduce the ability of elderly to perform efficiently and safely some daily activities. The purpose of the current study was to investigate the underlying causes of age-related motion sensitivity losses.

Older observers could be less sensitive to motion because they have more internal noise (e.g., distortions or spontaneous neural activity within the visual system) or because they are less efficient at detecting a noisy signal (i.e., lower calculation efficiency). To test these hypotheses, the current study used an external noise paradigm (Pelli, 1981; Pelli and Farell, 1999) to factorize motion sensitivity into the equivalent input noise, which is a measure of the impact of the internal noise on motion sensitivity, and calculation efficiency, which is related to the signal-to-noise ratio required to detect the signal. In other words, we used this paradigm to determine whether age-related motion sensitivity losses are due to an increase in imprecision in the transmission of the visual signal (internal noise) or a decrease in the ability of the visual system to detect a motion signal in noise (calculation efficiency).

Given that there is internal noise at all processing stages within the visual system, including the stochastic absorption of photons by photoreceptors and neural noise such as spontaneous neural activity, the current study further investigated more precisely the impact of aging on various sources of internal noise. To do so, we used the internal noise paradigm (Silvestre et al. 2018 and chapter 5) enabling to break down the equivalent input noise into the temporal modulation transfer function (tMTF, which correspond to temporal blur that modulates the impact of neural noise) and 3 different sources of internal noise: the stochastic absorption of photons by photoreceptors (i.e. photon noise), neural noise occurring at the retina level (i.e. early noise) and neural noise occurring at the cortical level (i.e. late noise). This psychophysical paradigm can quantify the impact of these different sources of noise based on two principles (Silvestre et al. 2018 and chapter 5): first, the sensitivity is noticeably affected only by the greatest noise source, the im-

pact of the others being negligible, and second, the impact of different sources of noise varies as a function of luminance intensity. The current study therefore evaluated the impact of healthy aging on various factors (photon noise, tMTF, early noise, late noise and calculation efficiency) by measuring the motion sensitivity for young and older healthy observers at different luminance intensities, temporal frequencies (TFs), and, with and without external noise.

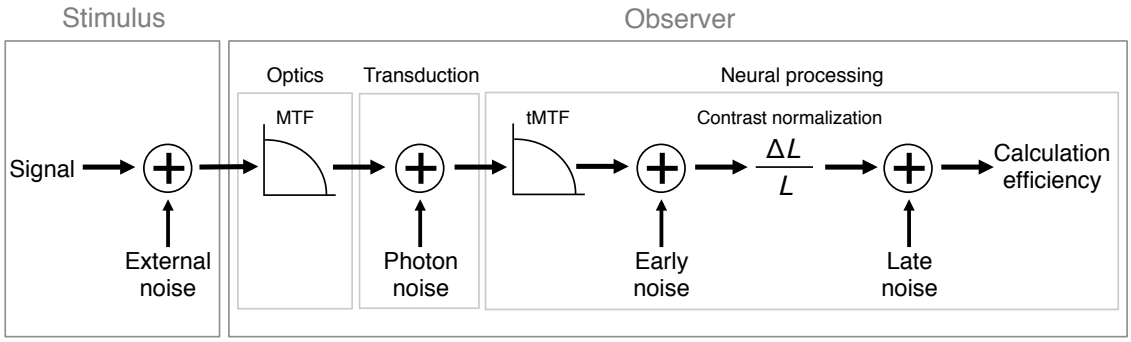

Figure 6.1: Observer's model comprising the photon noise, tMTF, the early noise, late noise and calculation efficiency (adapted from the model in chapter 5). The photon noise represents the fluctuations of phototransduction. The tMTF models the contrast gain as a function of the TF due to temporal blur modulating the relative impact of neural noise. The early and late noise represent internal noise occurring before and after contrast normalization.

6.2 Experiment 1

In the first experiment, motion sensitivity was measured at different temporal frequencies and luminance intensities to investigate which factor was most affected with aging.

6.2.1 Methods

Observers

The first experiment was conducted on twenty young adults (mean age = 26.5 years, SD = 3.79 years) and twenty-two older adults (mean age = 75.7 years, SD = 4.23 years) from the

Silversight cohort (Institut de la Vision, Paris). These participants were selected based on the following inclusion criteria: they had no ocular pathology (e.g., glaucoma, amblyopia, strabismus), no cognitive, neurobiological or vestibular disorders and participants were required to have a good visual acuity ($\geq$6/7.5, i.e. $\geq$0.8 in decimal units) with their dominant eye. For three older adults, one of the three noises had a negligible impact under all conditions, so its impact could not be quantified. The results of these three participants were not included in the analysis.

The visual correction of each participant was measured by an orthoptist before the experiment. The participants were wearing trial frames with trial lenses corresponding to their optimal correction for the distance to the screen (2 m).

Ethical approval was obtained from the (CPP Ile-de-France V) and the clinical screening was carried out under the supervision of the Clinical Investigation Center of Quinze-Vingt Hospital, Paris and informed consent was obtained.

Apparatus

Stimuli were presented on a 22.5-inch VIEWPixx LCD designed for psychophysical measurements. The refresh rate of the display was 120 Hz and the mean luminance intensity was 50 cd/m^2. At the viewing distance of 2 m, the spatial resolution of the screen was 128 pixels/degree of visual angle. The screen was the only source of light in the room. The Noisy-bit method (Allard and Faubert, 2008) implemented independently with each color gun made the 8-bit display perceptually equivalent to an analogue display having a continuous luminance resolution. The output intensity of each color gun was carefully linearized using a Minolta spectroradiometer CS-1000.

Stimuli and procedure

Observers were asked to discriminate the drifting direction (left or right) of a sine wave grating by pressing one of two keys. Auditory feedback was provided after each answer.

Motion sensitivity was measured by presenting on a screen a stimulus in motion in the absence and in the presence of noise at different temporal frequencies (0.9375, 1.875, 3.75, 7.5, 15, and 30 Hz) and at different luminance intensities (from 0.35 to 351 Td) using

neutral density filters. The spatial frequency of the grating was fixed to 0.5 cpd.

Stimuli were presented for 500 ms plus an onset and offset ramp (half-cosine) of 250 ms resulting in a total duration of 1 second. The spatial window was a circular aperture of 4 degrees of visual angle plus a smooth edge following a half-cosine of 0.5 degrees of visual angle. Stimuli were presented in the center of an 8.4×8.4 degree of visual angle grey square and were observed by the dominant eye through a 3 mm artificial pupil placed on the trial frame, at a distance of two meters from the screen.

The contrast thresholds were measured on a uniform grey background (condition without external noise) and on a noisy background (condition with external noise). The external noise added to the stimulus was a truncated filtered noise (Jules Étienne et al., 2016) with a low-pass filter with a cutoff at 2 cpd, temporally white (refreshed at 120 Hz), truncated at 1 standard deviation and set at 50% contrast. The energy of the noise was 323 μs.deg^2.

To evaluate calculation efficiency, contrast thresholds were measured in the presence of high external noise (Pelli and Farell, 1999). Given that calculation efficiency varies modestly with luminance intensity (Allard and Arleo, 2017), this measurement was carried out only at the highest luminance intensity (351 Td) and was assumed to be independent of the luminance intensity (but see experiment 2).

It was not possible to estimate the calculation efficiency in noise at 30 Hz (contrast thresholds of the elderly were to high), the calculation efficiencies measured for the other TFs (0.9375 to 15 Hz) were fitted with a quadratic function (Allard and Arleo, in preparation), which was then used to extrapolate and estimate the calculation efficiency at 30 Hz.

Contrast thresholds in the absence of external noise were measured at different luminance intensities and temporal frequencies, in order to discern three sources of internal noise and the tMTF. To do this, the conditions (luminance intensity and temporal frequency) were selected to evaluate the model's components from a previous study (chapter 5) that evaluated the sources of noise limiting contrast sensitivity as a function of temporal frequency and luminance intensity. Late noise affects motion sensitivity at high luminance intensities and drops with TF (chapter 5), so contrast thresholds were measured at all

temporal frequencies (0.9375 to 30 Hz) at the highest possible luminance intensity (351 Td). Photon noise affects motion sensitivity at low luminance intensities and low temporal frequencies, so contrast thresholds were measured at 0.9375, 1.875 and 3.75 Hz for which the observer had a retinal illuminance of 1, 3.51 and 11 Td respectively, obtained by using neutral density filters placed on the trial frame worn by the observer. Early noise affects motion sensitivity at high temporal frequencies, so the latter was measured at 3.75, 7.5, 15 and 30 Hz, values for which the retinal illuminance was set to 0.35, 3.51, 35.1 and 110 Td, respectively.

The contrast threshold was measured using the 3-down-1-up method (Levitt, 1971) in which the contrast of the stimulus increased or decreased depending on the observer's response with a step size of 1.25. The staircase was interrupted after 14 inversions and the contrast threshold was estimated as the geometric mean of the last 10 inversions. Such a staircase converged to a criterion level of 79% correct response. Two staircases were performed for each condition. The contrast threshold for a given condition was estimated as the geometric mean of the two measurements.

The experiment was conducted in two sessions of approximately two hours each. For each participant, the sessions were performed approximately one week apart. In the first session, the contrast thresholds were measured at the highest luminance intensity and in the second session they were measured at low luminance intensities. For the latter, the observers were light-adapted for 30 minutes by wearing on the trial frames neutral optical density filters of 3. For each session the order of the TFs was randomized and the two staircases for each TF were blocked. For the first session at the highest luminance intensity, two contrast thresholds were measured for each TF to estimate the equivalent input noise and the calculation efficiency: one in absence of noise and the other in high noise (except at 30 Hz where the contrast threshold of the elderly could not be measured because they were not sensitive enough to perceive the signal at the maximum contrast). For the second session, the participants adapted for the lowest luminance intensity (0.351 Td), were tested at that luminance intensity and then were tested at 1, 3.51, 11, 35.1, 110 and 351 Td.

The calculation efficiency (k) was estimated from equation (6.2.1) where E is the energy threshold, which is proportional to the squared contrast threshold (Bennett et al., 1999;

Pelli and Farell, 1999)

$$k = \frac{(d' + \sqrt{0.5})^2 N_{ext}}{E(N_{ext}) - E(0)} \tag{6.2.1}$$

The estimated calculation efficiencies as a function of the TF of each observer were fitted with quadratic functions (Allard and Arleo, in preparation) and these fits (i.e. k_{fit}) were then used to estimate the calculation efficiency at each relevant TF (0.9375 to 30 Hz) and estimate the equivalent input noise at the various luminance intensities:

$$N_{eq} = \frac{k_{fit}}{(d' + \sqrt{0.5})^2} E(0) \tag{6.2.2}$$

where $E(N_{ext})$ is the energy threshold in high noise, $E(0)$ the energy thresholds in absence of noise, and d'=1.16.

The yellowing of the lens, occurring with healthy aging, filters out primarily the short wavelengths, which reduces the retinal illuminance. To evaluate its potential effects, stimuli were also presented on a red background. Indeed the long wavelengths (red) are little affected by the yellowing of the lens that filters mainly shorter wavelengths. Therefore, if the age-related yellowing of the lens reduces considerably the retinal illumiance, it would increase the impact of the two noise sources that depend on luminance intensity (i.e., photon noise and early noise) and the age-related sensitivity loss would be less important with red stimuli for which the effect of lens yellowing would be negligible. This control was performed at 35.1 Td and at 15 Hz, at which the observer was limited by early noise, and at 2 Hz with an optical density filter of 1, at which the observer was limited by photon noise.

Model

The recently developed model (chapter 5) was adapted and applied on the estimated equivalent input noise of each observer ($N_{eq}(L,F)$) to the different luminance intensities (L) and temporal frequencies (F), which made it possible to estimate the tMTF and the 3 sources of internal noise according to the following equation:

$$N_{eq}(L, F) = \frac{N_{photon}}{L} + \frac{1}{tMTF^2(F)} \left(\frac{N_{early}}{L^2} + N_{late}(F)\right) \tag{6.2.3}$$

where N_{photon} is photon noise, N_{early} is early noise, and N_{late} is late noise.

Fitting the observer's model (Figure 6.1) to the equivalent input noise data ($N_{eq}(L,F)$) enabled to estimate the tMTF, and 3 sources of noise: photon noise, early noise and late noise. This model has 5 degrees of freedom: one for the photon noise (constant with respect to the TF), one for the early noise (constant with respect to the TF), two for the late noise (linear function with respect to TF), and one for tMTF (see chapter 5 for more details).

6.2.2 Results

Motion sensitivity

Motion sensitivity functions at different luminance intensities for the young and older adults are represented in Figure 6.2. At the highest luminance intensity, the motion sensitivity function follows the typical band-pass function peaking around 8 Hz. Older adults were less sensitive than the young adults at all TFs and all luminance intensities. The age-related decline was greater at low luminance intensities and at the highest TF.

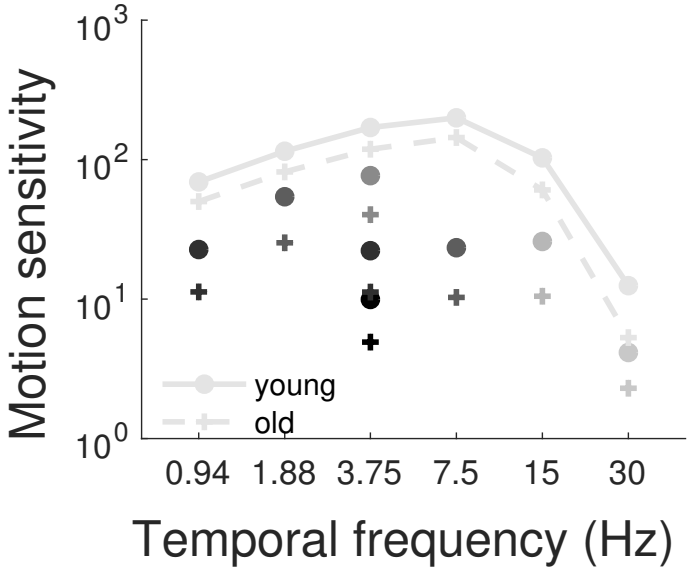

Figure 6.2: Motion sensitivity of young (circles) and older (crosses) observers. The color gradation from the darkest to the lightest gray represents the lowest to the highest luminance intensity, respectively. Motion sensitivity at the highest luminance intensity (i.e. 351 Td) was measured at all TFs (from 0.94 Hz to 30 Hz), so for clarity the markers were connected with lines for the young adults and dashed lines for the older adults. The error bars represent the standard error of the mean (most of them are not visible because they are smaller than the size of the marker).

Calculation efficiency

The calculation efficiency for young and older adults at high luminance intensity (351 Td) is shown in Figure 6.3. A two-way analysis of variance (ANOVA; age × TF) did not show any significant effect of the age ($F(1,37)=1.87$, $p=0.179$), but a significant effect of the TF ($F(4,148)=49.5$, $p<0.001$). A significant interaction between age and TF, ($F(4,148)=4.64$, $p<0.01$) was found, which can be explained by the greater calculation efficiency decline at high (e.g. 15 Hz) and low (1 Hz) temporal frequencies. Note that at 30 Hz, contrast thresholds in noise could not be measured, but was extrapolated from the fits.

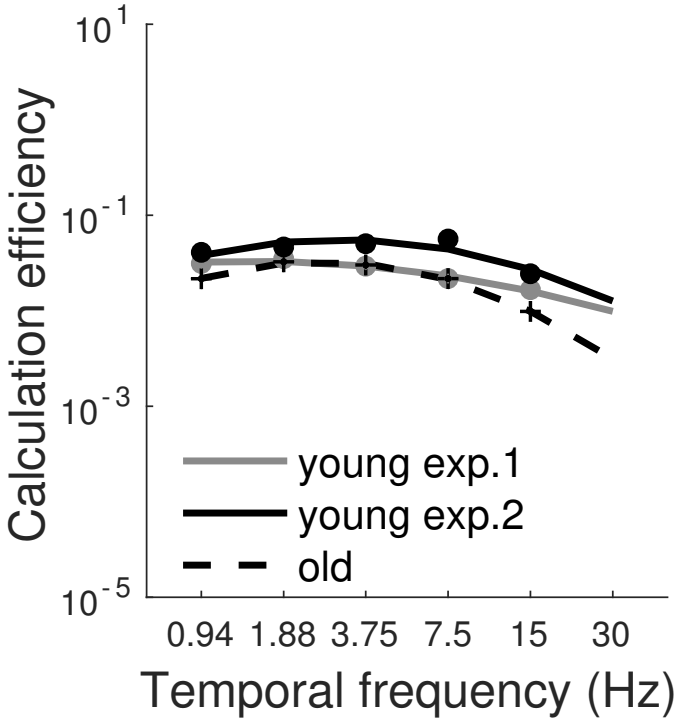

Figure 6.3: Calculation efficiency. Calculation efficiency as a function of TF at 351 Td for the young observers (grey circles, from experiment 1), for the older observers (black crosses, from experiment 1) and for the young observers at 111 Td (black circles, from experiment 2). The solid lines and dashed lines represent the fits (i.e. quadratic functions). The error bars represent the standard error of the mean (most of them are not visible because they are smaller than the size of the marker).

Equivalent input noise

Given equation (6.2.2), the equivalent input noise for young and older adults (Figure 6.4), at different luminance intensities and different TFs, was derived from the motion sensitivity measured in the absence of noise (Figure 6.2) and the fits of the calculation efficiency from the calculation efficiencies estimated at the highest luminance intensity (Figure 6.3), which was assumed to be independent of luminance intensity. Equivalent input noise was generally greater for the older observers, especially at low luminance intensities.

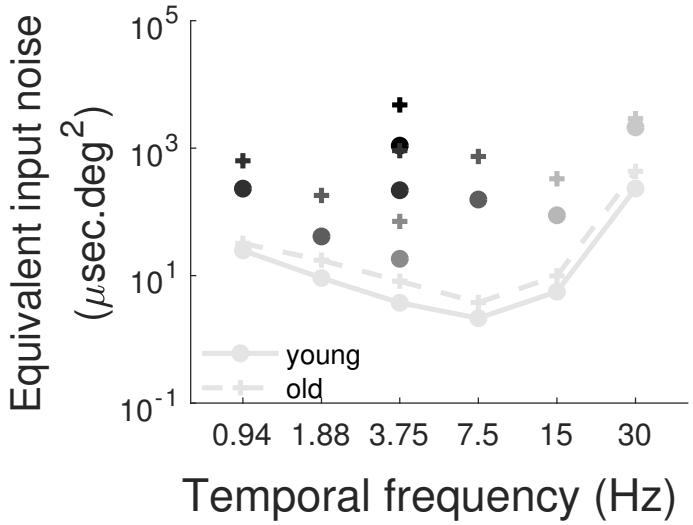

Figure 6.4: The equivalent input noise. The equivalent input noises for the young observers (circles, experiment 1) and for the older observers (crosses). The color gradation from the darkest to the lightest gray represents the lowest to the highest luminance intensity, respectively. The data at the highest luminance intensity (i.e. 351 Td) were connected for clarity, with lines for the young adults and dashed lines for the older adults. The error bars represent the standard error of the mean (most of them are not visible because they are smaller than the size of the marker).

Internal noise sources

Using the observer's model (Figure 6.1; equation (6.2.3)) on the equivalent input noise derived at different TFs and luminance intensities, the equivalent input noise was decomposed into photon noise, early noise, late noise and tMTF. The impact of these 3 sources of internal noise as well as temporal integration as a function of TF are represented in Figure 6.5 for young and older adults. The aging effects on these parameters are summarized in Figure 6.6.

Photon noise, which had only one degree of freedom as it was assumed to be temporally white (top left graph of Figure 6.5), was significantly affected with aging ($t(38)$=-4.85, p<0.01). More specifically, the effect of age on photon noise induced a decrease in sensitivity of a factor of 3.41 in energy units. This result suggests that photoreceptors of the elderly absorbed 3.41 times less photons than the ones of young adults.

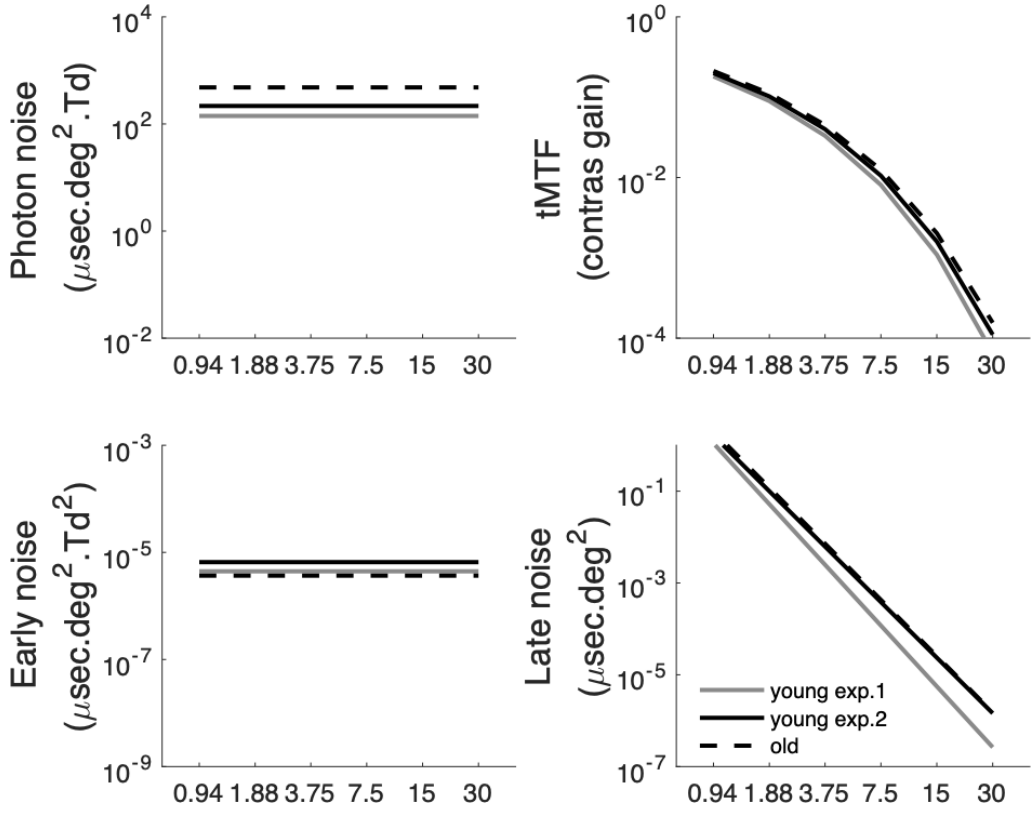

Figure 6.5: Sources of internal noise. The top left graph represents the photon noise as a function of TF (independent of TF). The top right graph represents the fitted tMTF. The bottom left graph represents the early noise (independent of TF). The bottom right graph represents the late noise as a function of TF (affine function). The mean fit of our model is represented by grey solid lines for the young observers in experiment 1, black dash lines for older observers (experiment 1) and black solid lines for the young observers in experiment 2.

The tMTF was also modeled by a single parameter representing the steepness of the low-pass temporal function (top right graph of Figure 6.5). A significant aging effect was also found ($t(38)=2.98$, $p<0.01$). Surprisingly, however, this result suggests that the visual system of the older observers attenuated less the high temporal frequencies (but see experiment 2). This result is unexpected given that sensitivity is more affected by aging at higher temporal frequencies.

Early noise was assumed to be temporally white (bottom left graph of Figure 6.5) and was fitted with a single parameter. No significant aging effect was found for early noise ($t(38)=0.35$, $p=0.73$), which suggests that healthy aging has little impact on early

noise.

The late noise, which drops with temporal frequency, was fitted by an affine function (bottom right graph of Figure 6.5). Older observers were found to have more late noise on average ($t(38)$=-2.13, p<0.05) as well as a shallower slope ($t(38)$=-2.09, p<0.05). This result suggests that the effect of aging on late noise tends to increase with temporal frequency (but see experiment 2).

Aging effect

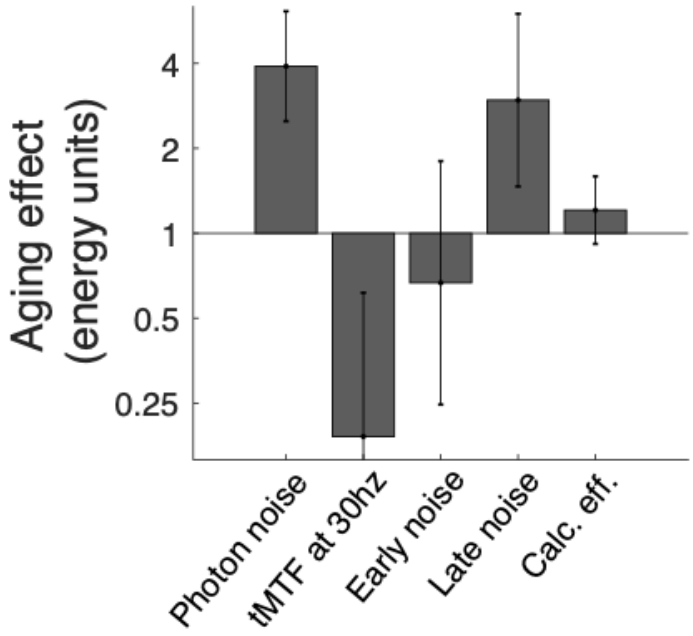

Figure 6.6: The aging effect on the different parameters of the model from experiment 1. The error bars represent a 95% confidence interval. An aging effect greater than 1 for photon noise and late noise represents more noise for elder observers. An aging effect smaller than 1 for early noise represents less noise for the elderly and for tMTF it represents a MTF that is less low-pass. An aging effect greater than 1 for calculation efficiency represents older observer being less efficient than the young observers.

Control of the yellowing of the lens

Results for the control of the yellowing of the lens occurring with healthy aging are shown in Figure 6.7. A three-way ANOVA (age × TF × luminance intensity) showed a significant effect of age ($F(1.152)$=130, p <0.001), that is, young observers had, on average, better

thresholds than older observers. A significant effect of the TF, ($F(1,152)=113$, $p<0.001$) was found, suggesting that all participants had better motion sensitivity at low temporal frequency. However, no significant effect of color was found ($F(1,152)=0.045$, $p=0.83$). There was no significant interaction between age and TF ($F(1,152)=1.2$, $p=0.27$). And there was no significant interaction between age and color, ($F(1,152)=3.12$, $p=0.08$) that is, the effect of aging was not statistically different for red and grey, suggesting a limited effect of the yellowing of the lens. Indeed, if age-related lens yellowing was responsible for a considerable portion of the effect of aging with grey stimuli, the effect of aging should have been significantly reduced with red stimuli.

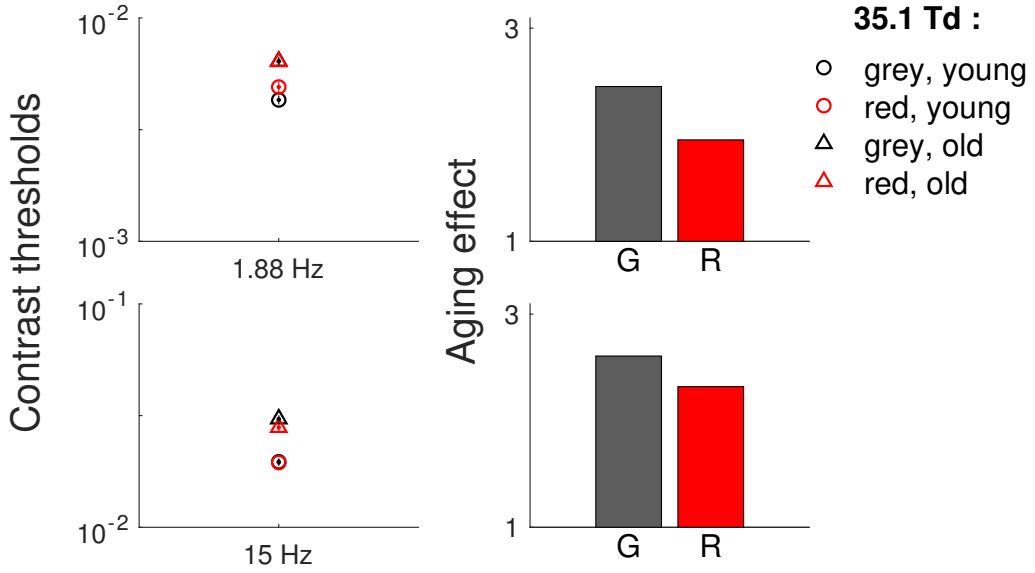

Figure 6.7: Experimental control of the yellowing of the lens. The left column represents the contrast thresholds for young and older observers when the stimulus was grey and red. The right column represents the aging effect in contrast units (contrast thresholds of older/young) for each condition. The first row represents the results of the experiment controlling the effect of low-frequency temporal lens yellowing for which photon noise was the dominant source of noise. The second row represents the results of the experiment controlling the effect of high-frequency temporal lens yellowing for which early noise was the dominant noise source. The error bars represent the standard error of the mean (most of them are not visible being smaller than the size of the marker).

6.3 Experiment 2

In the first experiment, a considerable aging effect was observed on photon noise suggesting that photoreceptors of older observers were absorbing about 3.4 times less photons. Given that calculation efficiency for motion sensitivity depends on luminance intensity (Allard and Arleo, 2017), a considerable lower absorption rate could have affected the measurement of the calculation efficiency. Thus, it is possible that the aging effect observed on calculation efficiency might have been biased by a lower absorption rate of the photoreceptors. Given that the equivalent input noise is derived from the threshold in absence of noise and the calculation efficiency, a bias in the calculation efficiency would also bias the equivalent input noise and could affect the other parameters derived from the equivalent input noise: photon noise, tMTF, early noise and late noise.

The aim of the second experiment was to evaluate the effect of aging on the calculation efficiency while roughly equating the amount of photons being absorbed. Given that elderly absorbed about 3.4 times less photons than the younger group on average (photon noise was 3.4 times greater for the older group in experiment 1), we evaluated the calculation efficiency (i.e., contrast threshold in high noise) of the young observers while reducing the retinal illuminance by a similar proportion.

6.3.1 Methods

The same apparatus, stimuli and procedure were used as for experiment 1. The study was conducted on the young participants of the experiment 1, but three of them were not available so only 17 were tested. The aging effect on the photon noise was corrected by a factor of 3.17 by an optical density filter of 0.5. The new measures of calculation efficiency were estimated in the same way as in the experiment 1 (equation (6.2.1)) and contrast thresholds were measured in noise at different TF (0.9375 to 15 Hz). Observers light-adapted for 2 min before the start of the experiment. Note that in this experiment 2 the contrast thresholds in noise were not measured at the same luminance intensity as in the experiment 1, (111 vs 351 Td), but this leads to comparable retinal illuminance as the elderly.

6.3.2 Results

Calculation efficiency

Reducing luminance intensity considerably affected the measurement of the calculation efficiency (Figure 6.3). As expected from a previous study (Allard and Arleo, 2017), reducing luminance intensity counter-intuitively improved the estimate of the calculation efficiency. Given that calculation efficiency depends on the amount of photons being absorbed and that young and older observers do not absorb the same amount of photons (different photon noises), the age-related effect on calculation efficiency per se should be compared under conditions in which both age groups absorb similar amount of photons, that is, the calculation efficiency measured under low luminance intensity for the young observers in experiment 2 and the calculation efficiency measured at high luminance intensity for the older observers in experiment 1.

A two-way analysis of variance ANOVA (age $\times$ TF) showed a significant effect of the age ($F(1,34)=23.4$, $p<0.001$), and a significant effect of the TF ($F(4,136)=42.9$, $p<0.001$). This is consistent with the polynomial function that fits the data. A significant interaction between these factors, age and TF, was also found ($F(4,136)=4.7$, $p<0.001$), suggesting that the effect of aging on calculation efficiency varies with the TF.

Equivalent input noise

Given that the equivalent input noise is derived from the calculation efficiency and the thresholds in absence of noise, changing the calculation efficiency has an impact on the estimate of the equivalent input noise. Thus, equivalent input noise needs to be reassessed. As shown in Figure 6.8, equivalent input noise for young and older adults were remarkably similar at the highest luminance intensity and a smaller aging effect compared to experiment 1 (Figure 6.4) was observed at low luminance intensities.

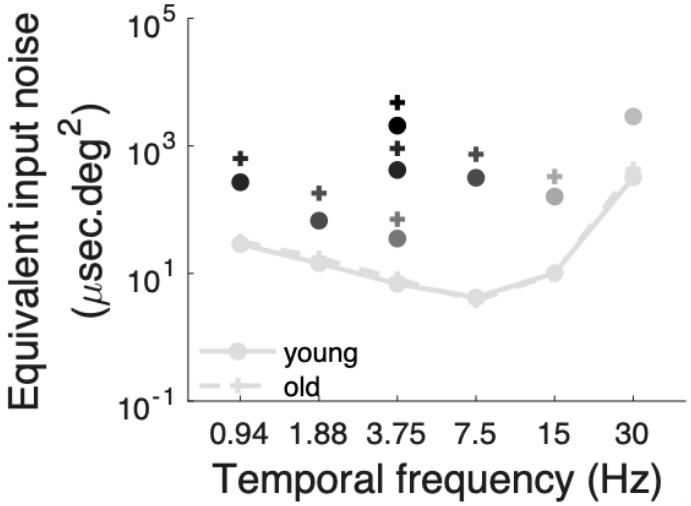

Figure 6.8: The equivalent input noise. The equivalent input noises for the young observers (circles, experiment 2) and for the older observers (crosses). The color gradation from the darkest to the lightest gray represents the lowest to the highest luminance intensity, respectively. The data at the highest luminance intensity (i.e. 351 Td) were connected for clarity, with lines for the young adults and dashed lines for the older adults. The error bars represent the standard error of the mean (most of them are not visible because they are smaller than the size of the marker).

Internal noise sources

The parameters of the model for young and older adults at different temporal frequencies and luminance intensities are represented in the Figure 6.6 and summarized in Figure 6.9. Photon noise was significantly affected by aging ($t(35)$=-2.82, p<0.01). This result suggests that elderly had more photon noise than younger adults. More specifically, older adults had 2.53 times more photon noise than the young observers. This result suggests that in the current study, photoreceptors of the elderly absorbed 2.53 times less photons than the ones of the young observers. No significant aging effect was found on tMTF ($t(35)$=1, p=0.32), or early noise ($t(38)$=0.35, p=0.73). The late noise being adjusted by an affine function, the effect of aging on its two parameters, the slope, and the mean have been studied: the effect of aging, on the mean (t(35)=-0.65, p=0.52) and the slope ($t(35)$=0.23, p=0.77) were not significant. Note that given that equivalent input noise at the highest luminance intensity is limited by late noise and no effect of aging was observed in those

conditions, it is not surprising that we observe no effect of aging on late noise and the tMTF (which modulates the impact of late noise).

Aging effect

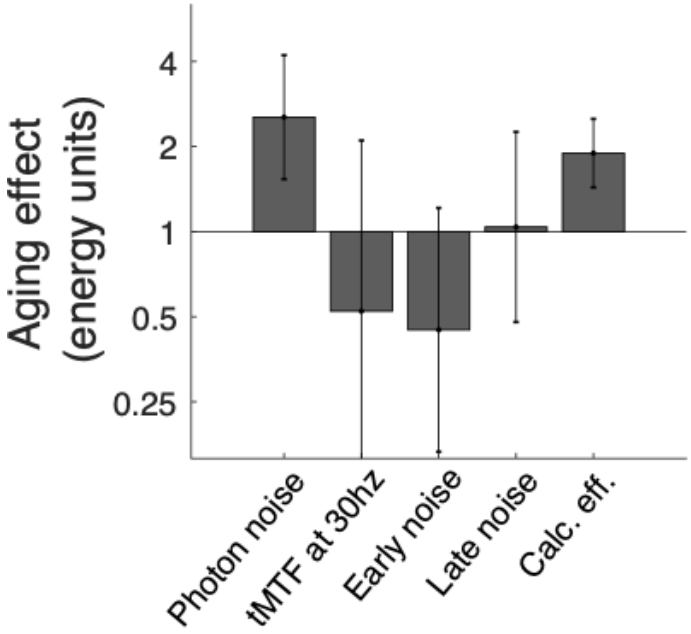

Figure 6.9: The aging effect on the different parameters of the model from experiment 2. The error bars represent a 95% confidence interval. An aging effect greater than 1 for photon noise and late noise represents more noise for elder observers. An aging effect smaller than 1 for early noise represents less noise for the elderly and for tMTF it represents a MTF that is less low-pass. An aging effect greater than 1 for calculation efficiency represents older observers being less efficient than the young observers.

The second experiment shows that equating the amount of photons being absorbed between young and older observers is important. The first experiment suggests that elderly had more late noise and less temporal blur, but after equating for the amount of photons absorbed (experiment 2), these aging effects disappeared.

6.4 General discussion

When roughly equating the amount of photons being absorbed by the photoreceptors between the two age groups, the current study found that elderly had more photon noise and a lower calculation efficiency, however no significant effect was found on tMTF, early noise and late noise. These results suggest that healthy aging affects the amount of photon absorbed by photoreceptors and require a greater signal-to-noise ratio to detect the signal. On the other hand, we found no evidence that aging affected the amount of neural noise within the visual system either at the retinal level (i.e., early noise) or cortical level (i.e., late noise), and no evidence that aging affected the tMTF (i.e., temporal blur due to the early integration time). So the loss of motion sensitivity with aging would be mainly due to an increase in photon noise and a decrease in calculation efficiency.

The increase in photon noise with aging suggests that photoreceptors in elderly absorbed 2.5 times fewer photons than those in younger adults. Two ocular causes could reduce the proportion of photons being absorbed by photoreceptors: senile miosis (reduction of pupillary diameter naturally related to healthy aging), and yellowing of the lens (tendency to filter the light of short wavelengths). In the current study, however, the effect of senile miosis was neutralized by the use of an artificial pupil, and controlled conditions reveal that similar aging effects were observed even when using long wavelengths (red light) that are little affected by the yellowing of the lens. This suggests that senile miosis and yellowing of the lens had little impact on the photon absorption rate of photons in the elderly. These results are analogous to the ones of our previous study investigating the effect of aging on contrast sensitivity (Silvestre et al., 2019), which suggests that the absorption efficiency of cones is affected with aging. Indeed, given that there is no considerable loss of cones with healthy aging, the fact that less photons are absorbed suggests that the absorption rate of cones is considerably affected with aging. As a result, elderly are expected to have more difficulty perceiving motion under dim light, such as when driving at night.

Regarding neural noise (early noise and late noise), whether at one level of treatment or another, it is not affected by aging, it is a surprising fact because some data from the literature suggests an increase of the spontaneous activity of neurons (Leventhal et al., 2003). It can therefore be concluded that there is no effect of aging on the transmission of

visual information. However, these data are not necessarily inconsistent with the current findings. Indeed, the internal noise paradigm used in the current study does not evaluate all sources of internal noise within the visual system, but only the ones that limit motion sensitivity. It is possible that a source of internal noise is affected with aging, but this source of noise does not noticeably affect motion sensitivity because of another noise having a greater impact, which happens to be little affected with aging. Indeed, there are many internal noise sources occurring early and late in the visual system and the psychophysical paradigm used here only measures the one that is limiting motion sensitivity.

Our study found no significant aging effect on tMTF, which were found to be remarkably similar in young and older observers. These results suggest that the temporal properties of cones and early neural processes are relatively preserved with healthy aging.

The age-related decline in calculation efficiency (when equating for the amount of photons being absorbed) shows that elderly required a greater signal-to-noise ratio to detect the signal. Indeed, in high external noise, the internal noise has a negligible impact and the contrast threshold only depends on the calculation efficiency. The current study cannot determine why older observers required a greater signal-to-noise ratio, but we can speculate. This age-related decline in calculation efficiency for motion sensitivity is analogous to the age-related decline in calculation efficiency for contrast sensitivity (Silvestre et al., 2019) and was attributed to a decline in the ability to integrate spatial information. Analogously, the age-related calculation efficiency decline for motion sensitivity could be due to an impaired spatial or temporal integration process, that is, elderly may focus on a smaller spatial area or may not be able to consider only the moments during the stimulus presentation. Further studies are required to test these hypotheses.

6.5 Conclusion

To conclude, our study tried to better characterize the origin of the loss of motion sensitivity related to healthy aging. The results suggest that the main causes of age-related motion sensitivity losses is the absorption rate of cones, which affects motion sensitivity under dim light, and the signal-to-noise ratio, which affects motion sensitivity under all brightness.

Surprisingly, the current study suggests that the temporal properties of early processes and the level of neural noise affecting motion sensitivity are little affected with healthy aging.

Part III

General discussion

Chapter 7

Discussion

7.1 The internal noise paradigm

7.1.1 Achievements

In this thesis, a new paradigm was developed to further understand the internal factors limiting the CSF and TCSF, which are estimations of the visual perception limits for the detection of stimuli with different spatial and temporal properties. This internal noise paradigm dissociates the equivalent input noise (i.e. estimation of the impact of the internal noise of an observer) into three sources of noise located at the photoreceptor level (photon noise), retinal level (early noise) and cortical level (late noise). This dissociation enable a better comprehension of the visual system limits and of the processing of visual information. Indeed these sources of noise being invariant to some properties of the visual stimulus (e.g. photon noise and early noise independent of TF), it gives us more information about the processing of visual information at a specific location of the visual system. This paradigm is a complement to the external noise paradigm, which factorizes contrast sensitivity into equivalent input noise and calculation efficiency, and adds another level of comprehension to the underlying causes of the limitation of the human's visual system.

The spatio-temporal properties found for the different internal noise sources relate to the

physiological processing of the different types of neurons involved in each of these sources of noise. The studies we conducted on the observer's model to find the best fitting functions for the three different sources of noise, gave us the following spatial and temporal properties in our final model (see Results section in chapter 3 and 5): photon noise was assumed to be spatially and temporally white fitting the characteristics of the transduction occurring at the photoreceptor level, which process a photon as an energy quantum only regardless of the spatio-temporal information it carries (i.e. photon absorption is uncorrelated over space ans time). Early noise was found to decrease as SF increased and assumed to be temporally white. Based on the internal noise paradigm it is assumed that this source of noise is at the retinal level between the photoreceptors and the ganglion cells. However, further studies of the physiological properties of the neurons located in this region (i.e. bipolar, amacrine and horizontal cells) need to be carried out to locate more precisely the main source of early noise. Late noise was found to decrease with SF and TF. However, the specific location or locations of this source of noise is still unclear. Based on its variation with SF (i.e. decreasing with a slope of -2) it was suggested by Pelli and Farell (1999) and Raghavan (1995) that this would be expected if neural density at the cortical level (i.e. visual area V1 for a detection task) was inversely proportional to receptive field size and receptive field size was inversely proportional to squared SF. In this thesis (i.e. chapter 3 and 5), similar conclusions were made. However, these findings alone are not strong enough to conclude that this source of noise is located solely in the visual area V1 and might in fact be generated by different regions of the visual system.

The internal noise paradigm also provides the spatio-temporal and luminance domain where each of the three noise sources limits contrast sensitivity. Chapter 3 and 5 show that photon noise limits visual perception over a wide range of spatial, temporal and luminance domain, which imply that our perception of the world is often limited by the first processing stage of the visual system. This finding confirms what Pelli (1990) had predicted with a smaller range of conditions. On the other hand, the spatio-temporal and luminance domain of the early noise and late noise have not been well characterized in the literature. Indeed, in chapter 3 and 5, late noise have been estimated for the first time at higher SF and TF. Early noise, to our knowledge, has never been estimated before and was therefore defined in this thesis for the first time. Indeed, early noise limits visual perception mostly at high

TF and no study have investigated internal noise limiting temporal sensitivity.

In summary, the internal noise paradigm developed in this thesis allowed us to further understand the underlying causes limiting visual perception by distinguishing three sources of noise from the equivalent input noise and characterizing their spatio-temporal properties and the spatio-temporal and luminance domain where each source of noise limits visual perception.

7.1.2 Implications

The internal noise paradigm is a simple approach that enables us to estimate three different sources of noise limiting contrast sensitivity in different luminance conditions. This internal noise paradigm presents some similarities and differences with Pelli's paradigm (Pelli, 1990; Raghavan, 1995). The main resemblance between the two approaches is to further decompose the equivalent input noise as the sum of different internal noise sources. Therefore, the main difference rely in the characterization of the different internal noise sources. The photon noise and late noise are defined quite similarly in both models, with photon noise being spatially and temporally white and late noise depending on SF. However, early noise is not defined in Pelli's model and ganglion cell noise is not define in our model. This is not surprising as early noise limits contrast sensitivity at high TF in photopic condition or at low SF at very low luminance conditions (mesopic condition), which are not conditions that have been investigated by Pelli. Likewise, peripheral vision, where ganglion cell noise dominates, has not been investigated in this thesis. One note of interest is that both models reduces the limitation of contrast sensitivity by internal noise to only three different sources.

The characterization in this thesis of the spatio-temporal and luminance domains of each source of noise could be useful for future psychophysical studies that want to investigate a specific processing stage of the visual system. Indeed, by looking at the 3-dimensional map reporting the boundaries of each source of noise could give the experimenter the temporal, spatial and luminance conditions in which he needs to measure the observer's threshold for the purpose of his experiment.

7.1.3 Perspectives

A prospect would be to extend the internal noise paradigm to peripheral vision to determine which internal noise sources limits contrast sensitivity in this condition and how these noises vary with eccentricity. Pelli and Yiltiz (2017) have recently extended their paradigm to the peripheral vision and found that ganglion cell noise (i.e. spontaneous activity at the retinal ganglion cell level) increased with eccentricity. Since our internal noise paradigm differs from Pelli's paradigm but do not invalidate it, it could be interesting to see how our approach conciliate with Pelli's findings.

Another interesting prospect for the internal noise paradigm would be to adapt it to clinic to be able to detect pathologies at an early stage. A drawback in clinic is how visual perception is evaluated, which is often not representative of the full potential of the human visual perception. Indeed, the clinical estimation of visual perception is visual acuity, which is generally measured with ETDRS (Early Treatment Diabetic Retinopathy Study) charts in a bright environment where the patient reports the smallest letter that he can read. This clinical quantification of visual perception is limited to central vision under a bright light condition (i.e. photopic vision) and to static visual input detection, which may not be sufficient to quantify vision loss due to eye pathologies affecting contrast sensitivity in peripheral vision or in low luminance conditions. I think the detection of eye pathologies at an early stage (i.e. before the apparition of symptoms) can be improved in clinic by adding a simple psychophysical experiment adapted to clinical screening and based on the internal noise paradigm. This new approach could, for instance, quantify photon noise and a predetermined scale could tell the doctor if the photon noise level is abnormal or not depending on the age of the patient. A higher level of photon noise could, for instance indicate that the patient has an AMD (age-related macular degeneration) at an early stage whereas a classical clinical approach using ophthalmoscopy to detect drusens (physiological mark of AMD) could miss an early detection of AMD since the approach is qualitative and is therefore subject to more variance. Furthermore, this internal noise paradigm could also be adapted for the detection of pathologies affecting visual perception at a higher cognitive level (e.g. autism, schizophrenia), where the late noise and the calculation efficiency will be of more interest than the photon noise.

7.2 Age-related contrast sensitivity loss

7.2.1 Achievements

The internal noise paradigm allowed us to evaluate how the three internal noise sources were affected with healthy aging and to further characterize the factors responsible for the age-related sensitivity loss. The results of the current thesis suggest that only two of the three internal noise sources were affected with aging: photon noise and late noise. Photon noise was found to increase considerably with aging, corresponding to fewer photons absorbed by the elderly than the young probably due to less efficient cones. Late noise was found to be affected by a factor of two when the visual input to detect was a static stimulus but was not affected by aging when the visual input to detect was a drifting stimulus. These different results for static and motion detection suggest that late noise might not originate from the same sources in these two conditions and that neurons processing temporal information (e.g. a drifting stimulus) is not affected by aging.

Calculation efficiency, which is another factor, besides internal noise, that limits contrast sensitivity was found to be affected by aging in both static and motion detection task. Based on the results in chapter 4 and a previous study (Allard et al., 2013b), we suggested that the decrease in calculation efficiency with aging was due to a decline of the spatial integration (i.e. the aging effect on calculation efficiency increases as the number of visible cycles of the signal increases).

Altogether these results give us a better comprehension of the underlying causes of the age-related contrast sensitivity loss.

7.2.2 Implications

Our findings of the underlying causes of the decline of the older adults' visual perception could help understand the loss of autonomy of the elderly for certain everyday tasks. For instance, studies have shown (Gruber et al., 2013) that the elderly population had more difficulties driving at night (e.g. more accidents were recorded). Our findings that the elderly population absorb fewer photons than the young due to less efficient cones (chapter

4 and 6) could account for the greater difficulties the elderly population encounters when performing tasks in dim light conditions. These findings on the factors affecting the age-related visual perception loss could be broadcast to the elderly population to help them understand the reasons of their limitations and help them adapt their daily activities accordingly in order to maintain their autonomy. Moreover, having a population that is more aware of its limitations and knowing that these limitations are part of a normal healthy aging process could help the older adults accept these changes and could avoid the seclusion and depression of this population. Furthermore, the main factor responsible for the age-related sensitivity loss being at the first processing stage of the visual input (i.e. at the photoreceptor level) it is more accessible for clinical observations and it might be easier to repair in a near future.

7.2.3 Perspectives

A prospect would be to develop a new clinical tool using the internal noise paradigm in order to follow-up early changes of the visual perception of the elderly population. Indeed, a short psychophysical experiment could be set up to measure contrast sensitivity in a condition where photon noise is the limiting noise source and a scale could be develop to determine if the photon noise level is abnormal. This clinical tool could be used during a normal ophthalmological check-up to give feedback to the older adult about his limitations so he could adapt his way of living (e.g. by no longer driving at night).

A future project in continuity with our findings is to develop a product to increase the visual comfort of observers and particularly of older adults. A patent was already filled with Essilor International company, which is the industrial application of the internal noise paradigm. The concept of this innovation is to develop eyeglasses that will be able to adjust their opacity automatically and in real time, according to the environmental luminance intensity. In other words, these eyeglasses will be able to adjust to the brightness of the environment, by for instance reducing glare in bright conditions while keeping the optimal sensitivity of the observer in this condition. These next generation eyeglasses Essilor is looking to develop could automatically become sunglasses according to the ambient light and the observer's sensitivity. This could particularly increase the older adults visual

comfort as they are particularly sensitive to glare. Indeed, reducing the light environment to decrease the older adult's glare without decreasing the light environment to much to not fall into a luminance condition where the observer is limited by de Vries-Rose law (i.e. limited by photon noise) as the sensitivity of older adults is greatly affected in this luminance condition. These eyeglasses for the elderly population will therefore allow them to reduce their glare in bright conditions without affecting their sensitivity (i.e. by staying in the Weber's law range, where late noise is the limiting source of noise).

7.3 Conclusions

In this thesis, the underlying causes of age-related vision losses were further characterized using our internal noise paradigm, which enabled the estimation of the impact of aging on internal noise sources located at different stages of the visual system. The elderly population absorb fewer photons than the young adults due to less efficient cones, which could explain their greater difficulties performing tasks in dim light conditions. Furthermore, the internal noise paradigm could be adapted to clinic as it would be a good tool to detect pathologies at an early stage and it could also be used in future fundamental psychophysical researches to further investigate the limiting factors of visual perception (e.g. in periphery).

Appendix A

List of contributions

Articles

Silvestre D., Arleo A. & Allard R. (2019), Healthy aging impairs photon absorption efficiency of cones, *Investigative Ophthalmology and Visual Science*, 60(2):544-551

Silvestre D., Arleo A. & Allard R. (2018), Internal noise sources limiting contrast sensitivity, *Scientific Reports*, doi:10.1038/s41598-018-20619-3

Silvestre D., Cavanagh P., Arleo A. & Allard R. (2017), Adding temporally localized noise can enhance the contribution of target knowledge on contrast detection, *Journal of Vision*, 2017;17(2):5. doi: 10.1167/17.2.5.

Patents

Allard R., **Silvestre D.**, (2018), Method and system for characterizing the visual system of a subject, EP18305379.2. 2018/03/30. France

Allard R., **Silvestre D.**, Chenguiti Y., (2017), Method and system for selecting a color filter, optical article comprising such a color filter, EP17306709.1. 2017/12/06. France

Poster presentations

Silvestre D., Arleo A. & Allard R. (December 18, 2017). Spatiotemporal maps of quantal noise, early and late neural noise limiting contrast sensitivity. Internal seminar, Essilor, Créteil, France

Silvestre D., Arleo A. & Allard R. (May 19-23, 2017). Spatiotemporal maps of quantal noise, dark light and late neural noise limiting contrast sensitivity. Vision Science Society, Florida, US

Silvestre D., Arleo A. & Allard R. (September 15, 2016). Internal noises limiting contrast sensitivity across different luminance levels. Internal Seminar, Institut de la Vision, Paris, France

Silvestre D., Arleo A. & Allard R. (May 13-18, 2016). Contrast sensitivity: Measuring late internal noise across spatial frequencies. Vision Science Society, Florida, US

Silvestre D., Arleo A. & Allard R. (September 11, 2015). Psychophysical study on contrast sensitivity using the external noise paradigm. Scientific day, Institut de la Vision, Paris, France

Oral presentations

November 29, 2018, Healthy aging impairs photon absorption efficiency of cones, Scientific Day, Institut de la Vision, Paris, France

August 30, 2018, Absorption efficiency of cones is considerably affected by healthy aging, European Conference on Visual Perception (ECVP), Trieste, Italy

March 13, 2018, Internal noise sources limiting contrast sensitivity: a healthy aging study, Vision and cognitive Neuroscience laboratory, McMaster University, Hamilton, Canada

Award

L'Oréal-UNESCO for Women in Science (15000€)

Bibliography

Allard, R. and Arleo, A. (2017). Factorizing the motion sensitivity function into equivalent input noise and calculation efficiency. *Journal of Vision*, 17(1):17.

Allard, R. and Cavanagh, P. (2011). Crowding in a detection task: External noise triggers change in processing strategy. *Vision Research*, 51(4):408–416.

Allard, R. and Faubert, J. (2008). The noisy-bit method for digital displays: Converting a 256 luminance resolution into a continuous resolution. *Behavior Research Methods*, 40(3):735–743.

Allard, R. and Faubert, J. (2013). Zero-dimensional noise is not suitable for characterizing processing properties of detection mechanisms. *Journal of Vision*, 13(10)(25):1–3.

Allard, R. and Faubert, J. (2014a). Motion processing: The most sensitive detectors differ in temporally localized and extended noise. *Frontiers in Psychology*, 5(MAY):1–5.

Allard, R. and Faubert, J. (2014b). To characterize contrast detection, noise should be extended, not localized. *Frontiers in Psychology*, 5:1–7.

Allard, R., Lagacé-nadon, S., and Faubert, J. (2013a). Feature tracking and aging. *Frontiers in Psychology*, 4(427):1–8.

Allard, R., Renaud, J., Molinatti, S., and Faubert, J. (2013b). Contrast sensitivity, healthy aging and noise. *Vision Research*, 92:47–52.

Artal, P., Berrio, E., Guirao, A., and Piers, P. (2002). Contribution of the cornea and internal surfaces to the change of ocular aberrations with age. *Journal of the Optical Society of America.*, 19(1):137–143.

Artal, P., Guirao, A., Berrio, E., Piers, P., and Norrby, S. (2003). Optical aberrations and the aging eye. *International Ophthalmology Clinics*, 43(2):63–77.

Baldwin, A. S., Baker, D. H., and Hess, R. F. (2016). Noise Studies Actually Measure ? Noise vs . Nonlinearity in Different Masking Paradigms. *PloS one*, pages 1–25.

Baldwin, W. R. and Mills, D. (1981). A longitudinal study of corneal astigmatism and total astigmatism. *American journal of optometry and physiological optics*, 58(3):206–211.

Barlow, H. B. (1956). Retinal noise and absolute threshold. *Journal of the Optical Society of America*, 46(8):634–639.

Barlow, H. B. (1957). Increment thresholds at low intensities considered as signal/noise discriminations. *Journal of Physiology*, pages 469–488.

Barlow, H. B. (1977). *Retinal and central factors in human vision limited by noise*. New-York Academic Press, New-York.

Bejjanki, V. R., Zhang, R., Li, R., Pouget, A., Green, C. S., and Lu, Z.-l. (2014). Action video game play facilitates the development of better perceptual templates. *PNAS*, 111(47).

Bennett, P. J., Sekuler, A. B., and Ozin, L. (1999). Effects of aging on calculation efficiency and equivalent noise. *Journal of the Optical Society of America*, 16(3):654–668.

Birren, J. E. and Schaie, K. W. (2006). *Handbook of the psychology of aging*. Elsevier, USA, 6th edition.

Bulmer, M. G., Howarth, C. I., Cane, V., Gregory, R. L., and Barlow, H. B. (1957). Noise and the visual threshold.

Charman, W. N. (1991). Wavefront Aberration of the Eye: A Review. *Optometry and Vision Science*, 68(8):574–583.

Chen, G., Hou, F., Yan, F.-F., Zhang, P., Xi, J., Zhou, Y., Lu, Z.-L., and Huang, C.-B. (2014). Noise provides new insights on contrast sensitivity function. *PloS one*, 9(3):e90579.

Cohen, J. (1988). *Statistical power analysis for the behavioral sciences*. Lawrence Erlbaum associates, second edi edition.

Cunea, A. and Jeffery, G. (2007). The ageing photoreceptor. *Visual Neuroscience*, 24(2):151–155.

Curcio, C. A. and Drucker, D. N. (1993). Retinal Ganghon Cells in Alzheimer's Disease. *Annals of Neurology*, 33(3):248–257.

Curcio, C. A., Millican, C. L., Allen, K. A., and Kalina, R. E. (1993). Aging of the human photoreceptor mosaic: Evidence for selective vulnerability of rods in central retina. *Investigative Ophthalmology and Visual Science*, 34(12):3278–3296.

Curcio, C. A., Sloan, K. R., Kalina, R. E., and Hendrickson, A. E. (1990). Human photoreceptor topography. *Journal of Comparative Neurology*, 292(4):497–523.

Dakin, S. C., Bex, P. J., Cass, J. R., and Watt, R. J. (2009). Dissociable effects of attention and crowding on orientation averaging. *Journal of Vision*, 9(11):1–16.

Davis, E. T. and Graham, N. (1981). Spatial frequency uncertainty effects in the detection of sinusoidal gratings. *Vision Research*, 21(5):705–712.

Davis, E. T., Kramer, P., and Graham, N. (1983). Uncertainty about spatial frequency, spatial position, or contrast of visual patterns. *Perception & psychophysics*, 33(1):20–28.

de Vries, H. L. (1943). The quantum character of light and its bearing upon threshold of vision, the differential sensitivity and visual acuity of the eye. *Physica*, 10(7):553–564.

Derefeldt, G., Lennerstrand, G., and Lundh, B. (1979). Age variations in normal human contrast sensitivity. *Acta ophthalmologica*, 57(1979):679–690.

Elliott, D., Whitaker, D., and MacVeigh, D. (1990). Neural contribution to spatiotemporal contrast sensitivity decline in healthy ageing eyes. *Vision Research*, 30(4):541–547.

Fechner, G. (1860). Elemente der Psychophysik. *Elemente dur psychophysik*, page 572.

Fernandes, T. M. D. P., Almeida, N. L. D., and Santos, N. A. D. (2017). Effects of smoking

and smoking abstinence on spatial vision in chronic heavy smokers. *Scientific Reports*, 7(1):1–7.

Fledelius, H. C. (1988). Refraction and eye size in the elderly. A review based on literature, including own results. *Acta ophthalmology*, 66(3):241–248.

Freeman, J. and Pelli, D. G. (2007). An escape from crowding. *Journal of vision*, 7(2):22.1–14.

Fry, G. A. (1969). Visibility of sine-wave gratings. *Journal of the Optical Society of America*, 59(5):610–617.

Gao, H. and Hollyfield, J. G. (1992). Aging of the human retina. Differential loss of neurons and retinal pigment epithelial cells. *Investigative ophthalmology & visual science*, 33(1):1–17.

Gartner, S. and Henkind, P. (1981). Aging and degeneration of the human macula. 1. Outer nuclear layer and photoreceptors. *The British journal of ophthalmology*, 65(1):23–8.

Giersch, A., Speeg-Schatz, C., Tondre, M., and Gottenkiene, S. (2006). Impairment of contrast sensitivity in long-term lorazepam users. *Psychopharmacology*, 186(4):594–600.

Greenwood, J. A., Bex, P. J., and Dakin, S. C. (2009). Positional averaging explains crowding with letter-like stimuli. *Proceedings of the National Academy of Sciences of the United States of America*, 106:13130–13135.

Gregory, R. L. and Cane, V. (1955). A statistical information theory of visual thresholds. *Nature*.

Gruber, N., Mosimann, U. P., Müri, R. M., and Nef, T. (2013). Vision and night driving abilities of elderly drivers. *Traffic Injury Prevention*, 14(5):477–485.

Habak, C. and Faubert, J. (2000). Larger effect of aging on the perception of higher-order stimuli. *Vision research*, 40:943–950.

Hecht, S., Shlaer, S., and Pirenne, M. H. (1942). Energy, quanta and vision. *The Journal of general physiology*, pages 819–840.

Hedges, L. V. (1981). Distribution theory for Glass's estimator of effect size and related estimators. *Journal of educational statistics*, 6(2):107–128.

Jules Étienne, C., Arleo, A., and Allard, R. (2016). Maximizing noise energy for noise-masking studies. *Behavior Research Methods*, 49(4):1278–1290.

Kandel, E. R., Schwartz, J. H., and Jessel, T. M. (2000). *Principles of neural science Fourth edition*. Mcgraw-hil edition.

Kelly, D. H. (1972). Adaptation effects on spatio-temporal sine-wave thresholds. *Vision Research*, 12(1948):89–101.

Kelly, D. H. and Wilson, H. R. (1978). Human flicker sensitivity: Two stages of retinal diffusion. *Science*, 202(4370):896–899.

Kim, C. B. and Mayer, M. J. (1994). Foveal flicker sensitivity in healthy aging eyes. II. Cross-sectional aging trends from 18 through 77 years of age. *Journal of the Optical Society of America. A, Optics, image science, and vision*, 11(7):1958–69.

Leventhal, A. G., Wang, Y., Pu, M., Zhou, Y., and Ma, Y. (2003). GABA and Its Agonists Improved Senescent Monkeys. *Science*, 300:812–815.

Levi, D. M. (2008). Crowding—An essential bottleneck for object recognition: A mini-review. *Vision Research*, 48(5):635–654.

Levitt, H. (1971). Transformed up-down methods in psychoacoustics. *The Journal of the Acoustical Society of America*, 49(2):Suppl 2:467.

Loewenfeld, I. E. (1979). Pupillary changes related to age. In Thompson, H. S. and Frisen, D. R., editors, *Topics in neuro-ophthalmology*, pages 124–150. Williams & Wilkins, Baltimore.

Lombardo, M. and Lombardo, G. (2010). Wave aberration of human eyes and new descriptors of image optical quality and visual performance. *Journal of Cataract and Refractive Surgery*, 36(2):313–331.

Losada, M. A., Navarro, R., and Santamaría, J. (1993). Relative contributions of optical

and neural limitations to human contrast sensitivity at different luminance levels. *Vision Research*, 33(16):2321–2336.

Lu, Z.-L. and Dosher, B. A. (1999). Characterizing human perceptual inefficiencies with equivalent internal noise. *Journal of the Optical Society of America. A, Optics, image science, and vision*, 16(3):764–78.

Lu, Z.-L. and Dosher, B. A. (2004). Perceptual learning retunes the perceptual template in foveal orientation identification. *Journal of Vision*, 4(1):44–56.

Lu, Z.-L. and Dosher, B. A. (2008). Characterizing observers using external noise and observer models: assessing internal representations with external noise. *Psychological review*, 115(1):44–82.

Mayer, M. J., Kim, C. B. Y., Svingos, A., and Glucs, A. (1988). Foveal flicker sensitivity in healthy aging eyes . I . Compensating for pupil variation. *Journal of the Optical Society of America*, 5(12):2201–2209.

Mellerio, J. (1987). Yellowing of the human lens: Nuclear and cortical contributions. *Vision Research*, 27(9):1581–1587.

Mendelson, D. N. and Schwartz, W. B. (1993). The effects of aging and population growth on health care costs. *Health Affairs*, 12(1):119–125.

Mueller, C. (1951). Frequency of seeing functions for intensity discrimination at various levels of adapting intensity. *The Journal of general physiology*, pages 463–474.

Mustonen, J., Rovamo, J., and Näsänen, R. (1993). The effects of grating area and spatial frequency on contrast sensitivity as a function of light level. *Vision Research*, 33(15):2065–2072.

Nagaraja, N. S. (1964). Effect of luminance noise on contrast thresholds. *Journal of the Optical Society of America*, 54(7):950.

Owsley, C. (2003). Contrast sensitivity. *Ophthalmology Clinics of North America*, 16(2):171–177.

Owsley, C. (2011). Aging and vision. *Vision Research*, 51(13):1610–1622.

Owsley, C., Sekuler, R., and Siemsen, D. (1983). Contrast sensitivity throughout adulthood. *Vision research*, 23:689–699.

Panda-Jonas, S., Jonas, J. B., and Jakobczyk-Zmija, M. (1995). Retinal photoreceptor density decreases with age. *Ophthalmology*, 102(12):1853–1859.

Pardhan, S. (2004). Contrast sensitivity loss with aging: sampling efficiency and equivalent noise at different spatial frequencies. *Journal of the Optical Society of America*, 21(2):169–175.

Pascolini, D. and Mariotti, S. P. (2012). Global estimates of visual impairment : 2010. *The British journal of ophthalmology*, 96(5):614–618.

Pelli, D. G. (1981). *Effects of visual noise*. thesis, Cambridge university.

Pelli, D. G. (1985). Uncertainty explains many aspects of visual contrast detection and discrimination. *Journal of the Optical Society of America. A, Optics and image science*, 2(9):1508–1532.

Pelli, D. G. (1990). The quantum efficiency of vision. *Vision: Coding and efficiency*, pages 3–24.

Pelli, D. G. and Farell, B. (1999). Why use noise? *Journal of the Optical Society of America. A, Optics, image science, and vision*, 16(3):647–653.

Pelli, D. G., Palomares, M., and Majaj, N. J. (2004). Crowding is unlike ordinary masking: Distinguishing feature integration from detection. *Journal of Vision*, 4(12):1136–1169.

Pelli, D. G. and Yiltiz, H. (2017). What internal noise source limits peripheral vision? *Journal of vision*, 17(10):775.

Raghavan, M. (1995). *Sources of visual noise*. thesis, Syracuse University.

Robson, J. G. and Graham, N. (1981). Probability summation and regional variations in contrast sensitivity curves across the visual field. *Vision Research*, 21(1):408–418.

Rose, A. (1942). The relative sensitivities of television pickup tubes, photographic film and the human eye. *P. Ire*, 30:293–300.

Rose, A. (1948). The sensitivity performance of the human eye on an absolute scale. *Journal of the Optical Society of America*, 38(2):196–208.

Rovamo, J., Donner, K., Näsänen, R., and Raninen, a. (2000a). Flicker sensitivity as a function of target area with and without temporal noise. *Vision research*, 40(28):3841–3851.

Rovamo, J., Luntinen, O., and Näsänen, R. (1993). Modelling the dependence of contrast sensitivity on grating area and spatial frequency. *Vision Research*, 33(18):2773–2788.

Rovamo, J., Mustonen, J., and Näsänen, R. (1994a). Modelling contrast sensitivity as a function of retinal illuminance and grating area. *Vision research*, 34(10):1301–1314.

Rovamo, J., Mustonen, J., and Näsänen, R. (1994b). Two simple psychophysical methods for determining the optical modulation transfer function of the human eye. *Vision research*, 34(19):2493–502.

Rovamo, J., Raninen, A., and Donner, K. (2000b). The effects of temporal noise and retinal illuminance on foveal flicker sensitivity. *Vision Research*, 39(3):533–550.

Shapley, R. (1986). The importance of contrast for the activity of single neurons, the vep and perception. *Vision Research*, 26(1):45–61.

Shapley, R. and Enroth-Cugell, C. (1984). Visual adaptation and retinal gain controls. *Progress in Retinal Research*, 3:263–346.

Silvestre, D., Arleo, A., and Allard, R. (2018). Internal noise sources limiting contrast sensitivity. *Scientific Reports*, 8(1):1–11.

Silvestre, D., Arleo, A., and Allard, R. (2019). Healthy Aging Impairs Photon Absorption Efficiency of cones. *Investigative ophthalmology & visual science*, 60(2):544–551.

Silvestre, D., Cavanagh, P., Arleo, A., and Allard, R. (2017). Adding temporally localized noise can enhance the contribution of target knowledge on contrast detection. *Journal of Vision*, 17:1–10.

Swenor, B. K., Wang, J., Varadaraj, V., Rosano, C., Yaffe, K., Albert, M., and Simonsick,

E. M. (2018). Vision Impairment and Cognitive Outcomes in Older Adults : The Health ABC Study. *Journals of gerontology: medical sciences*, pages 1–7.

Thibos, L. N., Hong, X., Bradley, A., and Cheng, X. (2002). Statistical variation of aberration structure and image quality in a normal population of healthy eyes. *Journal of the Optical Society of America*, 19(12):2329.

Tulunay-keesey, U., Ver Hoeve, J. N., and Terkla-mcgrane, C. (1988). Threshold and suprathreshold spatiotemporal response throughout adulthood. *Journal of optical society of America*, 5(12):2191–2200.

Tyler, C. W. (1989). Two processes control variations in flicker sensitivity over the life span. *Journal of the Optical Society of America. A, Optics and image science*, 6(4):481–90.

United Nations (2017). World population prospects: The 2017 revision, Key findings and advance tables.

van Meeteren, A. and Vos, J. J. (1972). Resolution and contrast sensitivity at low luminances. *Vision Research*, 12(5):825–833.

Van Nes, F. L. and Bouman, M. a. (1967). Spatial Modulation Transfer in the Human Eye. *Journal of the Optical Society of America*, 57(3):401.

Virsu, V. and Rovamo, J. (1979). Visual resolution, contrast sensitivity, and the cortical magnification factor. *Experimental Brain Research*, 37(3):475–494.

Watson, A. B. (1986). Temporal Sensitivity.

Watson, A. B. (2013). A formula for the mean human optical modulation transfer function as a function of pupil size. *Journal of vision*, 13(2013):1–11.

Weale, R. (1963). *Aging eye*. Lewis, London.

Wesner, M. F. and Tan, J. (2006). Contrast sensitivity in seasonal and nonseasonal depression. *Journal of Affective Disorders*, 95(1-3):19–28.

Wyart, V., Nobre, A. C., and Summerfield, C. (2012). Dissociable prior influences of signal probability and relevance on visual contrast sensitivity. *PNAS*, 109(9).

Xie, F., Liang, P., Fu, H., Zhang, J. C., and Chen, J. (2014). Effects of normal aging on

myelin sheath ultrastructures in the somatic sensorimotor system of rats. *Molecular Medicine Reports*, 10(1):459–466.

Zhang, C., Hua, T., Li, G., Tang, C., Sun, Q., and Zhou, P. (2008). Visual function declines during normal aging. *Current science*, 95(11):1544–1550.

Zhao, Y., Lu, Z.-L., and Dosher, B. A. (2015). Sustained spatial attention excludes external noise and narrows the perceptual template. *Journal of vision*, 15(12):1049.